Article:
Finnigan, J, Ayotte, K, Harman, I et al. (2020) Boundary-Layer Flow Over Complex Topography. Boundary-Layer Meteorology, 177 (2-3). pp. 247-313. ISSN: 0006-8314

https://doi.org/10.1007/s10546-020-00564-3

Boundary Layer Meteorology-50th Anniversary Volume
Boundary-layer flow over complex topography

John J. Finnigan[1] • Keith W. Ayotte[2] • Ian N. Harman[3] • Gabriel G. Katul[4] • Holly J. Oldroyd[5] • Edward G. Patton[6] • Davide Poggi[7] • Andrew N. Ross[8] • Peter A. Taylor[9].

Received: DD Month YEAR/ Accepted: DD Month YEAR/ Published online: DD Month YEAR

Abstract We review developments in the field of boundary-layer flow over complex topography, focussing on the period from 1970 to the present day. The review follows two parallel strands: the impact of hills on flow in the atmospheric boundary layer and gravity-driven flows on hill slopes initiated by heating or cooling of the surface. For each strand we consider the understanding that has resulted from analytic theory before moving to more realistic numerical computation, initially using turbulence closure models and, more recently, eddy-resolving schemes. Next we review the field experiments and the physical models that have contributed to present understanding in both strands. For the period 1970-2000 with hindsight we can link major advances in theory and modelling to the key papers that announced them but for the last two decades we have cast the net wider to ensure that we have not missed steps that eventually will be seen as critical. Two important new themes are given prominence in the 2000-2020 period. The first is flow over hills covered with tall plant canopies. The presence of a canopy changes the flow in important ways both when the flow is nearly neutral and also when it is stably stratified, forming a link between our two main strands. The second is the use of eddy-resolving models as vehicles to bring together hill flows and gravity-driven flows in a unified description of complex terrain meteorology.

Keywords Boundary-layer meteorology . Turbulence . Complex topography. Gravity-driven flows . Turbulence Modelling.

John J. Finnigan
John.finnigan@csiro.au

1. Australian National University, Research School of Biology, Canberra, Australia;
2. Windlab Systems Pty. Ltd. Canberra Australia;
3. CSIRO Oceans and Atmosphere, Canberra Australia
4. Nicholas School of the Environment & Department of Civil and Environmental Engineering, Duke University, Durham, NC 27708-0328, USA
5. Department of Civil and Environmental Engineering, University of California, Davis, CA, USA
6. National Center for Atmospheric Research, P.O. Box 3000, Boulder, CO 80307-3000, USA
7. Politecnico di Torino. Dept. of Environment, land and Infrastructure Engineering.
8. Institute for Atmospheric Science, School of the Environment, University of Leeds, U.K.;
9. Department of Earth and Space Science and Engineering, Lassonde School of Engineering, York University, Toronto, Ontario M3J 1P3, CANADA

1 Introduction

It is over 70 years since the similarity theory of Monin and Obukhov (MOST) was developed in the USSR and over 50 years since experiments on the sweeping plains of South Eastern Australia and the mid-West of the USA validated it for the first time (Monin and Obukhov 1954; Dyer, 1967; Kaimal and Wyngaard, 1990). Since then MOST has occupied a central position in boundary-layer meteorology and forms the foundation for climate and weather models used around the world. It is the point of departure for new theory and the benchmark against which experimental data are assessed. However, at the most fundamental level MOST applies only to flat homogeneous terrain and most of the earth's surface is not flat but topographically complex on scales from hillocks to mountains so it is no surprise that the study of airflow over hills and valleys has a history as long as MOST.

Everyday experience continually reminds us of the influence of topography on winds and climate and the motivation for studying and quantifying these influences comes from all areas of atmospheric science and engineering. The unique characteristics of mountain weather and climate were well known by the early 20th century and the first general theories of large scale hill and mountain flows in the 1940s were driven by the need to include topographic drag in numerical weather models. Much of the work we will review in this paper however concerns smaller scales. In agriculture and forestry we are concerned with topographic influence on wind damage to crops and forests, on seed and pathogen dispersal, water use and CO_2 uptake, and on heat stress and frost formation. In wind engineering we must allow for locally enhanced forces on structures and at larger scale the impact of severe hill and mountain flows on urban regions or airfields. Air quality is strongly conditioned by steep terrain and pollutants can be concentrated in separated flow regions or by downslope gravity currents. More recently, two new applications have guided the research effort. First, in the rapidly growing wind energy industry, wind farm designers seek topographic enhancement of their atmospheric feedstock but need to avoid the impact of increased turbulence on their turbines. Second, in developments that link back to the earliest general hill flow theories, the demand for greatly increased spatial resolution in weather and climate predictions is now entraining small scale hill-flow dynamics into weather and climate models.

Faced with the challenge of reviewing this field over the 50 year span that Boundary Layer Meteorology has recorded it, an author naturally starts by looking at earlier reviews. These in themselves form a useful chronology of the development of conceptual ideas and

theory as well as a history of the experiments that prompted and tested them. A list starting with Hunt (1980) then Taylor et al. (1987), Finnigan (1988) and Blumen (1990), augmented by the substantial preambles in the contemporary papers devoted to theoretical or experimental advances and culminating in the splendid syncretic survey by Wood (2000), allows us with hindsight to distinguish distinct stages in the development of our current understanding.

From roughly 1940-1960, hill flow studies were dominated by the theoretical advances of Queney (1948) and Scorer (1949). Their efforts were motivated by weather forecasting and focussed on the larger scale effects of disturbances to the stratified troposphere and, although Scorer's later papers acknowledged the importance of the turbulent boundary layer, those early analyses in the main assumed laminar flow. Starting in the early 1970s, the next fifteen years were marked by an upsurge of interest in boundary layer flow over hills initiated by the numerical models of Peter Taylor and his Canadian colleagues and, almost simultaneously, by the analytic linear modelling led by Julian Hunt and announced by the scene-setting analysis of Jackson and Hunt (1975). That first step by Jackson and Hunt was quickly followed by extensions and alternative analytic approaches with critical advances being made by Mason and Sykes (1979), Sykes (1980) and Hunt et al. (1988a). For a time, the parallel developments in numerical modelling were strongly influenced by the advances in analytic theory and both were provoked or guided by experiments over isolated hills and in wind tunnels and towing tanks. Over a similar 1975-1990 period the study of buoyancy-driven katabatic and anabatic flows on simple extensive hill slopes proceeded alongside the study of isolated hill flows but with surprisingly little overlap.

From 1990-2010, as more accurate and mature numerical schemes became widely available, driven in part by the needs of the growing wind energy industry, the community began to address the problem of extending the by-now extensive corpus of knowledge derived from simple hill configurations to complex topography on a larger scale, including the use of eddy resolving models of coarse resolution as foreshadowed by Wood (2000). The last two decades from 2000-2020 have also seen analytic and numerical advances in the study of hills covered with tall plant canopies. New physics appears in this situation and has provided insights into some existing theoretical problems as well as essential input to the increasingly critical problem of measuring carbon exchange between the terrestrial biosphere and atmosphere. Eddy-resolving numerical models have increasingly come to the fore, being used both with coarse resolution to characterize regional flow over complex mountain topography and at fine scales to model the detailed turbulence dynamics on boundary layer

hills. With major field campaigns like MAP-Riviera, Matterhorn-X and Perdigao (see Section 6), this period has also seen a revival of the community's appetite for the large scale cooperative field experiments that provided so much impetus in the 1980s. We hope that the events that defined these stages will become clear in the sections below.

1.1 Scope and Structure of this Review

This review has several goals. First, it attempts to survey the developments in theory and understanding of boundary layer flows over topography from the sudden spontaneous upsurge of effort in the mid 1970s to around 2000. We will highlight key steps and the papers in which they were recorded. Second, it will attempt to do the same for the parallel field of gravity-driven flows on complex topography, although we note that experiments and theoretical advances in this field lagged the study of flow over simple hills by around a decade. Surprisingly most reviews thus far have treated only one or the other of these subject areas or, when they are both studied as part of a single major campaign, they are discussed separately (e.g., Blumen, 1990). Third, we will discuss the advances that have been made in each area in the two decades 2000-2020. Over this period especially we will highlight new areas of interest such as the radical changes to hill and slope flows that occur when a tall plant canopy is present and the growing use of eddy resolving numerical models in both hill and slope flow simulation.

Since time has not yet winnowed the large number of papers from this period down to those that will eventually be seen to be key, we will provide a more comprehensive guide to the publications that seem to us at this time to be most worthy of note. We apologize in advance to authors, whom we should have included and didn't. Where we can, we will assess the strengths of weaknesses of the state of the art with the aim of highlighting shortcoming's and new research directions. Finally we will briefly touch upon the latest efforts at bringing together hill and slope flows as components of general complex terrain meteorology. These involve bridging the gap between eddy resolving models of resolution coarse enough to calculate the large scale flow patterns forced by topography and those with grids fine enough to resolve the near-surface 3D turbulence, whose interaction with hills and valleys produces those same emergent large scale responses. This latter is a subject that is now ripe for a review of its own.

We have organized our review around a set of key topics rather than following a strict chronology. The topic areas are, insofar as is possible, self-contained so that they can be used as independent sources of reference but there is substantial cross referencing between sections. The key topic areas we shall cover are:

2. Boundary layer flow over isolated hills - theory and mathematical modelling;
3. Canopies on hills - theory and mathematical modelling;
4. Gravity driven flows;
5. Field experiments;
6. Physical modelling - wind tunnel and flume studies;

and finally in a summary section 7, we attempt to draw some lessons and suggest fruitful new directions for analysis.

1.2 Boundary layer flow over topography-definitions

Belcher and Hunt (1998) defined turbulent boundary layer flow over hills by the criterion that the flow is only perturbed over a horizontal length scale L that is comparable to or shorter than the depth of the atmospheric boundary layer, z_i, so that most of the boundary layer does not have time to come into equilibrium with the distortion. This implies that special attention must be paid to modelling the turbulent stresses. It also restricts attention to low hills. Kaimal and Finnigan (1994) offered a different definition, noting that the troposphere is stably stratified over most of its height except within the daytime atmospheric boundary layer (ABL). As a result, the vertical movement of air parcels as wind flows over a hill is accompanied by a gravitational restoring force. If the hill is large enough to disturb the whole ABL and the overlying stable troposphere, then buoyancy effects are important at any time of day; conversely, flow patterns around a hill on scales much smaller than the ABL depth are only affected by buoyancy when the ABL itself is stably stratified.

We can quantify this condition by comparing the time an air parcel takes to traverse the hill (and therefore the time during which it is displaced vertically) with the period of its vertical oscillation in a stable density gradient. This period is the inverse of the Brunt–Vaisala or buoyancy frequency N, where,

$$N = \sqrt{\frac{g}{\Theta_0}\frac{\partial \theta}{\partial z}} \tag{1}$$

Taking the lengthscale of the hill as L, the half width of the hill at half height, and the characteristic velocity in the ABL as U_0 , the time scale ratio is the Froude Number, F_L

$$F_L = \frac{U_0}{NL} \tag{2}$$

For $F_L << 1$, the hill flow is significantly affected by buoyancy forces; for $F_L >> 1$ a balance between inertial forces and turbulent friction dominates (although this balance may itself be

affected by the influence of buoyancy on the turbulent stresses). The ratio U_0/N is typically 1km so flow over hills of kilometre length scale may be free of strong buoyancy influences for much of the daylight hours and when winds are strong. In contrast, since the H/L ratios of natural topography are roughly 1:10, hills of much larger scale, say L~5km, are subject to direct buoyancy influences all of the time.

A different set of scaling arguments obtains when we consider local, gravity-driven flows on topographic slopes. Katabatic or anabatic flows, respectively down or uphill, are driven by the component of the vertical hydrostatic pressure gradient resolved along the hill slope. This will dominate the hydrodynamic pressure gradient, generated by the deflection of the ABL flow over the hill, when the Froude number F_L formed from the ratio of these two pressure gradients is small i.e. $F_L \ll 1$. In this case F_L is defined by Belcher et al. (2012) as,

$$F_L = \frac{U_0}{L}\left[\frac{g}{\Theta_0}\frac{\Delta\bar{\theta}}{L}\right]^{-1/2} \quad (3)$$

where $\Delta\bar{\theta}$ is the characteristic temperature difference between the thin hot or cool layer on the sloping hill surface and the temperature of the surrounding ABL at the same geopotential height. Cool surface layers are commonly generated by radiative cooling at night and the resulting katabatic flows are important in many practical circumstances. We discuss them in detail in Section 4. Anabatic flows are usually less important in daytime as strong surface heating usually generates convection cells spanning the ABL and the 'footprints' of these cells impose transient but relatively strong horizontal winds at the surface over scales of kilometres or more (e.g. Patton et al., 2016) but when synoptic winds are light, topography of appropriate scale can interact with convection to organize these convection cells (Dörnbrack and Schumann, 1993). Anabatic flows generated by combustion of vegetation of course are a critical issue in wildfire prediction and control but we do not address that issue here.

Large areas of significant topography such as the European pre-Alps, the Pyrenees or the foothills of the US Rocky Mountains and Sierra mix all scales promiscuously. Nevertheless, most of the theoretical development in hill flow studies thus far has concentrated on isolated hills in well-defined approach flows. In contrast, buoyancy-driven flows on simple slopes have been studied both in idealized conditions and in the context of large scale hill-valley wind systems. We will look first at the developments in the theory and understanding of boundary-layer hill flows and, in contrast to the somewhat restrictive criteria given above, we will adopt a more relaxed definition and include any hill-flow phenomena that are determined primarily by processes located within the boundary layer.

1.3 Notation and Definitions

For convenient reference, notation and definitions of parameters used throughout this review are gathered here.

Hill Flows-Coordinates and velocity components

x, y, z denote components of a right handed coordinate frame, which can be Cartesian, surface-following or streamline according to context. *x* is taken in the streamwise and *z* the surface normal direction. u, v, w are the corresponding velocity components $u = U + u';\ w = W + w';\ v = V + v'$, where capitals denote time means and primes turbulent fluctuations. An overbar indicates time averaging so $U = \bar{u}$, etc. $\bar{\tau} = -\overline{u'w'}$ is the mean kinematic turbulent shear stress.

θ is potential temperature and θ_v virtual potential temperature. Θ_0 is a reference temperature in degrees K and *g* the acceleration of gravity so g/Θ_0 is the thermal expansion coefficient of the atmosphere. $\overline{w'\theta'}$ is the eddy flux of θ in the *z* direction and $\theta^* = -\overline{w'\theta'}/u^*$ is the temperature scale of the logarithmic temperature profile.

c represents a generic passive scalar with $C = \bar{c};\ c' = c - C$ and $\bar{f}_c = \overline{w'c'}$ the eddy flux of *c*.

Δ denotes perturbations to mean quantities induced by the hill so $\Delta U, \Delta W, \Delta\bar{\theta}, \Delta\tau, \Delta\bar{f}_c$ are the perturbations in mean streamwise and surface normal velocity, potential temperature, shear stress, and scalar flux, respectively.

$U_B(z)$ denotes the undisturbed mean wind profile approaching a hill. In analytic theory $U_B(z)$ is usually assumed to follow the logarithmic law with displacement height, *d* and roughness length, z_0. $u^* = \sqrt{-\overline{u'w'}}$ is the friction velocity of the undisturbed upwind flow and κ is von Karman's constant

U_0 is the characteristic mean streamwise velocity scale. In analytic hill flow models $U_0 = U_B(h_m)$, where h_m is the middle layer height defined in Figure 2.

$\Delta S(x, y, z)$ denotes the mean velocity speed up over the hill and $\Delta S_{\max}$ is its maximum value, usually located above the hill top.

Hill length and Velocity Scales

H is hill height and L hill length, defined as the horizontal distance from the summit to the half-height point. Hill slope is defined as H/L. In the analytic theory of HLR88, the depth of the shear stress layer is h_i and of the middle layer h_m (Fig. 2) and $U_0 = U_B\left(h_m\right)$.

Buoyancy parameters

The Brunt–Vaisala frequency is defined as $N = \sqrt{\frac{g}{\Theta_0}\frac{\partial\theta}{\partial z}}$ and the Froude Number based on hill length as $F_L = \frac{U_0}{NL}$. We also use when appropriate a Froude Number based on hill height, $F_H = \frac{U_0}{NH}$ and a Froude Number taken as the square root of F_p, the ratio of the hydrodynamic and hydrostatic pressure gradients on a slope. $\sqrt{F_p} = F_L = \frac{U_0}{L}\left[\frac{g}{\Theta_0}\frac{\Delta\bar{\theta}}{L}\right]^{-1/2}$, which we identify with F_L.

Canopy parameters

h_c is the canopy height, C_d the dimensionless drag coefficient of the foliage and a the foliage area per unit volume. The momentum absorption length scale of the canopy is formed from average values of C_d and a, $L_c = \left(C_d\, a\right)^{-1}$.

Gravity-Driven Slope Flows-Coordinates and velocity components

s,n denote along-slope and slope-normal coordinates with s positive downslope. Along-slope and slope-normal velocity components are identified with a subscript s or n respectively as in u_s and w_n. The slope makes a positive angle α with the local geopotential surface. H_s, L_s and U_s are the depth, length and velocity scales, respectively, of a gravity current. Where appropriate, e.g. when the gravity current is on a hill, we assume $H_s = L$ and $U_s = U_0$. $\Delta\bar{\theta}$ is the characteristic potential temperature difference between a gravity current and the ambient air. $\bar{e}$ denotes the local turbulent kinetic energy; Λ is the local Obukhov length in the s-n coordinate frame.

2. Boundary layer flow over isolated hills- Theory and mathematical modelling

2.1 Analytic models

The general features of airflow over isolated 2D hills or ridges in strong winds have long been known (Fig.1a). Along streamlines close to the surface the wind decelerates slightly at the foot of the hill before accelerating to peak at the crest then decelerates in the lee. If the hill is steep enough downwind a 'separation bubble' forms with reversed mean flow and enhanced turbulence levels. Whether a separation bubble forms or not, a turbulent wake with a general velocity deficit extends downwind. On axisymmetric hills, the upwind deceleration region disappears and is replaced by a region of flow divergence as the streamlines separate to pass around the hill. These general features are shown in a different way as perturbations to an upwind logarithmic velocity profile in Figure 1b. The task of research has been to quantify these changes for the wide range of hill shapes and atmospheric conditions found in nature.

Our conceptual understanding of boundary-layer flow over hills has been hugely influenced by the seminal work of Jackson and Hunt (1975) (henceforth JH75) and a series of follow up papers. JH75 developed an analytic model for neutral flow over a rough hill by linearising the equations of motion about a background logarithmic wind profile. Their key insight was that the flow can be divided into two layers: a thin inner layer of depth h_i near the surface where perturbations to the turbulent Reynolds stress terms are important, and an outer layer, where the flow perturbations are essentially inviscid (Fig. 2). Scaling analysis yields different leading order terms in each layer and leads to a separate analytical solution in each layer. These can then be matched asymptotically to give an overall solution. The various assumptions made to approximate the equations limit the solutions to low hills where the slope is small and where the roughness length z_0 is also small compared to the characteristic width of the hill.

a

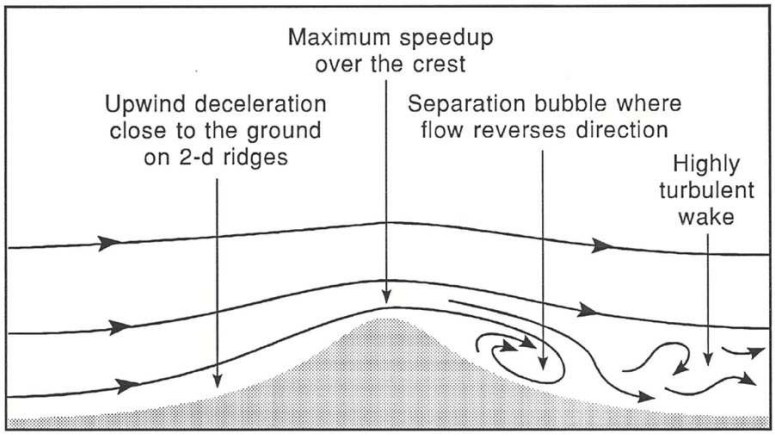

b

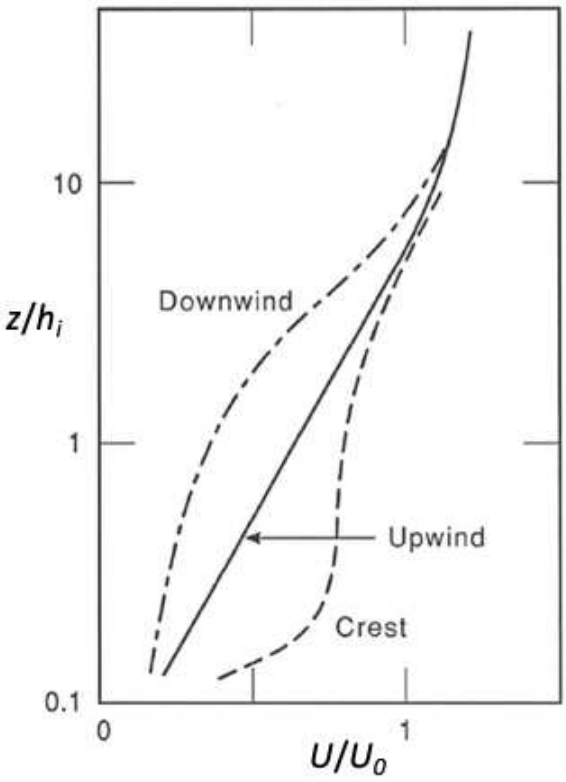

Fig 1. Main features of flow over low hills. a) flow over a 2D ridge. b) perturbation to an upstream logarithmic mean velocity profile. See Figure 2 for definitions of h_i and U_0. (After Kaimal and Finnigan, 1994)

The key result from the JH75 analysis was that there is much greater speed up than the magnitude of the hill slope would suggest. For example, if the slope of the hill is 1/5 then the wind speed at the crest is increased by a factor of about 1.5 (Belcher and Hunt, 1998) This is because the hydrodynamic pressure gradient that deflects the wind over the hill is proportional to the square of the approach velocity $U_B(z)$ well above the inner layer but the

resulting strong pressure gradient then acts on the much slower moving air layers close to the surface to produce a greater proportional acceleration. According to convention, the fractional speed-up is defined as,

$$\Delta S(x,z) = \frac{U(x,z) - U_B(z)}{U_B(z)} \tag{4}$$

where the origin of the x coordinate is the hill top. The peak speed-up, $\Delta S_{\max}$ occurs some distance above the hill top (Fig. 1b) and predicting its location and magnitude was the focus of much early research and served as a convenient test of theory against measurements. In JH75 and other analytic theories, ΔS was intimately related to the thickness of the inner layer, h_i and the several competing definitions of h_i that emerged from different approaches to scaling the equations of motion were tested against field data (Taylor et al. 1987) and wind tunnel simulations. For example, Britter, et al. (1981) compared the JH75 theory to the numerical model of Taylor (1977a,b) and to wind tunnel experiments (Finnigan, 1988). For a hill with a slope of H/L=0.26 the mean velocity predicted by the analytic model compared well with experimental data and numerical results on the upwind slope and near the crest of the hill, but not in the wake region.

Taylor et al. (1987) reviewed the application of JH75 to low hills and recommended using the speed-up formula,

$$\Delta S_{\max} = \left[\frac{U_B^2(L)}{U_B^2(h_i)}\right].\left[\frac{H}{L}\right]\zeta(x,z) \tag{5}$$

where ζ is a function that factors the precise shape of the hill into the formula. For values of H, L and z_0 typical of low hills with smooth contours, $\zeta \approx 1$ so that $\Delta S_{\max} \sim 2H/L$, the value recommended for 2D ridges in JH75. Taylor and Lee (1987) went on to formulate simple guidelines for wind speed changes over small scale topographic features. Over 3D axially symmetric hills they recommended $\Delta S_{\max} \sim 1.6H/L$, over 2D escarpments, $\Delta S_{\max} \sim 0.8H/L$ and over 2D ridges, $\Delta S_{\max} \sim 2H/L$. However, Finnigan (1988) noted that there exists an upper limit $\Delta S_{\max} \approx 1.25$, which is imposed by the appearance of a separation bubble on steeper hills. Once steady separation is established, the effective hill length, which determines the magnitude of the driving pressure perturbation through the hill steepness ratio H/L, is set by the geometry of the hill *plus* the bounding streamline of the separation bubble. We discuss experimental results on separation in Section 6 below.

Five years after the appearance of JH75, Sykes (1980) presented a rigorous asymptotic analysis which pointed to some weaknesses in the earlier model. He showed that the no-slip surface boundary condition, where the normal gradient of shear stress must match the tangential pressure gradient, could not be accommodated in the single shear stress layer of JH75. He also pointed out that the turbulent stresses in the JH75 upper layer should be well described by rapid distortion theory. These insights were incorporated in the more complex analytic model of Hunt et al. (1988a) (Henceforth HLR88), which refined JH75 by splitting each layer into two sub-layers. The outer region of JH75 was subdivided into a middle layer, where the mean vorticity is dynamically important, and an upper layer, which is inviscid and irrotational. The inner region was divided into a shear stress layer as in JH75 and a thin inner surface layer below, across which the shear stress varies only slightly but its gradient changes rapidly to match the hill-induced streamwise pressure gradient at the no-slip surface boundary condition (Fig. 2). Again, different terms in the momentum equation dominate in each layer, giving different solutions which can each be matched asymptotically to the adjacent layers.

From the point of view of weather models, one of the key motivations for studying flow over hills is to understand and predict the drag they exert on the atmosphere. For neutrally stratified flow this is entirely due to pressure or 'form' drag. In the JH75 and HLR88 analytic models, the solutions in each layer are obtained by series expansions in terms of a small parameter and terms of the same order are matched across the layers. The leading order pressure term comes from the solution of the inviscid irrotational (potential) flow in the upper layer and so is symmetrical about the hill and can exert no drag but it does produce an asymmetrical velocity perturbation through the effect of the shear stress in the inner layers. At second order, this asymmetrical velocity perturbation generates asymmetry in the pressure field also and, consequently, pressure drag on the hill. In the prescient analysis of Sykes (1980), his third major advance was to continue his asymptotic analysis to second order, whence he was able to deduce an expression for the pressure drag on a small hill.

In a similar way, Belcher et al. (1993) were able to extend the HLR88 model to second order to calculate the pressure drag. In contrast to the earlier calculation of Sykes (1980), Belcher et al. (1993) were able to include the effect of upstream shear, which significantly increased the form drag. They showed that the dominant mechanism for drag over low hills is 'separated sheltering', the thickening of the boundary layer in the lee of the hill. In an important clarification, Belcher et al. (1993) also showed that a traditional mixing length eddy-viscosity formulation overestimated the turbulent stresses in the HLR88 outer

layers and consequently overpredicted form drag by a factor of two. As a result they altered their analytic formulation to use a truncated mixing length. This overprediction of the turbulent response had been implicit in the results of Sykes (1980) and HLR88 as well as in the wind tunnel measurements of Britter et al. (1981), who all agreed that the turbulent stresses above the shear stress layer should follow rapid-distortion rather than flux-gradient physics. Wood and Mason (1991, 1993) went on to investigate the sensitivity of the Belcher et al (1993) numerical solutions to the turbulence closure assumptions and also extended the analysis to three dimensions. They used their solutions to develop an approximate expression for the 'effective roughness length', the apparent roughness length $\langle z_0 \rangle$ one would obtain from fitting a logarithmic form to the horizontally-averaged mean velocity profile well above the hill. This concept is often used in numerical weather prediction (NWP) models to represent the effects of sub-grid scale topography on the low level flow.

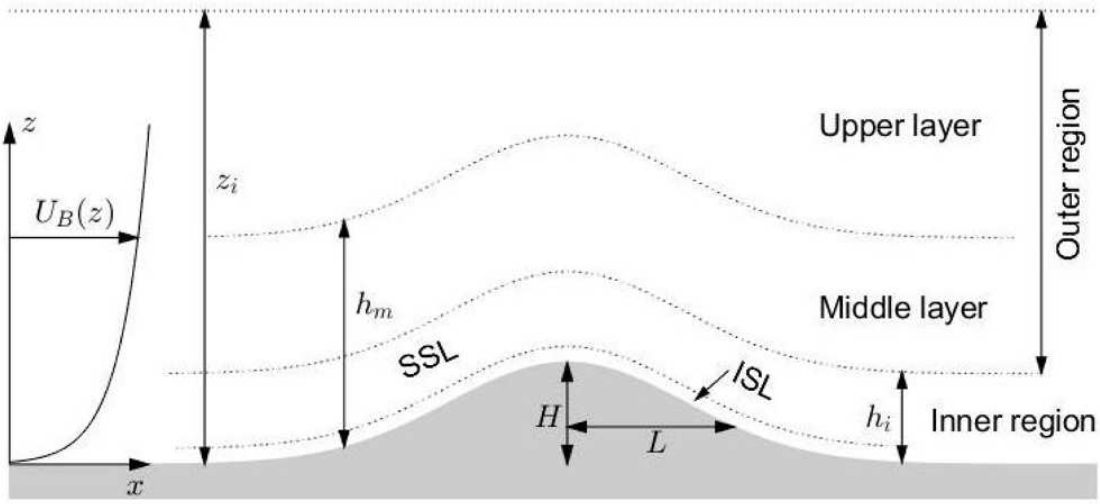

Fig. 2 Definitions of hill scales and HLR88 layers. SSL denotes the layer and ISL the inner surface layer. h_i is the shear stress layer depth and h_m the middle layer depth. $U_B(z)$ is the undisturbed approaching wind profile.

Another important feature of neutral boundary layer hill-flow is the onset of separation (Fig.1). Although this is an inherently non-linear process, linear theory has proved effective in predicting the critical slope at which flow separation can be expected to occur. Nanni and Tampieri (1985) and Tampieri (1987) derived an expression for the slope needed to cause separation over a two-dimensional hill, using the original analytic JH75 solution. Wood (1995) extended this, using the more complete analytic solutions in Belcher (1990) and Belcher et al (1993) as well as generalising to three dimensions. The analytic expression of

Wood (1995) for the critical slope angle depends on the hill geometry through the inner and middle layer heights, and also on the surface roughness. Wood also showed that these estimates from linear theory compare well with the numerical simulations of Wood and Mason (1993). Belcher and Hunt (1998) provide an excellent summary of the early developments of the JH75 model for neutral flow. A comparative review of earlier studies of flow separation, many from wind tunnel comparisons of hills of different geometry, can be found in Finnigan (1988). That comparison showed that separation on rough 2D ridges occurred at slope angles greater than ~15 degrees. But on axisymmetric hills, the critical angle was ~20 degrees. In all the cases reviewed, the nature of the surface roughness at or just upwind of the separation point was critically important.

Stratification is an all-pervading feature of the atmosphere and a number of studies have attempted to incorporate this into the JH75 framework. Carruthers and Choularton (1982) extended the JH75 solution to include an inversion layer between the neutral inner layer and a stratified outer layer. The model of HLR88 was also extended by Hunt et al. (1988b) to include the effects of several different upwind stratification profiles, although their solution is limited to $F_H = (U_0/NH) >> 1$, where F_H is a Froude Number based on hill height. At such large Froude Numbers the airflow goes over the hill rather than being blocked and forced to go around the hill by the stratification. A comprehensive treatment of these 'high Froude Number' cases, where the influence of buoyancy is largely exerted through changes to the shear in the approach flow, can be found in Carruthers and Hunt (1990). Blocked flow is fundamentally non-linear and is not amenable to this type of linearised analysis (Kaimal and Finnigan, 1994).

Belcher and Wood (1996) presented a more detailed analysis of flow over a hill with stratification, based on the work of Belcher et al. (1993). In the presence of stable stratification there is the possibility of generating internal gravity waves in the boundary layer, and hence there may be wave drag as well as form drag acting on the hill. From their solution Belcher and Wood (1996) derived expressions for both the pressure drag and the wave drag and showed how the relative importance of these depends on the stratification and on the hill shape, factors explored later both in field experiments (e.g. Vosper and Mobbs, 1997), numerical models and wind tunnel simulations (e.g. Ross et al. 2004; Allen and Brown, 2006).

2.2 Numerical models–Reynolds Averaged Navier–Stokes (RANS) Models

We divide the discussion of numerical models into those that use closure assumptions to relate the turbulent fluxes to the mean wind and temperature fields, collectively known as Reynolds Averaged Navier–Stokes or RANS Models, and those that resolve the energy-containing eddies of the turbulent flow directly, known as eddy-resolving or large eddy simulations (LES). These are treated next in Section 2.3. We can trace two main threads of RANS model development starting in the 1970s. One was initiated and led by Professor Peter Taylor and involved his many students and colleagues from Southampton and York universities, and loosely associated with the Canadian Atmospheric Environment Service. Much of their later work was motivated by the nascent wind energy industry. A parallel thread can be linked back to Dr Paul Mason at the United Kingdom Meteorological Office (UKMO) and his colleagues there and at the Universities of Cambridge and later, Reading. Both threads were strongly influenced by the analytical modelling ideas coming from Prof. Julian Hunt and colleagues at Cambridge. A strong motivator of the UKMO work was the effect of orographic drag on numerical weather prediction (Mason, 1985). It will be convenient in this section to describe first the 'Taylor family' of models and then the 'UKMO family' rather than swapping between the two chronologically although the many places where the two threads tangled will be obvious.

Numerical models of turbulent flow over low hills actually preceded the appearance of the JH75 analytic theory. In the mid 1970s Taylor and co-workers developed a non-linear numerical model of flow over low hills (Taylor and Gent, 1974; Taylor et al., 1976; Taylor, 1977a,b), while Deaves (1975) and Clark (1977) independently presented their own non-linear numerical scheme. These models employed more complex parameterizations of the turbulent stresses than the simple mixing-length closures used in the analytic models. Most used a so-called *k-l* or 1½-order closure scheme, where an eddy diffusivity was formed from the product of a velocity scale and a length scale. The velocity scale was taken as the square root of the turbulent kinetic energy (TKE), referred to in this context as *k*, and a length scale usually taken as the height above the surface at low levels merging smoothly to a constant value at greater heights (e.g. Taylor, 1977a). *k-l* closures require the solution of an equation for the TKE in addition to the momentum and continuity equations and so increase the demands on available computing power. Those demands could just about be satisfied in the mid 1970s but even today, when computing resources are more abundant, *k-l* schemes remain the default closure in many RANS hill-flow models because of their robust and predictable behaviour. They do have some significant shortcomings, however, which shall discuss below.

Following the appearance of JH75 and its clarification of the fundamental physics governing flow over low hills, several numerical models were developed that adopted the JH75 formalism as the basis for computationally efficient numerical schemes e.g. those of Walmsley et al. (1982) and Taylor et al. (1983). These models were based on linearised flow equations and made direct use of analytic formulations with various layers in the flow asymptotically matched to provide an approximate solution for hills of small slope. Within the limits to accuracy set by simply adding the impacts of surface roughness to those of topography, as permitted by their linear structure, these models allowed predictions of flow over terrain with changing surface roughness and elevation (Walmsley et al. 1986). In the wind energy industry the models most used were WAsP (Troen and Petersen, 1989) and to a lesser degree MS3DJH, originating from the work of Taylor et al. (1983). Both models are still used today in the wind energy industry.

These models structured on linear theory were very useful in that they allowed rapid calculation of complex flow fields over arbitrary topography but they were limited to gentler slopes. Because of their linear approximations they lost accuracy when used over terrain with slopes above ~0.2. This was mainly a result of their ignoring the strongly non-linear part of the advection terms in the model formulation and the weakly non-linear terms in the turbulent closure. Another area of weakness was in their vertical representation of the flow. The analytic theories of JH75 and HLR88 divided the flow into layers, in the case of HLR88, two inner and two outer, and this type of vertical decomposition tended to be overly restrictive, often not representing the real atmospheric boundary layer particularly well. At least partly in response to this, Beljaars et al. (1987) formulated a model that was less analytical in that it did not use explicit vertical layers. Though still using linearisations, the model used a mixed spectral-finite difference (MSFD) formulation, in which the terrain-following dimensions were spectral (Fourier modes) and the multi-layered analytic formulation was replaced by a finite-difference boundary-value solution of the equations for the mean and turbulent flow. Rather than explicitly imposing a layered structure on the solution, in which various analytical solutions held, this type of model accomplished a natural and smooth transition between the regions in the flow where different force balances dominated. Upstream mean and turbulent flow parameters (zero-order parts in the linearisation used within the model formulation) were provided by analytic forms of the boundary layer equations or, more commonly, by integrating the full set of boundary layer equations to a steady state over a horizontally homogeneous domain.

In addition to removing restrictions on the vertical structure accommodated within the model, this approach allowed more complex and arguably more realistic representations of turbulent flow. Examples of this were the use of higher-order turbulence closures (Newley, 1985; Zeman and Jensen, 1987; Ayotte and Taylor, 1994), full boundary layer formulations including rotation (Ayotte and Taylor, 1995) and adjoint data assimilation of upstream flows containing more realistic measured wind profiles (Ayotte, 1997). In the context of wind energy or wind engineering applications, which were key drivers for these developments, these changes to the model formulations moved away from the analytic restrictions noted above but still did not address the errors introduced by linearisation. Those ranged in type and magnitude from the more obvious misrepresentation of mean separation in the lee of steep slopes to the more gradual errors associated with the linearisation of modelled advection. The latter errors scaled with the hill slope and were manifested in an over-estimation of speed-up at the hill crest and an under-estimation of deceleration in the lee of hills of even modest slope. Evidence of this for atmospheric boundary layer flows was present in the literature quite early, for example in comparisons of modelled flow and field measurements over Askervein Hill (see Walmsley and Taylor, 1996). It was also explored more systematically in the wind tunnel measurements of flow over axisymmetric hills of varying steepness and roughness performed by Ayotte and Hughes (2004). Within the wind energy industry, these errors were understood to exist but were poorly quantified in flow over real terrain (Bowen and Mortensen, 2004) and were often compensated for in a practical sense by the use of such things as the Ruggedness Index (Mortensen et al., 2008), which was meant to allow the user to adjust solutions for these errors or at least be aware of them in particular modelling applications.

Another source of error when it came to the practical application of these models was their separation of the roughness and topographic influences on the flow. As noted above, the linear models of Walmsley et al. (1986) or Troen and Petersen, (1989) did combine both topography and roughness changes but allowed no feedback between the two influences on the flow. However, HLR88 had revealed the important influence of the shear in the middle layer of the upstream flow on the hill-top acceleration and so, because surface roughness changes clearly affect shear at mid-levels, the coupling between orographic accelerations and upstream surface roughness is unavoidable. Ayotte (1997) showed how upstream roughness changes and the associated changes in vertical shear in the approach flow can result in significant changes in the hill-top speed-up.

Although the simple linearised models such as WAsP, MS3DJH and MSFD in one of its many variants were subject to a number of the potential errors listed above, to the extent that these models were used over quite low slopes (*H/L* less than ~0.2) and in terrain where the surface cover did not change dramatically as well as in the near-neutrally stratified conditions of most interest to windfarm developers, the errors were acceptable and of the same order as other uncertainties in wind turbine siting. Recalling the available computing power of the day it is easy to see the attraction of these simplified models. They were easy to use (particularly the WAsP model), fast enough to give an answer quickly and accurate enough to give commercially acceptable uncertainties when used within the parameter space for which they were designed. However, they were often used outside this parameter space (sometimes unwittingly) and as such gained an undeserved reputation for being inaccurate. Some effort was made to address the shortcomings of linear models with weakly non-linear extensions to the MSFD model (Xu and Taylor, 1992, Xu et al., 1994). However, by the early 2000's with computing power becoming much cheaper and more available, the focus had shifted away from linear to non-linear formulations and to models in which the full set of Reynolds Averaged Navier–Stokes (RANS) equations were being solved.

Returning now to the 1970s and the UKMO modelling effort, Mason and Sykes (1979) had extended the 2D JH75 model to 3D and used a numerical implementation of their theory to successfully model flow around an isolated hill, Brent Knoll. There then followed a series of publications where numerical models with *k-l* closure were applied to successive 2D ridges (Mason and King, 1984), to an isolated hill (Mason and King, 1985) and, comparing the predictions of several numerical models, to the drag of small scale topography (Taylor et al. 1989). As part of his PhD thesis at Reading University, where Mason was one of his supervisors, Wood developed the non-linear BLASIUS model, which incorporated many of these earlier ideas and also employed *k-l* closure. This model was used to study orographic drag in neutrally stratified flow by Wood and Mason (1993) and later by Brown and Wood (2001) and then extended to stably stratified flow to calculate both pressure and wave drag on 3D hills by Brown et al. (2003). More advanced closure schemes also began to be implemented in BLASIUS and Ross et al. (2004) were able to compare 1½ order and 2nd order closure simulations of neutrally stratified and stable hill flow with wind tunnel modelling while Lewis et al. (2008a) used a series of mixing length simulations to explore the impact of surface heating on flow separation.

Although non-linear formulations were standard by the mid 1990s, we can see with hindsight that non-linear modelling began as early as the mid-1970's (Taylor and Gent,

548 1974, Taylor et al., 1976, Taylor ,1977a,b, Mason and King, 1984, Newley, 1985) but was
549 greatly hampered by insufficient computing power. Models of this type usually had an
550 incompressible pressure formulation and used a non-orthogonal, regular grid, loosely
551 following the formulation of Clark (1977). Ayotte (2008) has described the progression of
552 non-linear modelling that followed, leading to the non-linear RANS calculations now used by
553 many within the wind energy industry. Employing the wind tunnel measurements of Ayotte
554 and Hughes (2004) as a benchmark, Ayotte (2008) highlighted the improvement in accuracy
555 afforded by the use of a fully non-linear model formulation. The parameter space addressed
556 by RANS simulations has also expanded to include stability-affected flows as routine. See for
557 example Lewis et al. (2008a), who were able to model the effect of surface heating on
558 separation or Bleeg et al. (2015), who modelled the effect of stable stratification on the wind
559 resource of a windfarm, and many other examples can now be found in the literature. In
560 addition widely used commercial or freeware modelling packages like WaSP or BLASIUS
561 offer a variety of closures to suit specific problems. However, despite their widespread use,
562 RANS models remain severely limited in their ability to simulate the abrupt increase in
563 turbulent scale and intensity that follows separation, a phenomenon that is of great practical
564 importance in a range of applications from wind turbine siting to dispersion of seeds and
565 pollutants in steep topography. As a result, the exponentially increased computational power
566 that has now become available has shifted the focus of effort to eddy-resolving calculations
567 and we discuss these approaches next.
568
569 **2.3 Turbulence Resolving Large Eddy Simulations**
570 Although, as we have seen in the previous Section, RANS approaches have contributed
571 enormously to the community's ability to usefully model turbulent flow over complex terrain,
572 capturing the interplay between atmospheric turbulence and the terrain-induced pressure
573 distribution in RANS models largely hinges upon turbulence parameterizations derived from
574 horizontally-homogeneous boundary layers. While such techniques perform reasonably well
575 for unseparated flow over hills of low slope, they struggle to simulate flow separation and
576 recirculation and the accompanying large-scale high-intensity turbulence. The intimate non-
577 linear coupling between turbulent velocity and pressure in steep terrain almost guarantees
578 erroneous solutions when RANS is used in such situations. In RANS models, such errors can
579 certainly be reduced to some extent by applying tuning parameters to the model closures (as
580 noted in the previous Section) but these tunings are 'situation specific' and rarely transfer to
581 novel conditions.

582 The advent of turbulence-resolving simulation in the 1960's and 1970's introduced a
583 new paradigm for studying turbulence. Using numerical methods to solve the non-linear
584 Navier–Stokes equations directly was pioneered at the National Center for Atmospheric
585 Research (see review by Fox and Lilly, 1972). The researchers involved quickly realized that
586 direct numerical simulation (DNS), where a simulation resolves the flow down to the
587 Kolmolgorov microscale, is impractical for studying the atmospheric boundary layer because
588 of the vast range of scales of motion to be resolved (mm's to km's), which greatly exceeded
589 the capacity of computers at that time (and in fact still does), and the varying character and
590 roughness of the underlying surface. However, the researchers also recognized that
591 discretizing the flow field on a finite grid represents a low-pass filtering operation and that, if
592 they placed that filter at a scale well into the inertial subrange, they could calculate the time
593 evolution of the largest energy-containing scales of motion directly while using theoretical
594 arguments to parameterize the smallest scales, which act to dissipate the energy in the
595 resolved scales. This technique is known as large-eddy simulation (LES). We note here that
596 the engineering and geophysical fluid dynamics cultures use the label 'LES' to mean subtly
597 different things. In the engineering communities, LES implies parameterising the sub filter-
598 scale turbulent motions while still retaining sufficient resolution to capture the near-surface
599 viscous wall layer, i.e. they retain the viscous terms in the equations. This is sometimes
600 referred to as 'wall-resolved' LES. In contrast, in the geophysical community, viscous terms
601 at solid surfaces are usually ignored because of the very large disparity between the filter
602 scale and the Kolmolgorov microscale. In those models, therefore, momentum transfer to the
603 surface must be completely handled by a wall model (i.e. an imposed drag law with
604 corrections for atmospheric stability and roughness). Engineering LES is sometimes referred
605 to 'finite Reynolds number LES', and geophysical LES as 'infinite Reynolds number LES'.
606 Turbulence-resolving simulations transformed the community's understanding of
607 atmospheric turbulence over horizontally homogeneous terrain, showing for example, that
608 instabilities create organization or coherent eddy structures in turbulent flows, whose
609 character depends on the balance of driving forces, see Deardorff (1970a,b, 1972a,b). It also
610 quickly became aparent (e.g. Gal-Chen and Sommerville, 1975) that numerically solving for
611 the time evolution of flow over an irregularly shaped surface requires application of one of
612 two broad concepts. Either a Cartesian grid framework is retained and special techniques
613 applied to represent the lower boundary, a concept that now has numerous names, such as
614 immersed boundaries or cut-cell methods. Alternatively coordinate transformation is used to
615 convert complicated domains into a Cartesian representation (e.g. Phillips 1957). Although

they allow one to match boundary conditions explicitly, coordinate transformations generate additional terms in the equations, which, depending on the method chosen, can complicate the pressure solution and can introduce unphysical singularities.

To our knowledge, Clark (1977) was the first to apply a turbulence-resolving simulation to flow over aerodynamically-rough hills using the grid-transformation method and demonstrating the importance of properly treating the surface boundary and turbulent inflow conditions when studying orographic drag. In the early 1990's, Schumann (1990), Walko et al. (1992) and Dörnbrack and Schumann (1993) began exploring atmospheric LES as a tool to interrogate the influence of buoyancy on turbulent flow over sloping terrain or interacting with two-dimensional topography. Schumann (1990) determined that the equilibrium state for heated turbulent flows over a sloping boundary depends solely on the slope angle and the ratio of the surface roughness length (z_o) to a buoyancy length scale related to the amplitude of the surface buoyancy flux and stratification in the free-atmosphere above the boundary layer. However, he acknowledged some uncertainty in his findings associated with his having applied MOST in heterogeneous terrain. Walko et al. (1992) showed that buoyancy in the zero mean wind boundary layer over repeating hills generates circulations with updraft plumes focused at the hill crests while Dörnbrack and Schumann (1993) found that the scale of the orography alters the character of the hexagonal turbulent convection cells that dominate free convection boundary layers. They also found that convectively driven turbulence eliminates recirculation zones that would otherwise persist in the lee of steep terrain at the wind speeds they studied. Gong et al (1996) applied Dörnbrack and Schumann's LES to neutrally-stratified flow over two dimensional ridges to explain the longitudinally aligned roll-like structures that they found in their wind tunnel measurements. These probably arise from a secondary instability mechanism induced by the hills such as a Craik-Leibovich type-2 instability (See Section 7.1). Using 'wall-resolved' LES over low-amplitude two-dimensional hills, Henn and Sykes (1999) confirmed the presence of an inner layer, about 5% of the hill wavelength in depth, in which velocity variances vary rapidly. They also noted dramatic increases in the lateral velocity variance on the windward side of their hills that they also speculate are associated with an un-determined terrain-induced instability mechanism.

In his seminal review, Wood (2000) outlined the difficulties associated with producing "well-resolved" LES of neutrally-stratified turbulent flow over hills. His key findings were that: the simulations must be 3-D; grids must be isotropic; the domain needs to be large enough to permit the largest eddies anticipated yet fine enough to resolve the small

eddies within the inner layer; the lowest grid point needs to be sufficiently close to the surface to allow application of law-of-the-wall boundary condition; and finally, simulations need to be run for long enough to generate stationary turbulence statistics. While such requirements made accurate simulations difficult to implement in 2000, computing resources available today make them attainable (e.g. Bou-Zeid, 2014; De Bruyn Kops and Riley, 2019). Nevertheless, Brown et al. (2001) circumvented Wood's fourth requirement by recognizing that, when using such high resolution, one begins to resolve some of the roughness elements such as tall trees and accounting for momentum loss to the canopy elements, which occurs primarily through pressure drag, minimizes the importance of near-surface processes beneath the canopy. Interestingly, Allen and Brown (2002) found that applying a canopy model rather than surface roughness over their simulated hill increased the depth and overall extent of their predicted separation bubble compared with observations. We shall see in the next section that this phenomenon is caused by the interaction between fundamental features of canopy flow and hill flow.

Because of its control over and influence on near-surface mean wind and momentum flux profiles, the sub-filter scale model formulation used to close the equations and represent the momentum transport can affect flow separation predictions in the lee of steep hills (e.g. Satoru and Kondo, 2004, 2006; Wan et al., 2007; Chow and Street, 2009, Wan and Porte-Agel, 2011). Silva-Lopes et al. (2007) noted that resolution can also impact the size, shape, intensity, and intermittency of the separation bubble. Many of the early LES applications simulated wind tunnel rather than field measurements in an attempt to reduce terrain complexity and maintain some control over the driving parameters (e.g. Gong et al, 1996; Henn and Sykes, 1999). However, researchers fully recognized that transferability of that knowledge to geophysical applications outdoors would require an understanding of whether Reynolds number similarity applies, how stratification alters the relationships between hill-induced pressure and turbulent momentum stress, and how terrain containing a broad spectrum of scales alters the relationships and theories developed for idealized terrain (see Section 7 below).

Through the 1990's and 2000's, the Askervein hill experiment (Section 5) served as the most complete field data set available, hence many LES studies began targeting data from Askervein as computing power became more readily accessible (e.g. Undheim et al., 2006; Chow and Street, 2009; Golaz et al. 2009). It was soon realized that, while Askervein hill was excellent for testing linear theories, the shallow slopes were insufficient to study the application of non-linear models to fully separated flow and that the Askervein hill

684 experiment lacked enough turbulence measurements to characterise the flow complexity
685 adequately. To address these issues with newly emerging remote sensing capabilities, the
686 wind energy community initiated a new set of field experiments that began with what is now
687 known as the Bolund experiment (Section 6). Bechmann et al. (2011) presented a blind
688 intercomparison of many RANS codes and a few LES codes upon which the wind energy
689 community relies with the most interesting result being that the highly-tuned RANS models
690 outperformed the few engineering-style LES codes that were included, however, the poor
691 performance of the LES codes was largely attributed to modeller skill. Follow-on efforts
692 using LES to target the Bolund experiment have shown substantially improved skill (e.g.
693 Diebold et al., 2013). Recent field campaigns targetting flow over hills for wind energy
694 resource assessment (e.g., Mann et al., 2017) should enable transformative new
695 understanding and turbulence resolving simulation capabilities; for example, Dar et al. (2019)
696 used LES to demonstrate hill-induced flow separation influences on the downstream
697 evolution of turbine wakes. Several modelling packages now widely used in the community
698 such as the previously mentioned WAsP and BLASIUS as well as the more mesoscale
699 orientated WRF (https://www.mmm.ucar.edu/weather-research-and-forecasting-model) offer
700 LES capability but these codes need to be treated with due appreciation of the caveats listed
701 above.

702 **2.4 Modelling Scalar Transport over Rough Hills**

703 Thus far we have focussed on momentum transport and flow patterns but, as noted at the
704 beginning of this section, many of the applications of hill flow research require information
705 on scalar transport. The examples we have already given, where the effects of buoyancy on
706 the windfield were calculated, implicitly required knowledge of heat as well as momentum
707 transport, however, modelling of scalar transport over hills dealt first passive scalars. Padro
708 (1987) used a quasi-analytical approach to deduce the perturbations to the field of a generic
709 scalar flowing over a 3D hill. He derived the wind field was from the Walmsley (1980)
710 numerical implementation of the JH75 theory as discussed in Section 2.2. Padro and
711 Walmsley (1990) extended this approach by including the concentration field calculations in
712 the formalism of the linearised MSFD, model (Beljaars et al. 1987), which employed an
713 improved *K-l* closure scheme. This combination provided a generally useful tool for
714 application. Hunt et al. (1998c) reviewed the general principles governing scalar fluxes to
715 hills in the light of the scaling arguments encapsulated in HLR88 and its stratified extension
716 (Hunt et al. 1998b), however, the first direct application of the then new linear analytic
717 HLR88 theory to scalars was the elegant study by Raupach et al. (1992), who analysed the

718 exchange of a generic scalar, $c(x,z)$ with a rough 2D ridge and then applied their model to a
719 classic problem in micrometeorology-the partition of solar energy into sensible and latent
720 heat at the surface.

721 As in HLR88, Raupach et al. (1992) (henceforth RWCH92) divided the flow-field
722 into an outer layer and a shear stress layer of depth h_i (Fig. 2). In the outer layer, scalar
723 perturbations are governed by inviscid dynamics while in the shear stress layer, changes to
724 the scalar flux also play a role at first order. The linearised mass conservation equation in the
725 outer layer is,

726 $$U\frac{\partial \Delta C}{\partial x}+\Delta W\frac{\partial C}{\partial z}=0 \qquad (6)$$

727 which implies that in the outer layer $\Delta C\left(x,z\right)$, the perturbation in the time mean
728 concentration of the generic scalar *c*, is entirely the result of distortion of the isopycnals of
729 $C(x,z)$ as streamlines converge and diverge. In the inner layer, where $\Delta\overline{f_C}$, the perturbation
730 in the eddy flux of the scalar is important, the linearised mass balance is

731 $$U\frac{\partial \Delta C}{\partial x}+\Delta W\frac{\partial C}{\partial z}=-\frac{\partial \Delta \overline{f}_C}{\partial z} \qquad (7)$$

732 RWCH showed that in this region two other mechanisms become important in determining
733 $\Delta C\left(x,z\right)$. The first is the changes induced by the hill in the eddy flux field $\Delta \overline{f}_C\left(x,z\right)$ itself
734 and hence in its divergence. The second is the change to the flux of *C* from the surface that
735 occurs because the surface shear stress perturbation, $\Delta\overline{\tau}\left(x,0\right)$ varies as the hill is traversed.
736 The mechanism for this in the RWCH92 model is the representation of the surface source by
737 a flux-gradient expression, $\Delta \overline{f}_C\left(x,0\right)=-K_C\,\partial\left(C+\Delta C\right)/\partial z$, involving the scalar diffusivity,
738 $K_C=\kappa u^* z\left(1+\Delta\overline{\tau}/2\right)$. In the shear stress layer this modulation of the surface flux boundary
739 condition is the dominant influence on $\Delta C\left(x,z\right)$. The RWCH92 theory was later used to
740 investigate the general influence of topography on meteorological variables at whole
741 landscape scale by Raupach and Finnigan (1997) and see also Huntingford et al. (1998).

742 It was not long before the leading numerical models were incorporating the effects of
743 buoyancy by carrying an equation for heat transport as well as momentum transport fully
744 incorporated in their analysis schemes. Belcher and Wood (1996) used such a version of the
745 BLASIUS model in their study of form and wave drag over low ridges while Weng (1997)

746 presented a version of the MSFD model called MSFD-STAB in a comparison with buoyancy
747 affected field measurements over a low ridge (Coppin et al. 1994). This approach was then
748 generalised to consider the generation of internal gravity waves over generalised topography
749 Weng et al. (1997). Since then the BLASIUS model has been applied to more complex
750 questions such as the impact of surface heating on separation (Lewis et al. 2008a) while
751 buoyancy calculations are now standard features of most hill flow model applications (e.g.
752 Bleeg et al. 2014).

753

754 ## 3. New Physics-Canopies on hills

755 By the early 1990's a new and powerful motivation for studying boundary layer flow over
756 topography had appeared: the quantification of the exchange of carbon and energy between
757 the atmosphere and the biosphere through direct measurement of the turbulent exchange flux.
758 Organised into the international FLUXNET program (https://fluxnet.fluxdata.org), this
759 methodology built on a 25 year legacy of direct eddy flux measurement by fast response wind
760 and scalar sensors. With today over 900 'flux towers' measuring exchange from different
761 biomes around the world, particularly from tall forests where the major living carbon stores
762 reside, FLUXNET comprises one of the largest geophysical experiments ever mounted.
763 However, from its earliest days it was clear that significant problems in interpretation were
764 posed when the flux towers were situated in hilly terrain, even when steeper slopes were
765 avoided. Raw 24 hour totals of net carbon exchange were often wildly at variance with
766 independent stoichiometric limits on photosynthesis and respiration (Finnigan, 2008). Since
767 most flux tower sites were located in relatively gentle topography, the extension of linear
768 theory to accommodate a tall canopy rather than a rough surface was an obvious step towards
769 understanding what might be going on. Interestingly, the study of canopy flow on hills
770 brought together two fields which over the previous two decades had independently
771 undergone rapid development to each arrive at a generally accepted understanding of their
772 essential dynamics but their interaction revealed some new and surprising physical
773 phenomena.

774 We have already described the development of the basic theory of hill flows but by the
775 mid 1990's a set of questions that had taxed canopy flow researchers for at least 25 years
776 were also being answered, particularly the origin and nature of the characteristic large
777 coherent turbulent eddies that dominate canopy flow. By then, these were known to originate
778 from a hydrodynamic instability of the inflected mean velocity profile that inevitably

779 develops when momentum is absorbed over a finite height range rather at a plane surface
780 (Raupach et al., 1996; Finnigan, 2000; Finnigan et al. 2009). An early indication of the new
781 phenomena that appeared when topography was added beneath a deep canopy came from the
782 wind tunnel experiment of Finnigan and Brunet (1995). By placing a well-studied model
783 canopy on a 2D ridge they observed strong modulation of the critical inflected velocity
784 profile with the inflection point disappearing on the upwind hill slope and being exaggerated
785 and squeezed up into the upper canopy on the crest. They also observed a large continuous
786 separation bubble although the hill steepness was only at the margin of what would trigger
787 separation on a rough hill.
788
789 **3.1 Basic Theory and Analytic Models**
790 A first step in extending linear theory was taken by Finnigan and Belcher (2004) (henceforth
791 FB04), who effectively replaced the inner surface (shear stress matching) layer of the HLR88
792 model by a two-layer canopy scheme. In the upper canopy the flow is linearised and the hill-
793 induced pressure gradient, which is calculated as in HLR88 from the outer layer inviscid
794 flow, is balanced by a combination of perturbations in the turbulent shear stress and in the
795 aerodynamic drag of the canopy elements. In the lower canopy layer, which is inherently
796 non-linear the pressure gradient is balanced predominantly by the non-linear canopy drag,
797 $F_D = U^2/L_c$, which is represented as proportional to the square of the mean velocity divided
798 by a momentum absorption length scale, $L_c=(C_d\, a)^{-1}$, which is the reciprocal of the
799 dimensionless foliage drag coefficient C_d times the foliage area per unit volume, a (Finnigan
800 and Brunet, 1995). The non-linearity of the lower canopy layer cannot be avoided as the
801 background mean velocity decays exponentially with depth into the canopy (see Figure 3a
802 and Finnigan, 2000). As a result, in a deep or dense canopy, the background mean velocity in
803 the lower canopy is smaller than the perturbations driven by the pressure gradient, which
804 passes through the foliage effectively undiminished.
805 The coupling of the lower and upper canopy and shear stress layer solutions by
806 turbulent stress divergence leads to significant differences between the magnitude and
807 vertical distribution of the velocity perturbations in the FB04 and HLR88 models. The
808 differences can be seen in Figure 3a, where the FB04 and HLR88 models are applied to a 2D
809 hill of Gaussian cross section and where the surface z_0 in the HLR88 solution matches the
810 canopy z_0 in the FB04 solution. The differences are even clearer in Figure 3b, where only the
811 normalised velocity perturbations are shown. The HLR88 solution only goes down to a level

812 $d+z_{0,}$ where d is the displacement height of the upwind logarithmic wind profile, but it is
813 evident that the nature of the solution is changed significantly through the depth of the shear
814 stress layer above the canopy. An immediate consequence of the differing forms of the
815 leading approximation to the momentum equation in the upper and lower canopy layers is
816 that the velocity perturbation, ΔU in the upper canopy, just as in the shear stress layer above,
817 is proportional to the pressure perturbation whereas in the lower canopy, ΔU follows the
818 streamwise gradient of the pressure perturbation. This can be clearly seen in Figure 4a, where
819 the velocity perturbations along streamwise transects above and within the canopy on the hill
820 are compared with the forcing pressure perturbation and its gradient.
821 The differences are even clearer in Figure 4b, where the velocity perturbations ΔU
822 from both models are plotted along streamwise transects through the shear stress, upper and
823 lower canopy layers. In the shear stress layer at $z=3hc$ the two solutions are close and both
824 models have ΔU approximately in phase with the pressure perturbation but at the canopy top,
825 $z=h_c$ the FB04 perturbation is significantly smaller than the HLR88 solution and peaks further
826 upwind. As we descend deeper into the canopy, the phase of ΔU changes to match the
827 pressure gradient in the lower canopy solution and the phase difference between ΔU in the
828 upper canopy and in the shear stress layer approaches $\pi/2$, following the phase difference
829 between the leading order pressure perturbation and its gradient. We reemphasize that it is the
830 coupling of the non-linear lower canopy solution with the linear upper canopy and shear
831 stress layer solutions by the turbulent shear stress that leads to these global differences.
832 The fundamental non-linearity of the lower canopy solution in the FB04 model leads
833 to several features that are not seen in fully linear models. First it allows the hill flow solution
834 to affect the background flow, at least in principle, unlike models of the JH75 and HLR88
835 type, where the background flow remains unchanged. Wood (2000) pointed out that from the
836 NWP perspective, where we are interested in global changes to topographic drag, this is an
837 important limitation on linear models. Second, FB04 predicts the appearance of a separated
838 region within the canopy on the lee slope and, when that separation bubble occupies the full
839 canopy depth, we expect the flow above to separate also. Indeed, flow separation occurs for
840 hills of lower slope (by a factor of 2-3) than if the hill were a rough wall. This has been
841 confirmed in wind tunnel (Harman and Finnigan 2013), flume (e.g. Poggi et al. 2008) and
842 large eddy simulations (e.g. Dupont et al. 2008, Patton and Katul 2009) and is also reported
843 in field observations (Zeri et al. 2010).

844 Third, the non-linearity leads to convergence of the perturbation flow in the lower
845 canopy towards the hill crest (see Figure 4b). The associated vertical motion is in anti-phase
846 with the leading order pressure perturbation and $\pi/2$ out of phase with the vertical motion
847 induced by the deflection of the mean flow by the hill, which peaks on the upwind slope. For
848 hills of short length scale, L, and tall but sparse canopies, the two components of the vertical
849 motion are comparable, leading to significant changes in the magnitude and phasing of the
850 perturbation pressure response and associated form drag (Poggi and Katul 2008, Poggi et al.
851 2008). Simple scaling suggests that the pressure response decreases by factor of $1 + F$ where
852 $F \sim (h_c^2 L_c / HL^2)^{1/2}$, with more complex variations in phasing. As we shall see in Section 3,
853 this feature has a significant impact on scalar transport.
854 **a**

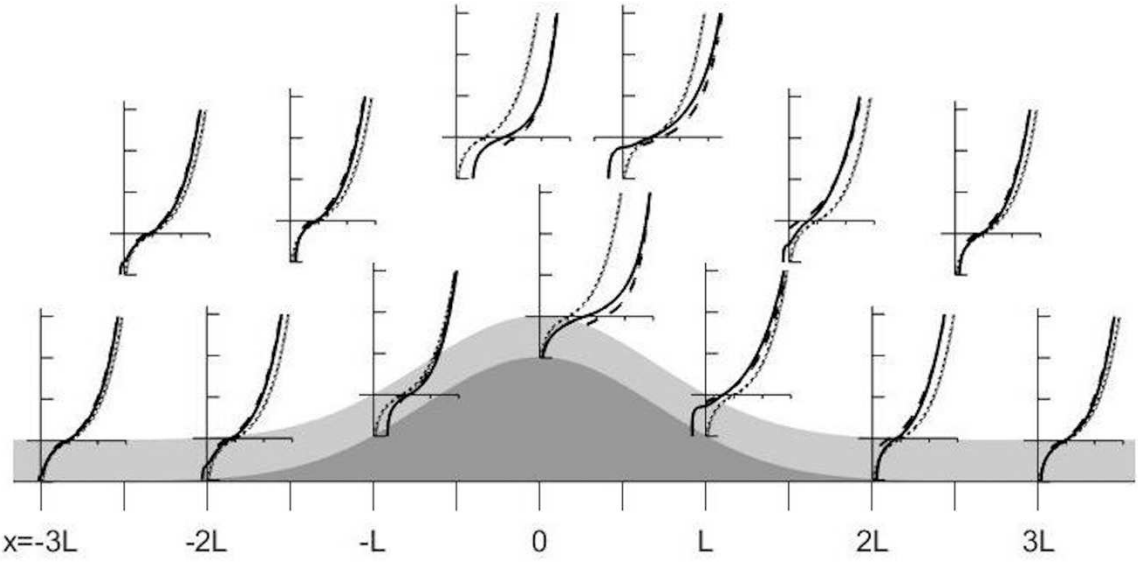

855
856 **b**
857

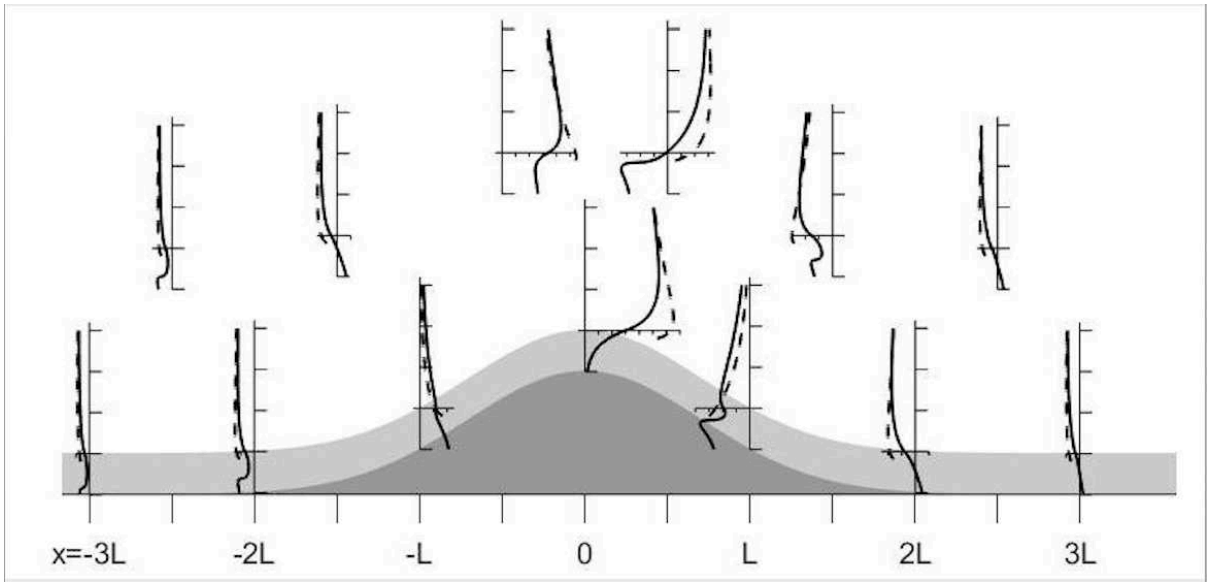

858

859

860 **Fig. 3** Profiles of wind speed above a Gaussian hill covered with a canopy calculated with FB04 and HLR88. **3a**
861 shows total mean wind profiles. The dotted lines show the wind profile in the absence of a hill; solid lines the
862 RB04 solution and dashed lines the HLR88 solution for the same effective z_0. Note the HLR88 solution extends
863 down only to $z=d+z_0$, where d is the displacement height and z_0 the roughness length of the upwind logarithmic
864 wind profile.
865 **3b**, as for Figure 3a but showing just the streamwise velocity perturbations for RB04 (solid line) and HLR88
866 (dashed line).

867 **a**

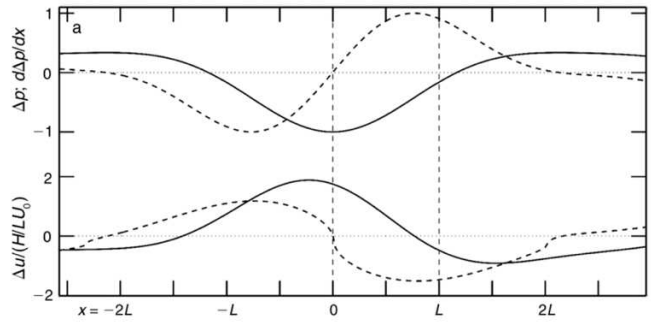

868

869 **b**

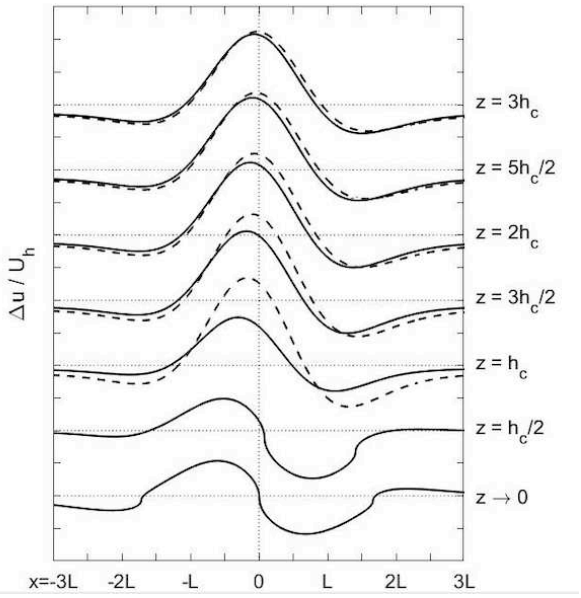

Fig. 4. (a) Phasing of forcing terms across the hill. Upper part of the panel shows variation across the hill of the pressure perturbation (solid line) and the pressure perturbation gradient (dashed line); perturbations have been normalized by the maximum value taken across the hill. The lower part of the panel shows variation of the normalized wind speed perturbation across the hill. Solid line is at z=3hc above the canopy, which is nearly in phase with the pressure perturbation. The dashed line is at z.= hc/2 within the canopy, which is in phase with the pressure perturbation gradient.
(b) velocity perturbations along streamwise transects through the shear stress layer and down into the canopy. Solid line denotes RB04 solution and dashed line HLR88.

The original FB04 model made a series of simplifying assumptions and these restrict its application to a relatively small region of a parameter space spanned by *H/L*, *h/Lc* and *Lc/L*, variables which provide a useful classification of experiments and model results (see Belcher et al., 2012). If we restrict our attention to hills where analytic theories like FB04 strictly apply, that is *H*<<*L*, Patton and Katul (2009) have collapsed the 3D parameter space of Belcher et al. (2012) into a 2D plane, which the competing influences of canopy height, canopy density and hill length divide into five regimes (Fig. 5). The envelope $h_c/L_c = 2\left(H/L\right)\left(L/L_c\right)^2$ marked by the slanting line in Figure 5 delineates regions in which the mean vertical velocity inside the canopy is expected to be large enough to affect the outer-layer pressure. Patton and Katul (2009) refer to flow regimes above this envelope to as 'interactive' pressure regimes, and flow regimes below this envelope as 'fixed' pressure regimes. FB04 is valid in the shaded area (Regime 1). Formalised extensions to the FB04 analysis, to cover a wider range of hill shapes and canopy densities have been presented by Poggi et al. (2008) and Harman and Finnigan (2010, 2013). The extensions include the effect

894 of advection in the upper canopy and better representation of the effect of the coupling
895 between the lower canopy flow and the upper canopy and shear stress layers on the pressure.
896 Finally, and of both theoretical and practical importance, FB04 demonstrated that,
897 even in the asymptotic limit of hills of very low slope, the canopy flow solution does not
898 converge to the HLR solution for a rough wall; a constant roughness length z_0 is not the
899 formal limit of a shallow canopy flow. This should not be too surprising since Harman and
900 Finnigan (2007, 2008), analysing flow in homogeneous canopies on flat ground, have
901 demonstrated that treating z_0 as a parameter determined by the surface geometry rather than
902 as a flow variable leads to significant errors in predicting the momentum and scalar fields in
903 the roughness sublayer. Since rough walls are themselves simply canopies of roughness
904 elements, they should be dynamically similar to tall canopies when correctly scaled (Raupach
905 et al., 1991).
906
907 **3.2 Effects of stability**
908 A further set of fundamental changes in the hill-canopy flow physics occurs when the
909 boundary layer becomes stably stratified, which typically occurs through radiative cooling at
910 night. These are discussed in detail in Belcher et al. (2008). Interestingly, these global
911 changes are the emergent result of differences in the microphysics of exchange processes at
912 leaf level. The efficiency of transport of a scalar between the foliage surface and the canopy
913 airspace is determined by the molecular conductivity of the scalar whereas, at typical natural
914 Reynolds Numbers, momentum transfer to the foliage is dominated by pressure drag. The
915 ratio of the efficiency of scalar to momentum transfer is expressed by the Stanton Number,
916 which is O[0.1] in natural canopies. As a result, the gradient of temperature in a radiatively
917 cooling canopy is much smaller than the gradient of mean windspeed produced as the foliage

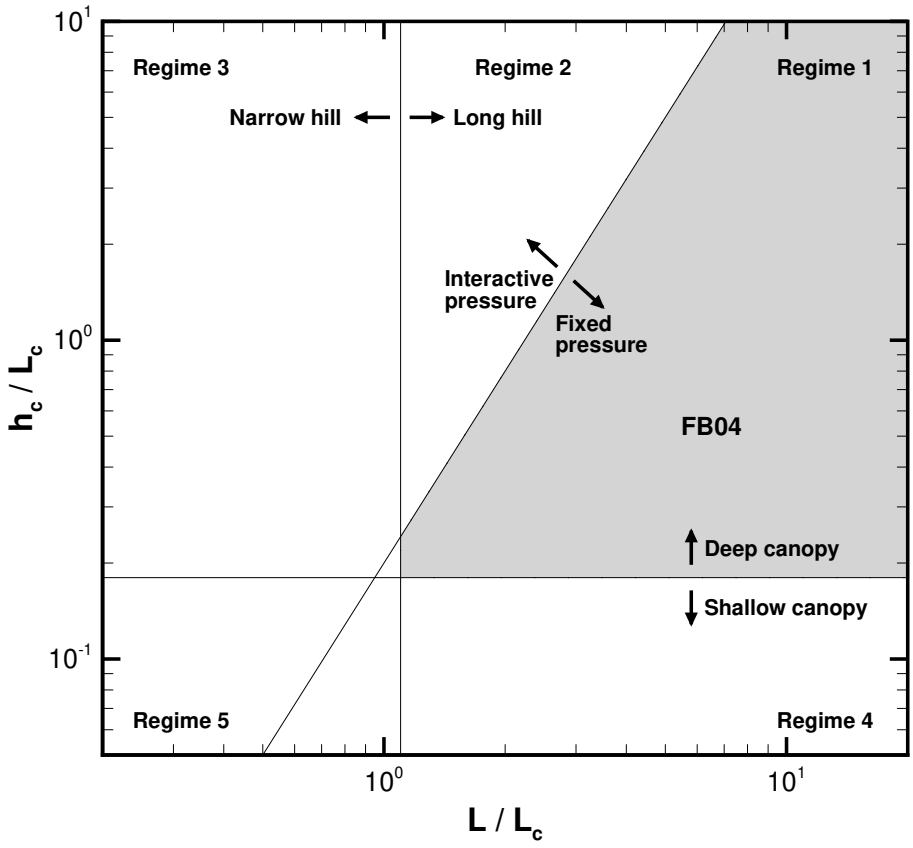

Fig. 5 Length scale regimes imposed by hill geometry and canopy morphology for low hills where $H << L$, after Poggi et al. (2008). Hills are classified as narrow or long and canopies as deep or shallow

absorbs momentum. Figure 6a shows profiles of temperature and windspeed computed using a simple mixing length model in a canopy with constant *Lc* and constant foliage surface temperature. Figure 6b shows the associated gradient Richardson Number $R_i = N^2 / \left(\partial U / \partial z\right)^2$, which has a minimum at $z=hc$, where the shear is largest, but quickly exceeds the critical value of Ri=0.25 within the canopy (Belcher et.al., 2008).

This rapid change in *Ri* typically leads to the existence of a subcritical region just above the canopy top within which $0.25>Ri>0$ and internal gravity waves can be supported. These are often observed at flux sites at night-time (van Gorsel et al., 2011) and add a level of complexity to the hill flow that has not yet been studied in any detail. When the within-canopy *Ri* becomes large enough, we see the situation modelled in a wind tunnel by Finnigan and Hughes (2008), where flow above the canopy was stably stratified but fully turbulent with Ri~0.1 while within the canopy Ri~10 and rotational turbulence was quenched, effectively decoupling the above- and within-canopy airflow. Within the canopy Finnigan and Hughes observed downslope gravity currents on both up and downwind hill slopes while

flow above the canopy behaved like flow over a rough hill (see Section 7.). Both the existence of large *Ri* in the night-time canopy, the decoupling of the within- and above-canopy flow and the consequent strong downslope gravity current seen in the idealised wind tunnel study were also observed in the field observations of Yi et al. (2005) at a FLUXNET site in the Front Range of the Rocky Mountains in Colorado. The gravity wave case (Van Gorsel et al., 2011; Lee and Barr, 2006) and the fully decoupled case are both of great importance to the carbon flux modelling community and we will return to them in Sections 4 and 5.

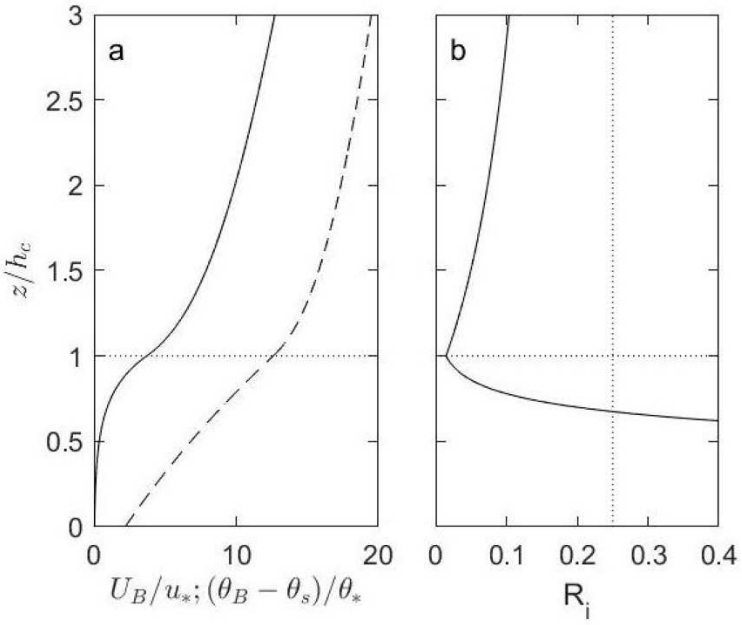

Fig. 6 Profiles of (a) windspeed (solid line) and temperature (dashed line) and(b) gradient Richardson Number, Ri through a canopy on level terrain . Note that for the moderate stratification of these plots, Ri remains sub-critical above the canopy, implying turbulent flow but supercritical within the canopy, implying collapse of the turbulence.

3.3 Numerical RANS models

Just as was the case over rough hills, numerical RANS models have played an important role when canopies are added to complex terrain. In order to represent canopy flow in a RANS model, an approach similar to that in analytic models like FB04 is typically taken, first by including a term in the momentum equation to represent the foliage drag, and second by modifying the turbulence closure to represent the different processes controlling turbulence in canopies. The canonical model is that the turbulence is dominated by eddies generated at the inflected shear layer near canopy top (analogous to a mixing layer). This motivates the choice of a constant mixing length l_m in the canopy. For 1½ order closure models with a prognostic

959 equation to compute the turbulent kinetic energy, there may also be an additional dissipation
960 term to represent the short-circuit in the energy cascade resulting from the small canopy
961 elements rapidly breaking up large eddies into smaller scale eddies (Baldocchi and Meyers,
962 1988; Wilson et al, 1998; Finnigan, 2000). Wilson et al (1998) tested the closure by
963 comparing with wind tunnel data from the Finnigan and Brunet (1995) "Furry Hill"
964 experiment and showed that the scheme worked as well as other more complicated closures
965 e.g. Sogachev and Panferov (2006) or Sogachev (2009).
966 Following the steps outlined above, Ross and Vosper (2005) modified the *K-l* closure
967 version of the BLASIUS model for canopy applications and inter-alia used this to validate the
968 linear analytic FB04 solution. They also used the numerical simulations to study the onset of
969 flow separation in a canopy and confirmed that a canopy on the hill surface indeed promoted
970 earlier separation than a roughness length parametrisation. Similarly they showed that the
971 canopy enhanced the form drag on the hill due to a shift in the pressure field as predicted by
972 FB04. Their model has subsequently been used to study the effects of canopy heterogeneity,
973 both variable canopy density (Ross, 2012) and hills partially covered by canopies (Ross and
974 Baker, 2013). Ross (2011) and Ross and Harman (2015) investigated the impact of source
975 distribution on tracer transport using the RANS model as a way of addressing the impact of a
976 canopy on flux variability over complex terrain even in neutral flow. As well as studying
977 idealised problems, the model has also been run over realistic terrain by Grant et al, (2016) to
978 compare to observations from the Arran canopy experiment described in Grant et al (2015).
979 Various RANS CFD models have also been applied to canopy flows. Yi et al (2005) used a
980 CFD model to study nocturnal drainage flows in forested complex terrain. More recently the
981 importance of canopy effects for assessing wind energy resources and for wind engineering
982 has led to a number of CFD studies including canopy effects (e.g. Chávez Arroyo et al 2014;
983 Desmond et al, 2017).
984 There has been debate in the literature over the applicability of simple RANS mixing-
985 length closure models in canopy flows. Eddy covariance observations do show counter-
986 gradient turbulent fluxes in some canopies, suggesting that local parameterisation is not
987 appropriate, however various studies have shown that in practice first order schemes are
988 useful (Grant et al, 2016). The assumptions and limitations of first order canopy closure
989 schemes are analysed by Finnigan et al (2015). There are a number of reasons for the
990 surprising success of first order closure schemes. First, analytic canopy models such as FB04
991 show that the leading order dynamics governing flow perturbations in canopy flows over hills
992 are inviscid (see Belcher et al., 2012), reducing the impact of the turbulence closure scheme.

Second, at least for momentum fluxes, the strongest shear is at the canopy top where the constant mixing length assumption works fairly well as demonstrated for example by LES studies like Ross, 2008 and in comparison with observations such as Katul et al, 2004 and Grant et al, 2015. The LES studies suggest that the mixing length may not be constant with height deeper in the canopy although the shear is generally low there and so this does not significantly impact on the momentum fluxes. However, it may be more important for scalar fluxes being emitted from the surface, although the impact of this has not yet been fully assessed.

3.4 LES Models

Although Brown et al. (2001) in their attempt to resolve competing requirements in LES modelling of neutral turbulent flow over a rough hill adopted Shaw and Schumann's (1992) strategy, which was developed to allow the incorporation of canopy physics in LES, canopy-resolving LES over hills really began with a pilot effort by Patton et al. (2006) who identified some of similarities and differences between flow over isolated and sinusoidally repeating 2D ridges. They demonstrated that resolving the canopy increases turbulence levels at the hill crest and confirmed the prediction of FB04 that, because a canopy primarily interacts with the flow through pressure drag, modelled flow over hills with resolved canopies will separate at much lower slopes than would flow over the same hill with an unresolved rough surface with the same z_0. A series of LES studies of hill-canopy flow followed. Tamura et al. (2007) simulated flow over an isolated three-dimensional canopy-covered hill and found that the flow took longer to recover from separation in the canopy case than in a smooth hill case. Next, Ross (2008) used LES to study the influence of 2D ridges on exchange processes at the canopy level and found that the turbulence is dominated by sweep/ejection events just as in homogeneous canopies but that the structure changes across the hill according to hill-induced modification of the mean flow.

Dupont et al. (2008) confirmed some additional flow characteristics predicted by the FB04 linearized theory, particularly that within-canopy flow accelerations on the upwind slope resulted in reduced canopy-top mean shear, that enhanced canopy-top shear at hill crest was responsible for increased turbulence kinetic energy production there and that, although canopy exchange occurs through similar mechanisms on either side of the hill, structures on the windward side of the hill are not correlated with those in the lee. From this they infer that such structures initiated on the windward slope end up being advected downstream of the hill in the region above the separation zone.

Patton and Katul (2009) investigated vegetation density influences on second-order flow statistics over gentle sinusoidal 2D ridges with key findings that included the fact that restricted domain heights can influence phase relationships between hill-induced perturbations in mean velocity and velocity variances, that an order-of-magnitude increase in canopy density does not significantly alter the broad phase relationship between pressure and the topography but can shift the pressure minimum downstream sufficiently to increase the hill-induced pressure drag by about 15%, and that hill-induced regions of increased turbulent momentum flux create regions of high amplitude pressure fluctuations. Ross (2011) used LES to study the transport of scalars emitted at a specified rate by a resolved canopy on a hill and found that those hill-induced pressure forces act like a pump to efficiently remove scalars from the canopy space, thereby reducing mean within-canopy scalar concentrations overall. However scalar concentrations exhibit high spatial variability with respect to location over the hill (see Section 4. below).

3.5. Scalar transport in canopies on Hills

Once direct measurement of carbon and energy exchange over hills using fast response sensors on 'flux towers' had become widespread significant problems began to appear. Uncorrected eddy flux measurements were often biologically unrealistic (Finnigan, 2008) and so to address this problem systematically in the early 2000s, detailed field experiments commenced at a number of sites in Europe (later formalized in the ADVEX initiative), where topographic complexity and canopy structure varied across sites (e.g. Lee and Hu, 2002; Feigenwinter et al., 2004). These studies showed that much of the imbalance between absorption or release of CO_2 and its vertical eddy flux is caused by the advective terms, especially under near neutral and unstable atmospheric stratification Aubinet et al. (2010). To further guide these field experiments and contribute to understanding the genesis of such imbalance, several model investigations of scalar transport in tall canopies on gentle hills were initiated.

Just as the FB04 model was developed as an extension of HLR88, and motivated by the same questions posed by direct eddy flux measurements of carbon exchange, a canopy extension of RWCH88 was developed for the case of a concentration boundary condition on the foliage (Finnigan, 2006). Like the momentum field in FB04, the scalar perturbation in the canopy was divided into a linearised upper-canopy solution and a non-linear, lower-canopy solution, which were matched asymptotically. In the upper canopy, on scaling grounds, the

scalar conservation equation reduces to a balance between the scalar eddy flux divergence and the perturbation to the canopy scalar source or sink.

In the lower canopy the scalar flux divergence becomes small, however, a sensible velocity perturbation ΔU continues to drive the scalar source term so that the conservation equation becomes a balance between advection of *c* along streamlines and the scalar source strength. Like its momentum equivalent in FB04 the lower canopy equation is non-linear but for a different reason. At leaf level, the leaf boundary layer conductance g_b, which for a constant concentration boundary condition controls the source strength, depends only on the magnitude of the wind velocity and not on its direction so that we must write $g_b = A\left|\overline{u}\right|^n$, where A is a constant depending on leaf morphology and *n* is an exponent between 0.5 and 0.8 (Finnigan and Raupach, 1987). In the upper canopy, where $U_B > \Delta U$ this dependence on absolute velocity need not be made explicit, but in the lower canopy, where $U \simeq \Delta U$, it is critical. Setting *n*=1 allows the equations to be solved analytically with results that are qualitatively the same as for the fractional values of *n*.

Two useful results follow from the analytic solution. First, the typical magnitudes of the velocity and scalar perturbations within the canopy, U_c and C_c, are respectively,

$$U_c = \frac{U_0^2 H L_c}{U_h L^2}; \qquad C_c = r U_c \frac{C_h}{U_h} \quad (8)$$

The magnitude of the velocity perturbation depends on the driving pressure gradient, which is $O\left[U_0^2 H / L^2\right]$, where U_0 is defined as the background velocity at the middle layer height, (Fig. 2) i.e $U_0 = U_B\left(h_m\right)$ and so is determined by the outer layer flow as well as by the momentum absorption in the canopy, which is characterized by L_c and U_h. Note that subscript *h* refers to values at the canopy top, $z=h_c$. With the choice of a constant concentration boundary condition on the foliage surface, the scalar perturbations are caused entirely by the windfield and not by variations in the source/sink strength and we see that they are relatively smaller than the velocity perturbations that drive them, the proportionality factor being the leaf-level Stanton number, *r*, which was introduced in Section 3.2. Second, changes to the concentration and flux fields above the canopy in the region where eddy flux towers are usually located, lead to changes in the relative phases of horizontal and vertical advection sufficiently large that a measurement of the vertical eddy flux at a point can differ

from the area average flux by around +/-50% (Finnigan, 2006). To test this result further we need to model the more complicated surface boundary conditions that control biologically active scalars like CO2 and water vapour and for this, numerical implementations of the linearised scheme or fully numerical models are necessary.

At roughly the same time as the linear analytic model development, Katul et al. (2006) produced a study where the analytic velocity field of FB04 was used to drive a scalar transport model with realistic parameterisation of energy and CO_2 exchange at the leaf surfaces and which was applied to a hill sufficiently steep that a separation bubble almost filled the canopy in the lee of the crest. The effects of topography and canopy on radiation attenuation were also considered and included in the leaf gas exchange equations. This more realistic but still simple model confirmed that streamwise and vertical advection are individually much larger than the biological sinks (leaf-area weighted photosynthesis) at many positions within the canopy and across the hill. As in the fully analytic model of Finnigan (2006), the two advective terms are usually opposite in sign but do not precisely cancel each other locally even when averaged across the hill. The imbalance between them is sufficiently large to decouple the local canopy photosynthesis from the local turbulent flux, implying that linking tower-based eddy-flux measurements to local biological sources and sinks on hilly terrain is difficult to impossible without knowledge of both advective terms.

The flow convergence caused by the non-linearity of the momentum and scalar solutions in the lower canopy described in Section 3.1, forces a plume of concentrated scalar to be ejected just behind the hill crest. In Figure 7 this is illustrated by a numerical solution of the scalar equations driven by the FB04 model for a very gentle hill (maximum slope 3 de.g.) covered with a tall dense canopy. The solution assumes a constant scalar source of unit strength and the appearance of a plume of low vertical eddy flux $\overline{w'c'}$ behind the hill crest is clear as is the compensating horizontal and vertical advection terms and a smaller contribution from the divergence of the horizontal turbulent flux of *c*.

More accurate quantitative modelling by Ross (2011), using a Lagrangian transport scheme embedded in the 1.5 order closure implementation of the BLASIUS model (Ross and Vosper, 2005) revealed the first-order effect of canopy source distribution on the overall transport and its spatial distribution and confirmed the qualitative results of the analytic modelling described above. In addition, Ross (2011) was able to assess the contribution of higher order terms in the turbulent transport of the scalar relative to advection more

accurately. Ross and Harman (2015) used the same RANS modelling framework to investigate the ecologically important case of a ground respiration source of CO2 combined with an upper-canopy assimilation sink, which is the typical state of a photosynthesising canopy during daytime. They modelled a very gentle hill, which would not a priori be expected to generate significant advective errors in any daytime eddy flux measurements, but showed that the differential advection in the lower and upper canopy would lead to significant underestimation of daytime carbon assimilation from a flux tower placed on a hill top, which is where towers are usually located.

Most of these examples involved relatively gentle hills but the presence of a recirculation zone within the canopy, which occurs even on quite gentle hills, if the canopy is deep and dense enough, has a large impact on scalar transport. This was the focus of recent LES work by Chen et al. (2019), who generalised the concept of differential advection by exploring passive and reactive scalar dispersion within canopies on gentle and steep hills, using Lagrangian particle tracking. In neutral flow conditions, two main pathways were identified for parcels of air to be transported out of the canopy volume: a "local path-way", corresponding to nearly vertical transport out of the canopy by turbulent ejection events with some lateral displacement associated with finite mean velocity, and an "advection path way", corresponding to parcels that travel horizontally from the source towards the recirculation zone on the lee side of the hill and reside at the separation point until they are transported out of the canopy by turbulence. The dominance of one pathway over the other was primarily determined by the relative time-scales for vertical transport by turbulence (dictated by $\overline{w'^2}$) and mean-wind advection and the height of scalar release.

For a wide range of hill and canopy conditions, it was shown that the local pathway is dominant for scalar releases in the upper part of the canopy whereas the advection pathway is dominant in the lower part. A major consequence of the advection pathway is that almost all source locations contribute air parcels to the total escape at the separation point, resulting in the 'chimney' effect that can be clearly seen in Figure 7. Sources near the ground will contribute more than sources in the upper canopy, but the collection of parcels from all source locations leads to a large total escape at the separation point on the lee of the hill crest. This pathway results in a probability density function of escape locations displaying a strong peak at the separation point, supporting the observations of elevated concentrations and fluxes in other models (Katul et al., 2006; Ross, 2011; Ross and Harman, 2015).

The LES results also show that vertical transport in the recirculation region is performed predominantly by turbulence, giving rise to the intermittent accumulation–ejection cycles observed in the flume experiments of Poggi and Katul (2007a) (see section 7 below). However, near the ground, where vertical velocity fluctuations are damped, mean vertical advection contributes significantly to transporting air parcels upward to levels of more intense turbulence, where they can then be readily transported out of the canopy by ejections. This vertical advection is responsible for a reduction in residence times for gases emitted in the bottom part of the canopy, as compared to flat terrain conditions, which in turn results in a larger escape fraction for reactive compounds. Thus, the increased out-of-canopy transport efficiency observed over topography in several studies (Ross, 2011) appears to be caused by the small but important effect of mean vertical advection near the ground in the vicinity of the separation point or recirculation region.

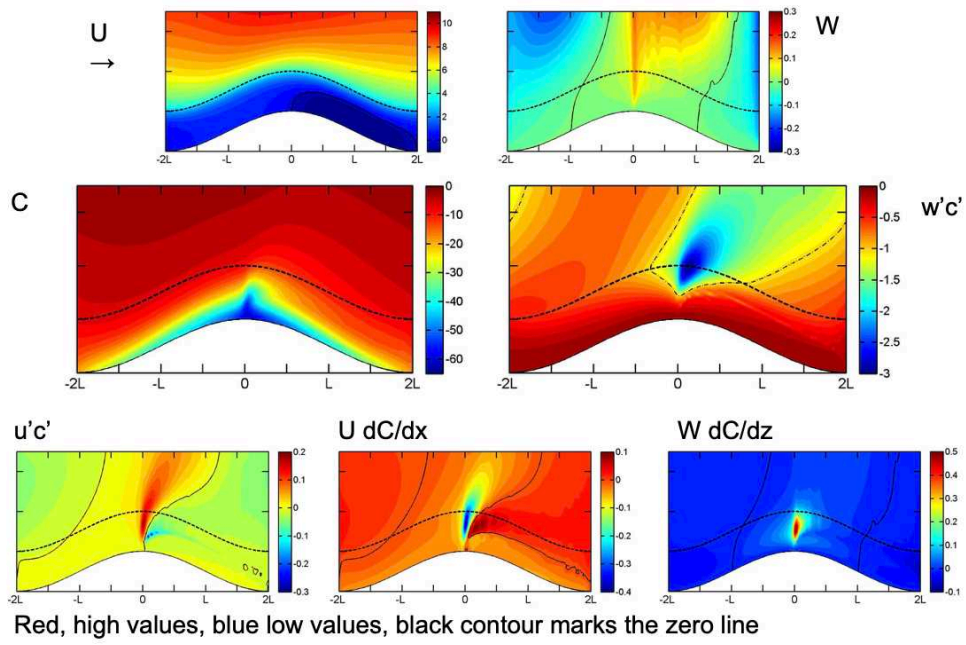

Fig. 7 Numerical calculation of scalar transport driven by the RB04 model. Cosine hill profile with H=20m, L=400m, hc=20m, Lc=30m, $u^*/U(hc)$=0.3, $S(z)$=$S0$=constant for $hc>z>0$. S_0=1. Figures from Dr I. N Harman.

It is clear that the fundamental non-linearity of scalar (as well as momentum transport) that is introduced when even a gentle hill is covered with a tall canopy opens the possibility of emergent changes to the mean transport efficiencies of scalars between biosphere and atmosphere at landscape scale. For some scalar fluxes, such as the photosynthetic

assimilation of CO_2 by vegetation or the evaporation of water, energy supply provides a global constraint on the landscape scale flux (Katul et al., 2006; Raupach and Finnigan,1997) but for other scalars, net changes in the rate of ventilation of the canopy could lead to sensible large scale changes (Ross, 2011). As a final comment it is necessary to point out that almost all these studies of scalar transport involving canopies have been carried out on 2D ridges. The magnitude of the driving velocity perturbation field is generally smaller on axisymmetric hills but recent unpublished measurements on 3D hills covered with canopies indicate much more complex flow patterns can occur in such cases according to unpublished results by Dr I. N. Harman and Dr E. G. Patton. The impact of these flow patterns on local exchange is probably significant but has not yet been quantified.

4. Gravity Driven Flows

Studies of slope flows, driven by gravity currents, have also been an important focus of complex-terrain meteorology, but have developed somewhat independently of boundary-layer hill flow studies. This disconnect has occurred in part through a separation in the dominant scales of motions but has been mainly driven by different scope and objectives. Where hill flow studies aim to understand how orographic features modulate boundary layer winds, slope flow studies ask how buoyant forcing from surface cooling or heating interacts with orography to drive slope-scale mean winds and turbulence. In practice, the resulting winds usually interact with larger scale terrain forcing causing those same near-surface temperatures and surface fluxes to evolve so that the problem is intrinsically non-linear. Nevertheless, just as hill flow studies have advanced through analysis of the simple cases of isolated 2D and 3D hills, many of the fundamental slope-flow studies have focussed on gravity flows over extensive uniform mountain slopes, over steep valley sides or over ice sheets and glaciers, treating these ‘simple’ flows as the building blocks of the more complex interactions that drive mountain wind patterns. Similarly, theory initially concentrated on idealised situations, where the flow did not affect the forcing that generated it, but as knowledge has advanced, more interactive situations are being modelled.

Modelling and prediction of the characteristic features of katabatic and anabatic slope flows dates back nearly eighty years, to the observations and theories of Prandtl (1942). However, earlier meteorology and weather reports had documented diel slope- and valley-wind patterns, mostly in the 1920s and 1930s in the European Alps (e.g., Wagner 1938), and their existence must have been known much earlier to explorers, mountaineers and

communities living in mountain regions. Slope flows occur most often with weak synoptic forcing under clear skies when virtual potential temperature differences between the surface and the adjacent air are greatest. When the sloping surface is cooler than the ambient air, for example at night as a result of radiative cooling, the downhill component of the hydrostatic pressure gradient generates downslope density currents or drainage flows whereas daytime surface heating generates upslope, or anabatic flow (Hahn 1981; Catalano and Moeng 2010).

In transitional periods during mornings and evenings, flow reversals can occur that last from a minute to an hour or more (e.g., Bader and Mckee 1983; Papadopoulos and Helmis 1999; Nadeau et al. 2012, 2018; Fernando et al. 2013; Zardi and Whiteman 2013; Jensen et al. 2017). Transitional regimes are typically characterized by quiescent winds prior to flow reversal and very weak turbulence. Over mountainous terrain, these periods can be difficult to compare or translate between sites because they can be triggered locally by topographical shading effects, propagating shadow fronts or localized insolation (Papadopoulos and Helmis 1999; Nadeau et al. 2012; Jensen et al. 2017). In general, transitional flows can exhibit a range of behaviours, driven by a variety of multi-scale mechanisms and more observational, theoretical and numerical studies will be necessary to understand these regimes better.

An excellent introduction to the basic physics of katabatic slope flows is provided by Mahrt (1982). Starting from the assumption that the flows are driven almost entirely by the surface energy balance, he was able to clarify the different assumptions implicit in earlier modelling and analysis. He used a rigorous scale analysis to classify different regions of the parameter space spanned by the downslope velocity scale, U_s, the slope length scale, L_s, the characteristic depth of the gravity current, H_s, the characteristic potential temperature deficit of the cool layer, $\Delta\overline{\theta}$, and α, the (positive) angle the slope makes with the local geopotential surface. By further restricting attention to 'nearly stationary' flows ,where inertial acceleration and advective effects roughly balanced the hydrostatic forcing and by also ignoring large scale Ekman-Gravity flows, where Coriolis effects were important (e.g., drainage flows over large ice sheets in Greenland and Antarctica; see Parish and Cassano, 2003), he was able to cover much of the parameter space corresponding to the scales we have considered in boundary layer hill flows. In this 'nearly stationary' regime, gravity currents could be roughly divided into 'Tranquil Flows', where the Froude Number based on the gravity current depth, $F_{Hs} = U_s^2 \Big/ \left[H_s \left(g\Delta\overline{\theta} \big/ \Theta_0 \right) \right]$ is small and 'Shooting Flows', where F_{Hs} is large. In 'Tranquil Flows' the thermal wind term, which is the contribution to the

hydrostatic pressure gradient caused by changes of gravity current depth or temperature deficit along the slope, is important and tends to oppose the other component of hydrostatic forcing, the vertical hydrostatic pressure gradient resolved down the slope. This trade-off tends to keep F_{Hs} low. In general, the thermal wind term can be ignored when $H_s/L_s << 1$, a condition that is satisfied in many or most of the large scale mountain- and hill -slope gravity currents that have been studied. Shooting flows in contrast are those for which $F_{Hs} >> 1$, which implies that $U_s \gg \left[H_s \left(g\Delta\overline{\theta}/\Theta_0 \right) \right]^{1/2}$. Shooting flows can be further subdivided into 'advective-gravity flow', where the buoyancy term leads to acceleration down the slope and 'equilibrium flow', where the buoyancy terms are approximately balanced by frictional effects on the ground and at the top of the gravity current. Marht (1982) goes on to derive useful idealised solutions for further subdivisions of these flow classes but to obtain models that apply to the more complex boundary conditions found in real life, more realistic representations of the flow dynamics are required.

4.1 Localized katabatic slope flows

A characteristic feature of buoyancy-driven slope flows is a jet-shaped mean velocity profile, exhibiting an elevated velocity maximum as first described by Prandtl (1942) and observed in a wide range of subsequent studies (Fig. 8). The jet shape develops as the air layer cooled by interaction with the cold surface accelerates down the slope but is decelerated by surface friction from below and the mixing of warmer air from above. Entrainment of the warmer ambient air also tends to deepen the gravity flow layer in the downslope direction (e.g., Manins and Sawford 1979b; Princevac et al. 2005; Grachev et al. 2016). Katabatic flows on open slopes tend to be extremely shallow so a current extending kilometres or more in the downwind direction will be only ~10-100-m deep with jet peaks as low as 1m (e.g., Horst and Doran, 1986; Oldroyd et al. 2014). These shallow flow depths facilitate tower-based observations, but are extremely difficult to resolve sufficiently in numerical models (Söderberg and Parmhed 2006). For example, the lowest grid cell in a typical NWP model could contain the entire katabatic layer. Gravity-driven flows over very large ice sheets, for example in Greenland and Antarctica, are stronger and deeper than those over isolated mountain slopes as they develop over long stretches of sloping terrain and hence, Coriolis forcing also becomes significant (King 1989).

Despite understanding some of the key features of slope flows and how they develop, systematically predicting their onset, the depth of the flow layer, the height of the jet peak and its strength remain a challenge. Currently, the biggest barrier to model improvement is devising better parameterizations of turbulent mixing. This is especially the case for wall models, which are critical for translating the surface forcing to the overlying atmosphere. Prandtl's (1942) slope-flow model, which assumed laminar flow and so a constant molecular kinematic viscosity, ν was initially used as an analogue for simple turbulent flow models that replaced ν with a constant eddy-diffusivity (e.g., Defant 1949). This so-called 'Prandtl model' is still used (e.g., Burkholder et al. 2011; Shapiro et al. 2012; Shapiro and Fedorovich 2014) but has also been extended using variable eddy-diffusivities to account for more complicated turbulence structure (Rao and Snodgrass 1981; Grisogono and Oerlemans 2001; Parmhed et al. 2004; Giometto et al. 2017a). Additional parameterizations can be included to model the momentum retardation effects of entrainment at the upper boundary of the cool layer and its effects on flow depth modulation (e.g., Manins and Sawford 1979b; Princevac et al. 2005, 2008).

A wide variety of other turbulence parameterizations have also been used, ranging from two-layer slab models (Manins and Sawford 1979b; Fitzjarrald 1984; Kondo and Sato 1988), through flux-gradient parameterizations based on local MOST closure schemes (Lee and Kau 1984; Ye et al. 1990; Oldroyd et al. 2014) to RANS closures of 1½ and higher order (Horst and Doran 1988; Denby 1999; Goger et al. 2018). However, most of these closures and associated empirical constants were originally derived for horizontal, homogeneous terrain and cannot, a priori, be expected to apply to wall jet slope flows, where simple surface layer scaling does not apply (Mahrt 1999; Skyllingstad 2003).

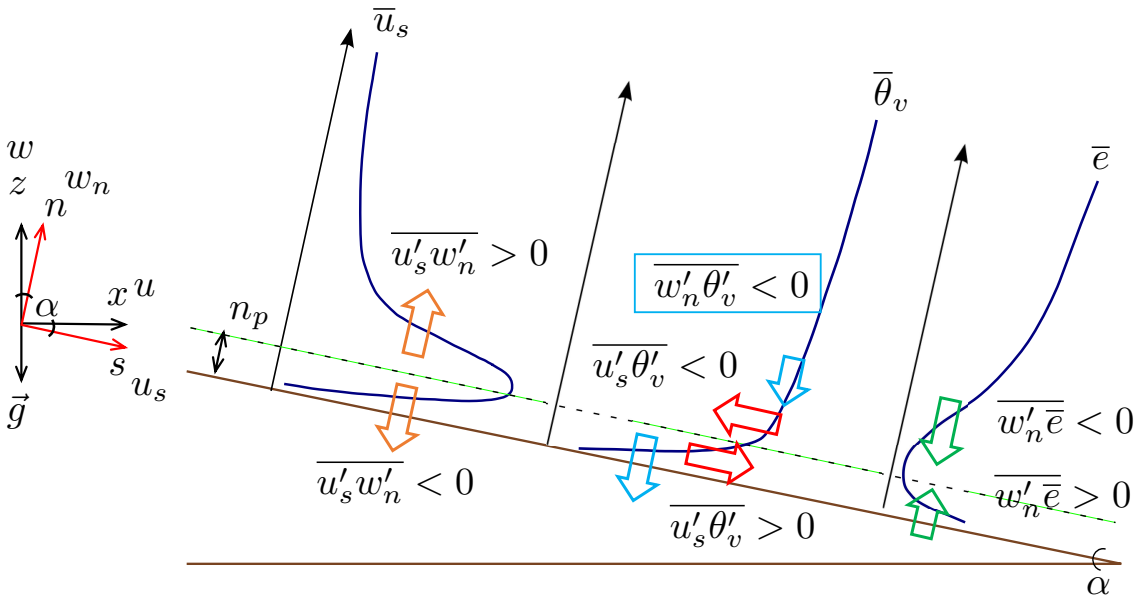

Fig. 8 Slope flow coordinate systems (black is aligned with gravitational acceleration and red is terrain following) and schematic of mean and turbulent flux quantities for katabatic flow (Horst and Doran 1988; Denby 1999; Grachev et al. 2016). The dashed line indicates the height of the katabatic jet peak, n_p, u_s *and* w_n are velocities in the downslope (s) and slope-normal (n) directions, respectively, θ_v is virtual potential temperature, and $\overline{e}$ is the mean turbulent kinetic energy (TKE) per unit mass. Block arrows indicate the relative directions of momentum fluxes (orange), buoyancy fluxes (red and blue) and slope-normal turbulent transport of TKE (green).

The earliest experimental studies of turbulence in katabatic flows had insufficient resolution to reveal the flow structure in complete detail. Despite this limitation, significant deviations from MOST turbulence theory such as large values of eddy flux divergence were observed, even below the jet peak (Horst and Doran 1986). More recent observational studies with higher vertical resolution both below and above the jet peak have confirmedsome of the earlier findings, conjectures and theories but also highlight novel features of the turbulence structure and the buoyancy driven dynamics (Nadeau et al. 2012; Oldroyd et al. 2014; Grachev et al. 2016). The following list highlights some of these key features of the turbulence structure as we now understand them:

- Significant surface-normal momentum flux divergence is characterised by negative momentum fluxes below the jet peak and positive above, crossing zero near the peak, where the streamwise velocity gradient also changes sign (Horst and Doran 1986, 1988; Denby 1999; Smeets et al. 2000; Oldroyd et al. 2014; Grachev et al. 2016). .
- Significant surface-normal divergence of the kinematic heat and buoyancy fluxes is characterised by stronger gradients from the ‘bulge’ of the jet down to the surface and a

weaker divergence above (Grachev et al. 2016). Radiative surface cooling causes surface normal heat fluxes to be negative (or close to zero) throughout the slope-flow layer.

- The slope-parallel kinematic heat and buoyancy fluxes also have a tendency to change sign near the jet peak (Horst and Doran 1988; Denby 1999; Grachev et al. 2016). This behaviour is expected when the shear and gradient production terms dominate in the rate equations for the eddy fluxes. Using a slope-aligned coordinate system with positive u_s directed down the slope (Fig. 8), the slope-parallel buoyancy fluxes are positive below the jet peak, indicating a warming flux down the slope, whereas they are negative above the peak, indicating a cooling flux down the slope (Horst and Doran 1988; Denby 1999; Grachev et al. 2016). The physical implications of this sign change are summarized in the next point.
- Buoyant production or suppression of TKE by the vertical buoyancy flux, $g/\Theta_0 \, \overline{w'\theta_v'}$, which on horizontal ground affects only $\overline{w'^2}$ the vertical component of velocity variance, affects both streamwise $\overline{u_s'^2}$ and surface normal $\overline{w_n'^2}$ components when the variance equations are rotated into the slope-aligned coordinate frame of Figure 8. Hence, the net vertical buoyancy term in the TKE equation contains contributions from the slope-normal buoyancy fluxes, which are negative and act to suppress TKE, and the slope-parallel buoyancy fluxes, which can be either negative or positive. As a result, the net vertical buoyancy flux can produce TKE when, $\overline{u_s'\theta'} \big/ \overline{w_n'\theta'} > \cot\alpha$ leading Horst and Doran (1988) and Denby (1999) to estimate that buoyant TKE production will occur over slopes with angles greater than 30° and 25°, respectively. Those estimates assume an approximately constant ratio of slope-parallel to slope-normal buoyancy fluxes, however, Oldroyd et al. (2016) show that the buoyancy flux ratio can be highly variable and that buoyant TKE production may occur over much shallower slopes. This has important implications for how various stability parameters can be used for turbulence modelling, as well as for how they should be used (i.e., in the surface-normal versus vertical coordinate frame) and interpreted (i.e., as a representation of stability versus as a scaling parameter) (Oldroyd et al. 2016).
- Profiles of mean TKE exhibit a local minimum near the jet peak, where shear production and the slope-parallel buoyancy flux approach zero (Fig. 8) (Horst and Doran 1986; Denby 1999; Grachev et al. 2016). The sign changes in momentum and slope-parallel

buoyancy fluxes may indicate turbulence decoupling from the surface near the jet peak (Horst and Doran 1988; Denby 1999; Grachev et al. 2016). Hence, turbulent transport acts to transfer TKE into the bulge of the jet both from below and above, serving as an important turbulence coupling mechanism maintaining non-zero TKE at the peak (Arritt and Pielke 1986; Smeets et al. 2000; Söderberg and Parmhed 2006; Giometto et al. 2017b). This is analogous to the situation in the lower part of a plant canopy flow, where shear production is small and TKE is maintained by transport from the region of strong shear production at canopy top (Finnigan, 2000). The critical inference is that, if both TKE and eddy fluxes near the jet peak are maintained by third moment transport terms, local eddy diffusivity-type closures are bound to fail there.

- In contrast to the shear production term for TKE, the gradient of mean virtual potential temperature and the slope-normal temperature flux are both large at the jet peak so the dominant gradient production term in the rate equation for the variance of virtual potential temperature, $\overline{\theta_v'^2}$, remains large and profiles of $\overline{\theta_v'^2}$ exhibit a local maximum near the jet peak (Denby 1999; Grachev et al. 2016). Compared to TKE, $\overline{\theta_v'^2}$ and its relation to turbulent potential energy (Zilitinkevich et al. 2009; Łobocki 2017) has received much less attention with the exception of variance similarity scaling efforts as discussed next.

4.2 Similarity scaling for katabatic flows

Clearly, the turbulence structure of slope flows does not conform to traditional horizontally homogeneous surface-layer behaviour. This poses several modelling challenges. Most critical, is that traditional MOST (Monin and Obukhov 1954; Obukhov 1971), which is used in nearly all NWP models in some form (Foken 2006), and the associated empirical parameterizations developed over idealized terrain (e.g., Businger et al. 1971; Dyer 1974) break down. As an alternative to MOST, local similarity scaling (Nieuwstadt 1984a, b) has been applied to slope flows but with mixed results for turbulent momentum fluxes and variances and very poor results for heat fluxes, especially at higher stabilities (Forrer and Rotach 1997; Smeets et al. 2000; Heinemann 2004; Nadeau et al. 2013; Stiperski and Calaf 2017; Sfyri et al. 2018; Stiperski et al. 2019). These mixed results with local scaling have prompted the use of other characteristic length scales, such as the height of the jet peak (van der Avoird and Duynkerke 1999; Smeets et al. 2000; Söderberg and Parmhed 2006) or local

1386 z-less (or n-less) scaling, which been shown to work relatively well for dimensionless
1387 velocity gradients $\left(\kappa z/u*\right)\partial U/\partial z$ (or equivalently $\left(\kappa n/u*\right)\partial U_s/\partial n$) above the jet peak,
1388 where turbulence is somewhat decoupled from the surface (Forrer and Rotach 1997; Grachev
1389 et al. 2016). However, a major challenge when using the height of the jet peak (or z-less
1390 scaling for regions above the peak) as the characteristic length scale is that this height is
1391 unknown a priori and can vary with time, stability, jet strength and distance along the slope.
1392 Summarising, while local similarity scaling has had mixed success, nearly all attempts
1393 at applying horizontal-terrain scaling parameterizations for the heat fluxes underestimate the
1394 turbulent mixing of the dimensionless temperature gradient $\left(\kappa z/\theta*\right)\partial\overline{\theta}/\partial z$ that occurs with
1395 relatively high stability ranges (typically $n/\Lambda > 1$, where Λ is the local, surface-normal
1396 Obukhov length). Furthermore, there is some evidence that turbulent mixing associated with
1397 the heat fluxes can, in some cases, actually increase with stability (Forrer and Rotach 1997;
1398 Smeets et al. 2000), which is most probably due to an accompanying increase in the slope-
1399 parallel buoyancy fluxes and subsequent reduction of buoyant TKE suppression or even TKE
1400 production, as discussed above; however, this has not yet been rigorously established from
1401 observational studies. Consequently, 'universally' appropriate turbulence length scales and
1402 velocity scales for katabatic flow are still being actively debated. Finally, a scaling
1403 framework for other scalars such as water vapour or CO_2 in katabatic flows has rarely been
1404 studied over bare or sparsely vegetated slopes (Forrer and Rotach 1997; Nadeau et al. 2013).
1405 Hence there is a set of critical open questions for katabatic flows, whose answers could have
1406 significant positive impact impacts on our modelling capabilities for complex topography
1407 flow in general.
1408
1409 **4.3 LES modelling of gravity flows**
1410 We discussed the development of turbulence closure parameterisations suitable for RANS
1411 modelling approaches in Section 4.1. However, just as in the case of hill flows (Section 2.3) ,
1412 in recent years LES has been applied to slope flows to try to resolve some of the difficulties
1413 listed above. We have already referenced (Section 2.3) the early efforts of Schumann (1990),
1414 Walko et al. (1992) and Dörnbrack and Schumann (1993), who addressed different aspects of
1415 buoyancy driven flow on slopes. Of more general application is the finding of Burkholder et
1416 al. (2011), who determined that, although their simulated mean fields were insensitive to the
1417 choice of sub-filter-scale model, the model choice did substantially impact the simulated
1418 second-order moments, especially the buoyancy fluxes and vertical velocity variances.

Skyllingstad (2003) used LES to demonstrate the role turbulence plays in controlling the strength and depth of katabatic flows while Smith and Skyllingstad (2005) studied the influence of multi-angle slopes on katabatic flows. They found that on a steep upper slope followed by a gentler lower slope, a rapid acceleration was generated on the upper slope followed by a transition to a slower evolving structure characterized by an elevated jet over the lower slope. In contrast, a case with uniform slope having the same total height change yielded a more uniform slope flow profile with stronger winds at the slope bottom. As well as these two modelling efforts, Axelsen and van Dop (2009a, b) simulated katabatic flows observed on glaciers while Grisogono and Axelsen (2012) compared their LES with the classic Prandtl modelling approach and ranked the reasons for the departures between them. All these models relied on MOST-based wall models, and so needed high vertical resolution below the jet peak to reduce the relative dependence on the MOST scaling assumptions. Over rough surfaces, this can generate problems with prescribing a 'surface-layer' model within the roughness sublayer (Basu and Lacser 2017).

Although generally limited to low Reynolds numbers, direct numerical simulations have also been performed (Shapiro and Fedorovich 2014; Umphrey et al. 2017). These tend to overpredict jet strength and under-predict the height of the jet peak. However, a recent set of DNS data at very high Grashof Number has delivered detailed information on both katabatic and anabatic flows of real relevance (Giometto et al. 2017b). That said, better understanding of the turbulence structure in katabatic flows and how best to model it remain critical open questions and we expect LES and even DNS to play an increasingly important role in answering them.

4.4 Gravity-driven flows in Plant Canopies

As emphasised in Sections 2 and 3, measurement of carbon exchange from flux towers has been a major driver of boundary layer hill flow research for the last two decades and the study of katabatic flows in canopies on relatively gentle complex terrain has been a necessary component of this. These flows tend to decouple fluxes of CO2 from the soil surface at night from the eddy flux measured on towers above the canopy and can lead to significant errors in 24 hour carbon budgets (Goulden et al. 2006; van Gorsel et al, 2011). Steeper canopy-covered slopes are also widespread in mountainous areas and have been studied as components of larger complex terrain field campaigns (e.g. van Gorsel et al., 2003). Unlike katabatic flows on open slopes, where the depth of the flow is set by a delicate balance

between cooling from the ground and the entrainment of warmer air from above, tall closed canopies like forests that are radiatively cooling at night develop very stable buoyancy profiles in the crown space that quench and decouple the canopy turbulence from the boundary layer above (see Figure 6 and the accompanying discussion in Section 3.2 *et seq.*).

Modelling of these flows has proceeded along several fronts. Watanabe (1994) calibrated one- and two-layer slab models of radiative and convective heat and momentum transfer in a canopy against a multi-layer model and then applied it to drainage flow but the vertical integration necessary to define his slabs precluded a detailed treatment of some of the important physics. Hatcher et al., (2000) studied a physical model of a turbulent gravity current through a canopy of obstacles in a flume, producing similarity solutions that can be used to describe the initiation of the slope flow in the atmospheric case. Here we will discuss the more directly relevant analysis of Belcher et al. (2008), who extended the FB04 canopy-on-hill model by adding a hydrostatic pressure gradient term, $g\bar{\theta}/\Theta \sin\alpha$ to the streamwise momentum equation. Because their canopy was assumed to be of constant height h_c and this was also assumed to be the top of the gravity current, $H_s = h_c$, the depth of the cool layer is constant so the thermal wind term was ignored. In their analysis Belcher et al. (2008) also equated the gravity current lengthscale *Ls* with the hill length scale *L*.

In forests, the time scale for the night-time radiative cooling of the canopy air layers is typically about four hours (Watanabe 1994). Within the canopy, the characteristic timescales of turbulent mixing h_c/u^*, and advection, $L/U(h_c)$, are much shorter, and so the flow caused by the cooling can be treated as if it is steady over time scales short compared with the radiative cooling time. As shown in Figure 6, the cooling leads to high Richardson numbers, and collapse of the turbulent mixing within the canopy and between the canopy and overlying boundary layer. Hence the canopy flow can be estimated by considering only the pressure forces acting on the canopy airspace. For dense canopies radiative losses occur predominantly from the top of the foliage, while the soil remains warmer, resulting in an unstable temperature profile between soil surface and crown (Kaimal and Finnigan 1994: Chapter 3). The air in the trunk space is convectively mixed, therefore, but entrainment of cooler air from above causes this mixed region to cool progressively. As a result, while the lower canopy may be locally unstably stratified, it is cooler than air at the same geopotential height outside the canopy and so subject to downslope buoyancy forces. on both sides of the hill crest.

As we saw in Section 2, neutral flow over a hill covered with a forest canopy generates a hydrodynamic pressure gradient, which also drives flow within the canopy. For small positive stability, the hydrodynamic pressure gradient changes little from that found for neutral flow over a hill and so within the canopy it drives flow perturbations towards the hill top on both sides of the crest. Hence, the hydrodynamic pressure gradient opposes the hydrostatic pressure gradient. Under these conditions the air within the canopy flows up the hill slopes toward the crest if the hydrodynamic pressure dominates, but flows down the slopes away from the crest if the hydrostatic pressure gradient dominates. The competition between these two processes, and the onset of drainage flows within the canopy, is measured by constructing their ratio.

The hydrodynamic pressure gradient generated by the flow over the hill can be estimated to be $d\Delta p/dx \approx U_0^2 H/L^2$ (Belcher et al., 2012) whereas the hydrostatic pressure gradient is estimated as $\left(g\Delta\overline{\theta}/\Theta_0\right)\sin\alpha \approx \left(g\Delta\overline{\theta}/\Theta_0\right)H/L$ so their ratio can be written as $R_p = \dfrac{U_0^2\,\Theta_0}{g\,L\,\Delta\overline{\theta}} \approx F_L^2$ which is effectively the square of the Froude Number F_L.

The big surprise here is that, while the slope of the hill *H/L* enters the estimate of both the hydrostatic and hydrodynamic pressure gradients, it cancels from their ratio. The outcome of the competition between the tendency for the hydrodynamic pressure gradient to force flow up the slopes against the tendency for the hydrostatic pressure gradient to force flow down the slopes is determined by the characteristic wind speed in the HLR88 outer layer U_0, the average temperature deficit of the air within the canopy, $\Delta\bar{\theta}$, and the length of the slope, *L*. Drainage flows occur when R_p drops below a threshold, which we expect to be about 1. For more stable conditions, the magnitude and form of the hydrodynamic pressure gradient also changes. The progressive impact of this on the velocity field that develops over a hill has been extensively studied in the context of mountain flows (Queney 1948; Scorer 1949; Kaimal and Finnigan 1994, Ch. 5).

Figure. 9 shows the variation of the hydrodynamic and hydrostatic pressure gradients in flow over 2D sinusoidal ridges and valleys, for a range of Froude Numbers, F_L. At neutral stability $\left(F_L \sim \infty\right)$ the hydrodynamic pressure gradient is antisymmetric about the hill, driving upslope flow within the canopy on both sides of the crest. As the stratification increases, F_L decreases and the hydrodynamic pressure forcing becomes smaller, while the hydrostatic pressure forcing increases so that by F_L=1.2, they almost cancel. For, F_L close to but just above 1 (Fig. 9c) the critical value of R_p has been exceeded and the net pressure gradient forces drainage currents down both the slopes. The hydrodynamic pressure becomes symmetric about the crest at $F_L \approx 1$ (Fig. 9d). As the Froude number reduces further, the flow above the canopy is stable enough to support gravity waves. The resulting hydrodynamic pressure gradient now augments the hydrostatic forcing and tends to increase the strength of the drainage flows (Fig. 9e).

The effect of these opposing pressure gradient forces on the flow within and just above the canopy is illustrated in Figure 10. For near neutral flow $\left(F_L \geq 1.5\right)$ we see convergence of the flow perturbations to the hill top within the canopy while above the canopy the maximum stream-wise perturbation is just above the crest as seen in Figures 3 and 4 of Section 3. As the influence of stability starts to make itself felt, the hydrostatic pressure gradient dominates near the crest and the convergence at the crest splits and moves up and downwind $\left(1 \leq F_L \leq 1.5\right)$ until by $F_L = 1$, the gravity current dominates

within the canopy and the flow perturbations above are starting to weaken. When the hydrodynamic pressure gradient flips around $\left(0.66 \le F_L \le 1\right)$, the two pressure gradient forcings are in the same direction over part of the hill, and we see that the perturbation above the canopy is in the same direction as within. For even stronger stabilities $\left(F_L \le 0.66\right)$ the gravity current is dominant within and above the canopy but we should be cautious about pushing the fundamentally linear FB04 analysis to Froude numbers any smaller than this.

The small timescale of turbulent adjustment compared to that of radiative cooling has permitted us to describe the evolution of the gravity current in the canopy as a sequence of steady states, however, in nature, other effects can confound this simple picture. For example, once the within-canopy flow near the crest starts to diverge $\left(\text{Fig. 10; } 1 \le F_L \le 1.5\right)$, conservation of mass demands that warmer air must be entrained into the canopy at the hill top, reducing the temperature deficit of the canopy airspace, $\Delta\bar{\theta}$ and so decreasing the hydrostatic pressure gradient. Anecdotally it is often observed that forest gravity currents accelerate after initiation but then weaken. Sometimes this effect can lead to oscillations throughout the night. As a final comment, it is also regularly observed that the gravity current can propagate upwind on level ground for many hill lengths as long as the within-canopy Richardson Number is large and turbulent entrainment of warmer air into the current is small. This phenomenon was observed in the wind tunnel simulation of Finnigan and Hughes (2008) (see Section 7 below) and has been noted at a flux tower site in the Amazon (Prof. Y. Malhi. *pers. comm*.).

1559

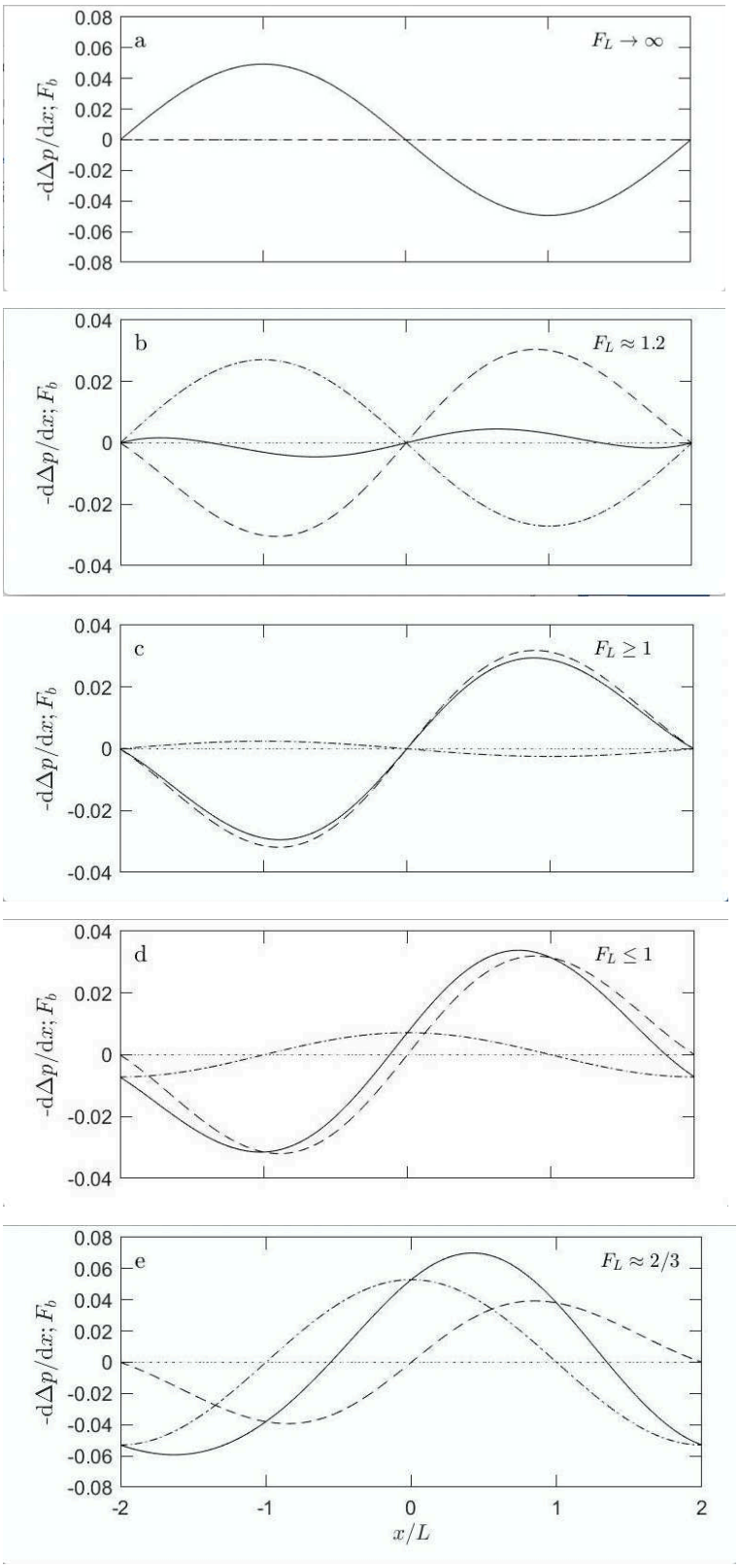

1560

1561

1562

1563

1564

Fig. 9 Hydrodynamic $-d\Delta p/dx$ and hydrostatic Fb pressure gradients within a canopy on a sinusoidal 2D ridge as the stability of the boundary layer varies. (a) $F_L \sim \infty$, (b) $F_L = 1.2$, (c) $F_L \geq 1.0$, (d) $F_L \leq 1.0$, (e) $F_L \approx 2/3$ The dashed line is the hydrostatic pressure gradient, Fb, the dash dotted line (-) the hydrodynamic gradient, $-d\Delta p/dx$ and the solid line shows the net forcing. Indicative pressure gradients in units of Pa/m for a hill of the scale shown in Figures 3 and 4 are given on the y axis.

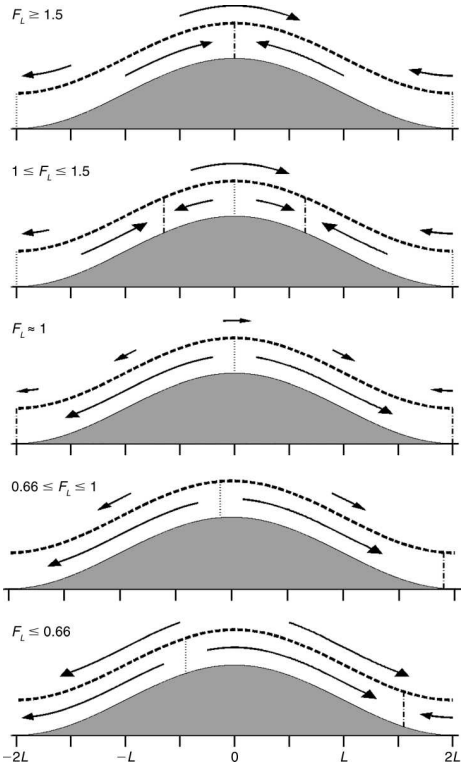

Fig. 10 Schematic showing forces on flow deep within and just above the canopy on a sinusoidal ridge from Figure 9. For a range of boundary layer stabilities as quantified by the Froude Number F_L. Above the canopy top (dashed line) arrows indicate the hydrodynamic pressure gradient only. Within the canopy (below the dashed line) arrows indicate the balance between the hydrodynamic and hydrostatic pressure gradients. Arrow lengths indicate the magnitude of the forcings. Dotted lines indicate regions of divergence within the canopy (and descent at canopy top). Dash-dotted line indicate regions of convergence in the canopy and ascent at canopy top.

4.5 Gravity driven flows in a wider context

In mountainous regions, buoyancy-driven valley and slope flows (Whiteman, 1990; Schmidli and Rotunno, 2010) often interact and significantly impact one another (Manins and Sawford 1979a; Mahrt and Larsen 1982; Fitzjarrald 1984; Arritt and Pielke 1986; Horst and Doran 1988; Doran et al. 1990; Mahrt and Larsen 1990; Doran 1991; Amanatidis et al. 1992; Smeets et al. 1998; Mahrt et al. 2001; Lehner et al. 2015; Mahrt et al. 2018). Valley flows and ambient winds can deflect slope flows from their natural fall lines, inducing directional shear (Manins and Sawford 1979a; Kottmeier 1986; Horst and Doran 1988) or can be strong enough to smear or overtake the slope-scale flow entirely (Mahrt and Larsen 1990; Litt et al. 2015). Down valley flows tend to limit the depth of the slope side wall inversions (Doran et al. 1990) and generate a 'skin-flow', or shallower, sheltered drainage flow, as opposed to a deeper, 'pure' katabatic flow (Manins 1992; Mahrt et al. 2001).

Katabatic flows can also contribute to the development of cold pools, in which cold air stagnates in basins and valleys (Gryning et al. 1985; Mahrt et al. 2010; Burns and Chemel 2014; Geiss and Mahrt 2015; Foster et al. 2017). Subsequently in the presence of a cold pool, katabatic flows can 'peel off', or intrude, into the cold pool (Mahrt et al. 2010; Whiteman et al. 2010; Haiden et al. 2010; Soler et al. 2014), generating waves (Burns and Chemel 2014, 2015) and instigating sloshing (Lehner et al. 2015) or seiches (Lareau and Horel 2015). Additionally, when approaching cold pools or adjacent horizontal surfaces (plains or oceans), a katabatic jump (analogous to a hydraulic jump) may develop, generating turbulence and strong vertical motions (Gallée and Schayes 1992; Yu et al. 2005; Yu and Cai 2006, Mayr et al. 2007. Interactions between slope and valley flows can generate significant vertical transport, cross-valley circulations (Hennemuth 1986; Kuwagata and Kimura 1997; Weigel et al. 2007; Choukulkar et al. 2012; Arduini et al. 2016) and meso-scale heat transport (Noppel and Fiedler 2002). Turbulent fluxes in valleys have been shown to scale better with the local slope-scale variables than with larger scale terrain features (Rotach et al. 2008), while the katabatic flows generated on sloping valley walls can extend a considerable distance into the horizontal terrain below, akin to an internal boundary layer (Mahrt et al. 2018). In extreme cases hydrodynamic and hydrostatic forcing can combine to produce dangerous phenomena like rotors and extreme downslope winds (Sheridan et al. 2004; Mobbs et al.

2005; Grubisic et al. 2008) and we can also observe hydrodynamically driven flows over hill tops and ridges effectively decoupled from the valley flows on either side (Lewis et al. 2008b)

At first site, understanding the interaction between the complex flows generated as synoptic winds encounter extensive steep topography and the multiplicity of valley-scale and slope-scale flows generated by solar heating and cooling seems an intractable problem. Almost all the theory and models we have surveyed so far address flows over simple idealised topographies but in nature hydrodynamic forcing and heterogeneous heating and cooling can generate multiple flows evolving at multiple scales and the number of possible combinations grows geometrically (Soler et al. 2002; Trachte et al. 2010; Martínez et al. 2010; Serafin et al. 2016). However, surprisingly, recent syntheses of field experiments are beginning to reveal useful simplifications and paths forward; see for example Rotach and Zardi (2007). We shall return to consider this paradox in the Discussion Section 7.

5. Field Experiments

5.1 Boundary Layer Hill Flows

Now we want to discuss in some detail the largest hill flow field campaign of the 1980s, Askervein in Scotland, and contrast it with the most recent, Perdigao in Portugal to provide a reference frame for the many other experiments, which have underpinned the theoretical developments that we have concentrated on so far. Many of the early theories and models from the 1970s and 1980s, discussed in Sections 2.1 and 2.2, were linked to field experiments on conveniently located hills of relatively simple geometry, for example Brent Knoll (Mason and Sykes, 1979), Black Mountain (Bradley, 1980), Ailsa Craig (Jenkins et al., 1981), Kettles Hill (Taylor et al.,1983; Salmon et al. 1988), Bungendore ridge (Bradley, 1983), and Nyland Hill (Mason, 1986). Indeed, Bradley's laboratory in Canberra Australia was literally at the foot of Black Mountain. Although some of the earlier experiments only measured windspeeds on an upwind and a hilltop mast, others added more measurement stations to track the flow development over the hill. Nevertheless there was an emphasis on measuring the speed up, ΔU as the touchstone for modelling success (Section 2.1). As new theory developed, however, the

search for field sites to test it unequivocally became more urgent as was the realisation that a field campaign able to deploy sufficient sensors to gather the information theory now demanded was probably beyond the capabilities of a single laboratory.

In the early 1980s, therefore, the search for an 'ideal' 2D ridge with uniform surface cover, where the predictions of theory would not be confounded by other influences like roughness changes or complex approach flows, sent two research teams to the Outer Hebrides of Scotland. The 1982 and 1983 Askervein campaigns (Taylor and Teunissen, 1985, 1987) on South Uist were a combined effort between researchers from the Atmospheric Environment Service, Canada, the Risø National Laboratory, Denmark, the University of Hannover, Germany, the University of Canterbury, New Zealand and both the Building Research Establishment, and ERA Technology Ltd. in the United Kingdom. It had been initiated at an International Energy Agency meeting with a view to supporting research related to wind farm siting. At the same time, in 1982 the UKMO mounted a campaign on another isolated hill, Blashaval on North Uist (Mason and King, 1985). In their review of field experiments up to that time Taylor et al. (1987) classified hills in terms of two parameters H/L and L/z_0. Most experiments up to that time had been on isolated hills or ridges of moderate slope and smooth profile, ($H/L < 0.7$) and, except for Black Mountain, which was forested, on hills with grass or scrub surfaces so that $L/z_0 \geq \sim 10^4$. The focus was on moderate to strong winds, near neutral stratification and overall terrain length scales, $4L \sim 1$ km. The prevailing westerly winds and uniform sheep-cropped turf on North and South Uist certainly conformed to those conditions.

The Askervein experiments generated by far the largest data set of the 1980's projects and the results were made widely available, being distributed as scanned copies of the Atmospheric Environment Service reports (available at https://www.yorku.ca/pat/research/Askervein/index.html). The data set has been used by many modellers as a test case-see for example Chow and Street (2009) who list seven other papers using Askervein-and it is one of the data sets still recommended for use in the wind energy community-https://windbench.net/askervein.

Askervein Hill (Fig. 11a) can be considered as a segment of a 2D ridge of total length 2km, oriented NW-SE and with width (4L) about 1 km. There is a good, relatively uniform, flat fetch to the SW beyond which lies the Atlantic Ocean, about 3 km to the

West. There are other hills to the East of Askervein but the predominant winds were from the West. As can be seen in the figure, there are no trees on the hill and the roughness length was relatively low, estimated as z_0=0.03m from reference mast profiles. The surface on the hill itself appeared similar to the reference site apart from a few mobile roughness elements (sheep) and it came as a great surprise when near-surface wind profiles at the hilltop appeared to have z_0 = 0.001m (Mickle et al, 1988). Walmsley and Taylor (1996) argued that this could be increased to 0.005m if cup anemometer over-speeding was accounted for while Niels-Otto Jensen of the Danish Riso laboratory, who spent a lot of time at the hilltop, estimated that the hilltop area surface would have z_0 = 0.01m. Based on an analysis in streamline coordinates, Finnigan has calculated that the anomalously small roughness length could result from ignoring the stabilising effect of the convex streamline curvature at the hill crest, the so-called 'curvature Richardson Number' effect (Bradshaw, 1969; Finnigan, 1988, Finnigan et al. 1990). Nevertheless, it remains something of a puzzle.

a

b

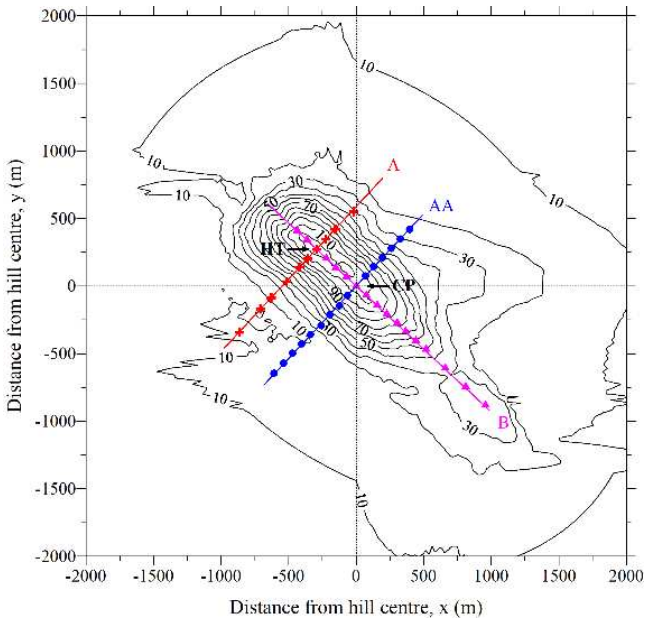

Fig. 11 *Askervein. (a) Photo, by Hans Teunissen, taken from the 50m reference mast. (b) topographic contours (m) and mast positions*

The Askervein experiment deployed a far more extensive sampling network than anything attempted to that time. This comprised 10m wind speeds along two lines (A, AA) of 10m masts (50 in total) across and one line (B) along the hill ridge (Fig. 11b). There were also 50m masts on the hilltop (HT) near the NW end of the ridge and at an "upwind" reference location about 3 km SSW of the hilltop, a 30m mast W of the hilltop and a 16m mast at a second ridge top location (CP) at the "centre point" of the ridge. Some 10m masts and the 16m CP mast had Gill UVW anemometers while others were making measurements with cup anemometers. The 50 m masts had sonic anemometers, Gill UVW anemometers and cup anemometers and in addition TALA kites were flown and line tensions measured to determine wind speeds to greater heights, including profiles up to 500m with multiple kites near the reference tower. Some radiosondes were released and confirmed near-neutral stratification. Wind directions were measured continuously with several systems. Mean wind speed profiles at the hilltop and reference sites provide speed-up information for different wind directions while data from the 10-m tower lines provide information on relative wind speeds at different positions on the hill, again for different background wind directions.

In the 1983 experiment, an extensive set of Mean Flow data was collected with wind speeds in the 5-15 ms^{-1} range. These were used to guide model development and showed that the earlier linearized RANS modelling approach of Beljaars et al. (1987) could be extended to a deeper and non-linear planetary boundary layer approach, which could better deal with flow reductions in the lee of the hill and better match hilltop profiles. (Weng and Taylor, 2011) as shown in Figure 12.

Turbulence measurements at Askervein were less extensive but still important. Two of the participating groups installed sonic anemometers, three groups used Gill UVW anemometers, one had gust anemometers and the standard deviations from cup anemometers were also used. The most reliable sonic anemometer data (Taylor and Teunissen,1985, Fig 4.5) showed reductions in hilltop profiles of $\overline{u'^2}$, $\overline{w'^2}$, and $-\overline{u'w'}$ relative to upwind values and an increase in $\overline{v'^2}$ in a middle layer (20m > z > 5m), in accord with Rapid Distortion Theory (Hunt and Carruthers, 1990). The $\overline{u'^2}$ reductions were also evident in the cup anemometer wind speed variance data. Mason and King (1985) and Mason (1986) had also found evidence of Rapid Distortion impacts in hill top turbulence profiles at Blashaval and Nyland Hill (Section 2).

a

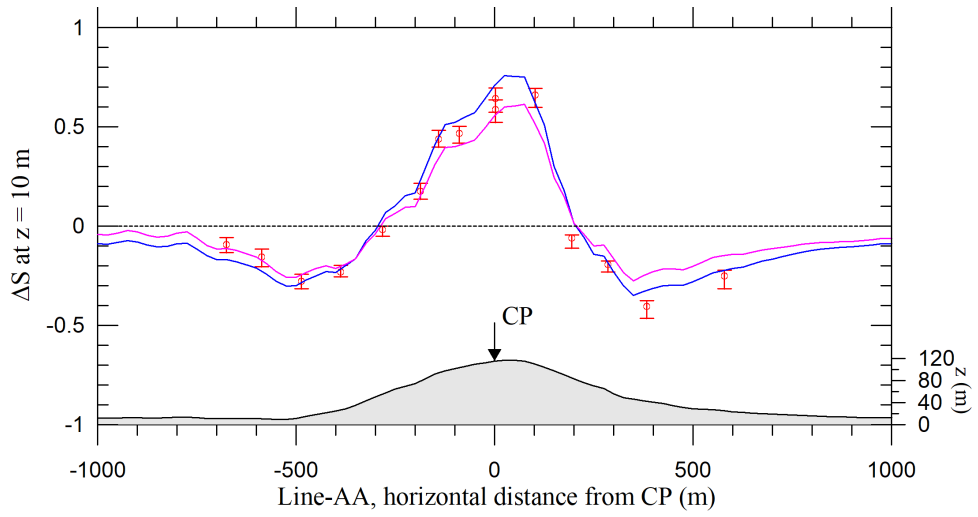

b

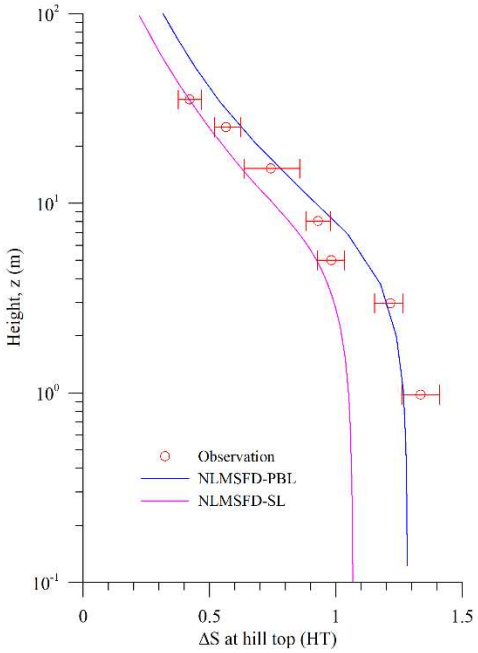

Fig. 12 Comparisons between model calculations (Weng and Taylor, 2011) and Askervein 1983 field data (Taylor and Teunissen, 1985) (a) 10m mean windspeeds along transect AA. (b) hilltop speed up profiles.

Since the Taylor et al (1987) review there have been other reviews and several notable field program reports on flow over topographic features. Coppin et al (1994) analyzed 1984/1985 measurements over Cooper's Ridge, a grass covered feature by the side of the Wollondilly river in New South Wales, Australia. The emphasis was on the effects of stratification. A previously unencountered source of anomalous data from Coopers Ridge proved to be the result of the mobile roughness elements on that hill (cows) finding that the sensor power cables provided a tasty alternative to chewing grass. Vosper and Mobbs (1997) directly measured the pressure drag on a large hill in NW England-as we noted in Section 2. topographic drag was an issue of major concern to the NWP community and there were few if any field data available up to that time with which to compare theory. The same scientific team based at Leeds University went on to perform a multi-season measurement campaign over Tighvein, a large $\left(H \approx 500m, L \approx 2000m\right)$ hill in the SW corner of the Isle of Arran, which is 22 km off the SW coast of the Scottish mainland (Vosper et al. 2002) As well as surface pressure they made detailed mean windspeed and turbulence measurements at multiple locations over the hill . As we would expect from

1756 the scaling criteria discussed in Section 1., Tighvein was subject to buoyancy influences
1757 and they found that at times when $F_L \geq 0.25$ there was a pressure minimum over the hill
1758 top, which was also the position of maximum near-surface speed-up, while for $F_L \leq 0.25$
1759 the pressure field is more asymmetric and the lee-slope flow is generally stronger than on
1760 the windward slope.
1761 A more complex terrain configuration but at much smaller scale was described by
1762 Berg et al. (2011) in their Bolund hill study. This low (H=12m) coastal hill involves a
1763 steep cliff and a transition from water (Roskilde fjord) to grass covered land and so added
1764 a roughness change and an abrupt upwind step to complicate modelling or interpretation
1765 but the relatively small scale of Bolund hill had advantages in characterizing the flow in
1766 detail. Sonic anemometers, plus some cup anemometers and thermometers were used to
1767 measure winds and turbulence at levels up to 9m on eight masts on the hill, with two
1768 other masts providing reference profiles. A companion paper (Bechmann et al, 2011)
1769 reports on an extensive modelling inter-comparison exercise (Section 2.3).
1770 An equally complex site on a larger scale than Bolund was studied by Grant et al.
1771 (2015). They made measurements over a partially forested hill on the NE coast of the isle
1772 of Arran. The hill height varied from 160m to 260m asl. over its 1.5km length and both
1773 its NE slope, which falls to the sea, and its SW slope are steep enough to ensure
1774 downwind separation. Measurements were made using sonic and cup anemometers on
1775 three 23m masts, one upwind of the SW slope and two on the crest. In addition 12
1776 automatic weather stations were deployed on SW-NE transects and recorded data at 2m
1777 height. As might be expected at such a complex site with patchy forest clearings and an
1778 abrupt roughness change from sea to forest cover in North Easterly airflows, the wind
1779 and turbulence field is complex with strong directional shear between the masts. The data
1780 were modelled by Grant et al. (2016) using a 1.5 order closure RANS model and quite
1781 satisfactory agreement was obtained under neutral conditions as long as the horizontal
1782 variability in canopy structure was explicitly represented. Data to allow such structural
1783 detail to be incorporated in the model are now readily obtained from airborne lidar
1784 measurements.
1785 On a larger scale than Askervein, both physically and in terms of the number of
1786 scientists involved, the Perdigão - 2017 field campaign in Portugal (Fig. 12) represents a

major step forward in characterising a complex large scale flow field. Fernando et al (2019) provide the background and some initial results while a series of papers have and continue to appear in EGU journals. A preliminary study, Perdigão – 2015 had used the site to develop scanning multiple lidar methodologies (Vasiljević et al, 2017). The UCAR and University of Porto web sites https://www.eol.ucar.edu/field_projects/perdigao, https://perdigao.fe.up.pt/ have multiple links, including public access to the data and a promotional video. There is also access to slide presentations from Perdigão workshops showing the latest progress with processing and interpreting the data.

The Perdigão project covers two parallel ridges, orientated approximately NW-SE with a broad valley between (Fig. 13). The scale is comparable to Askervein ($L \sim 250$ m, $H \sim 150$m) but one big difference is in the land cover, which is mostly forest with trees of mean height 10 m. There is also a large wind turbine, the focus of some wake studies. The surrounding terrain is complex, and thermal and larger scale topographic effects are very present and have a major impact. Fernando et al (2019, Figure 4) shows that while the dominant winds 60m above the ridge top are from W to SW or NE directions, i.e approximately normal to the ridge, winds in the valley are generally from the NW or SE or calm ($< 1 ms^{-1}$). There is a slight SE to NW gradient along the valley contributing to these low velocity valley winds, downslope at night and upslope during the afternoons. While the details may be site-specific the valley wind effect is a common feature in moderately complex terrain (see Section 4.) and Perdigão will provide an important data set for testing models that can resolve and accurately predict this feature. Palma et al (2019) demonstrate this possibility with models that nest from global (GFS) through mesoscale (WRF) to the micro-scale (VENTOS©/M) and successfully reproduce local flow behaviour at Perdigão over a 24-hour period.

(a)

(b) Photo by Mr. Nuno Soares, Smart Box, Comunicação Audiovisual, Portugal

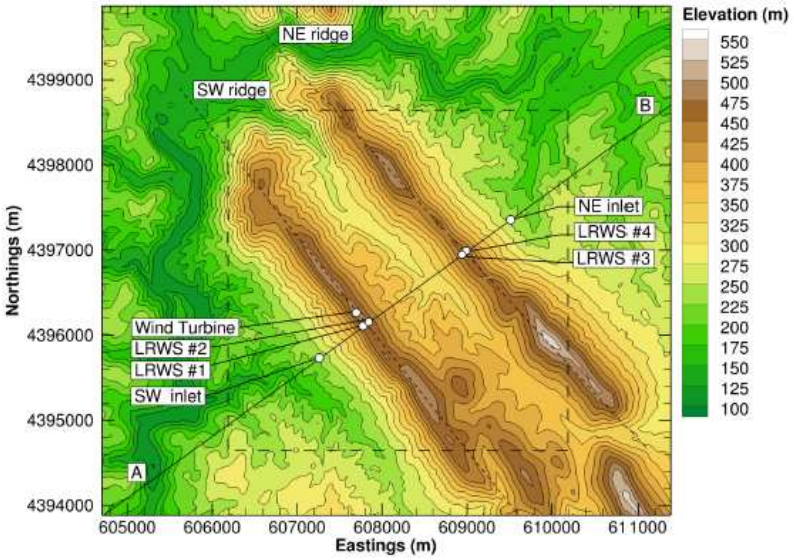

(c) Image reprinted from Palma et al. (2019)

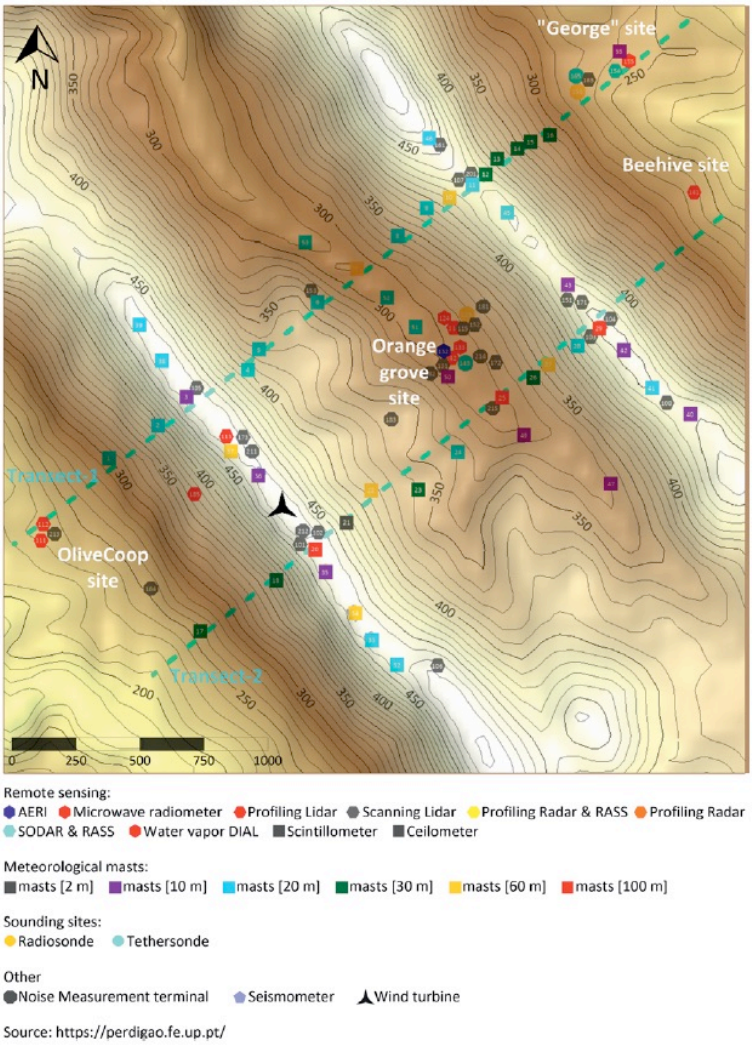

Fig. 13 Perdigão Field site, Portugal. (a) photo, (b) contour map of the region, (c) sensor locations

5.2 Gravity-Driven flows

Most thermodynamically driven slope flows develop both in space and time so characterising them properly requires measurements at multiple heights at multiple positions along a slope over an extended period. Only a few field experiments have achieved this and this has contributed to the difficulty of deriving simple general rules for the structure of gravity flows with the generality of the JH75-type linear hill flow models. As we shall see in the next Section 6, it is also the case that physical modelling has not played as large a role in gravity flow studies as it has in hill flows so what we do know comes primarily from the interplay of field observations and theory.

1833 It is possible to roughly divide the field studies into three groups. First, dedicated
1834 studies of katabatic flows driven by radiative cooling on simple slopes usually at shallow
1835 angles (<5 degrees). Second, studies of flow on valley sides driven by radiative
1836 heating/cooling as part of larger scale campaigns targetting mountain-valley systems.
1837 These are often on much steeper slopes (~30-40 degrees) and also deal with transitional
1838 flows and shadow effects. Third, flows over glaciers, often focussing on the interaction
1839 between larger scale and katabatic forcing. As we shall see, many of the simple slope
1840 studies were performed as elements of larger scale mountain meteorology campaigns
1841 such as ASCOT (Blumen et al., 1990), MAP-RIVIERA (Rotach et al., 2004), VTMS
1842 (Monti et al., 2002), CASES-99 (Mahrt et al., 2001) and MATERHORN (Fernando et al.
1843 2015) and so the local slope measurements were often supported by extensive
1844 climatological data.
1845
1846 **5.2.1 Flows on simple slopes.**
1847 Although drainage winds (particularly in valleys) had been studied in the past, few
1848 detailed measurements had been made of katabatic flows on simple slopes prior to the
1849 late 1970s. Mahrt (1982) for example was able to list only eight cases from six
1850 observational studies that measured profiles of both wind and temperature. The study of
1851 Manins and Sawford (1979a) on a long gentle slope using a combination of balloon
1852 profiling equipment and virtual potential temperature measurements was one of the first
1853 to produce detailed data. They concluded that the 1D models then current were
1854 inadequate to describe their observations. Their major findings were that even on a
1855 simple slope, the flow was significantly 3D and that the main cause of flow retardation
1856 was entrainment from the boundary layer above rather than surface friction. Their study
1857 prompted the development of their two-layer slab model (Manins and Sawford, 1979b).
1858 A series of fruitful experiments over simple slopes followed through the 1980's
1859 with, in several cases, multiple towers or observation points equipped with fast response
1860 sensors, which allowed the spatio-temporal development of the flow to be recorded as
1861 well as the turbulent fluxes that maintained it. An early example was the study by
1862 Clements, and Nappo (1983), employing two towers and 2 weather stations on a 1 km
1863 slope but more influential were the measurements of Horst and Doran (1988), who

measured at two sites as part of the US DoE ASCOT field campaign. Their two sites differed markedly in surface roughness; the first slope was covered by 1-2m bushes and 10-30m trees while the second consisted of 10-30cm grass and scattered bushes. At the second site, which more closely approximated a simple tilted plane, they were able to follow flow development using four 20m towers and fast response turbulence sensors and produced valuable data on turbulent fluxes above and below the observed low level jet peak.

A gap of over a decade intervened before more simple slope studies appeared with the measurements of Monti et al. (2002) in the Salt Lake Basin of Utah as part of the Vertical Turbulence and Mixing (VTMX) campaign. Their measurements showed the influence of internal waves on entrainment and the data were also used by Princevac et al. (2005) in their parametrisations of entrainment. More recently, the study by Whiteman and Zhong (2008) at the same Salt Lake Valley site and also as part of VTMX used four tethered balloon profiles along a 1km downslope transect and reported a much thicker and stronger katabatic current than the earlier studies had found for similar slope and thermodynamic configurations. Most recently, the detailed sampling of small scale turbulence structure by Grachev et al. (2016), used four comprehensively instrumented towers on a slope on Granite Mountain during the 30-day long MATERHORN field campaign in 2012 to produce a data set with unprecedented temporal and spatial resolution of turbulence structure (see Section 4.1).

Moving away from simple slopes, Mahrt and various collaborators (Mahrt et al. 2001; Soler et al. 2002) had focussed on the interaction of shallow drainage flows with both the ambient wind and with larger scale drainage flows developing over the major landscape features. Using mainly data from the CASES99 experiment, he was able to develop a general understanding of this complex situation which is important in many biometeorological applications.

5.2.2 Flow on valley sides

The development of both anabatic and katabatic flows on valley sides has been studied primarily in the context of campaigns to characterise mountain-valley wind systems more generally. As noted by Whiteman (1990) such flows can be expected to differ from those

on simple slopes because of two factors. First, the formation and growth of a surface-based inversion over the valley floor will mean that the ambient stratification in which the valley side flow develops will change as the inversion deepens. Second along-valley circulations will affect the structure and evolution of the shallow slope flows so that these are fundamentally 3D and unsteady. Despite these complications we can contrast two experiments both of which have provided valuable data. First, as part of the large scale MAP-RIVIERA campaign (Rotach et al., 2004) measurements were made from a single tower equipped with six 3D sonic anemometers and other sensors in a 13m high mixed deciduous forest on a 35 degree slope on the side of the Riviera valley in the Italian Alps. We have already noted these results in the context of slope flows in canopies (van Gorsel et al. 2011; Section 4.2) for which they provide valuable data.

A useful contrast is provided by the measurements of Oldroyd et al. (2014) who also made detailed wind and turbulence measurement from a single tower on a slope also of 35 degrees in Val Ferret, Switzerland. However, their measurements were made over a surface of short grass and a classic wall jet type wind profile was observed. Their data have provided a valuable input to our understanding of turbulent structure in this 'classic' situation (Oldroyd et al. 2016) but also of more complex flow dynamics during transitional periods (Nadeau et al. 2018). The experiment of Oldroyd et al. (2014) followed the earlier study at the same 'SLOPE' field site by Nadeau et al. (2013) who used a comprehensive instrument array, comprising two turbulence towers, two weather stations, five surface temperature measurement stations and a tethered balloon system deployed down a 400m slope transect to study the transitional flow generated by advancing shadow fronts.

5.2.3 Flow over ice and snow surfaces

The strong katabatic winds in Antarctica have long been a subject of study and analysis (e.g. King, 1989; Parrish and Cassano, 2003) but the difficulty of doing tower based measurement in that hostile environment has meant that studies have mainly been at the synoptic scale. At a smaller but still whole-of-mountain scale, the KABEG'97 experiment (Heineman, 1999) combined aircraft and surface measurements to disentangle the effects of synoptic and katabatic forcing on a tundra and ice sheet in West Greenland.

On the smaller slope-flow scale, there has been continuing interest in katabatic flows developing over European glaciers. To some degree this has been motivated by general research into the structure of stable equilibrium boundary layers (e.g. Smeets et al. 1998) but the turbulence structure of katabatic winds developing over an extensive Austrian glacier was recorded by Smeets et al., (2000), who showed the important role played by the turbulent energy fluxes in the mass balance of the glacier ablation zone.

Reviewing this necessarily incomplete survey of slope flow field experiments, we are struck by several things. First, the very large range of different hill and valley combinations and the similarly large range of 'typical' flow responses, has meant that many of the field data sets cannot be directly compared. Even in the most obvious case of simple, thermodynamically driven slope flows, finding data free of secondary synoptic forcing so that they can directly inform theory is difficult. Second, the wide range of important configurations to be studied has meant that the effort has been spread thin with only a few useful data sets for each archetypal situation-slope flow, valley flow, glacier flow, etc. This is in quite stark contrast to boundary layer hill flows where, even if ideal hills are hard to find, most field experiments have contributed to a single theoretical framework. The wide spread of local slope flow data can be best understood, therefore, in the context of the larger scale dynamics of hill-valley flows as addressed for example in the 1990 meteorological monograph edited by Blumen (1990) and in the summaries of the more recent large scale field campaigns such as MAP-RIVIERA (Rotach and Zardi, 2007). These problems are well recognized by workers in the field, see for example Stiperski and Rotach, (2016). We will return to consider this context in the Discussion, Section 7.

6. Physical modelling: Wind Tunnel and Flume Studies

Partly as a result of the elusive nature of 'simple isolated' hills in nature and partly because it is very difficult in field experiments to sample with sufficient resolution and range to fully characterize the flow, physical modelling has played an important part in developing theory and understanding. This has particularly been the case for separated flow, where field exploration of the separation bubble was almost always restricted to the layer that towers could reach, whereas the bubble depth is O[H]. The extensive

deployment of lidars and boundary layer profilers at Perdigão is the first time that the complex dynamics of the separation bubble have been fully characterized in a large scale hill flow experiment (Palma et al. 2019). In this section we first discuss the benefits and limitations of physical modelling before looking at the more recent efforts in modelling canopy covered hills. For a comprehensive review of earlier simulations of flow over rough hills, the reader is referred to Finnigan (1988).

The scaling laws that govern physical modelling set limits on what can be modelled and also determine how we must interpret results. For neutrally stratified flow, the key dimensionless group to match between real life and the model experiment is the Reynolds Number, $\mathrm{Re} = U_0 L/\nu$. However, characteristic Re values for boundary layer hills in the atmosphere are $10^8 - 10^9$ whereas the largest Re values achievable in boundary layer wind tunnels or flumes, where topography is reduced in size by factors of 10^3-10^4, are only about 10^5. Operating windspeeds in boundary layer wind tunnels are typically 10-30 m/s while water flumes run at a tenth or less of that velocity but, since the kinematic viscosity of water is about ten times that of air, they achieve similar Re values to wind tunnels. This reduction in model Re implies significant differences in the balance of viscous and inertial forces between real and simulated flows but experience has shown that, if the modelled flow is 'aerodynamically fully rough', then acceptable turbulent boundary layer characteristics can be reproduced.

Fully rough flows occur when the momentum absorption at the model surface is almost entirely through pressure drag on the surface roughness elements. This requires the roughness Reynolds Number, $\mathrm{Re}^* = \left(u* z_0/\nu\right)$ to be 5 or greater (Raupach et al., 1991). Re^* almost always exceeds 5 in atmospheric flows but in a wind tunnel or flume, it requires the model surface to be far rougher than strict geometric scaling would imply unless the prototype hill is covered with a tall plant canopy or buildings. If the roughness elements of a real hill covered with turf or rocks were scaled down in the same ratio as the gross hill dimensions, *H* and *L*, then the model surface would be aerodynamically smooth or transitional $\left(\mathrm{Re}^* \sim 1\right)$ and momentum would be absorbed predominantly as viscous rather than pressure drag. As a result the turbulence dynamics of the near-surface model layer can be significantly different from that over the real hill. Conversely, if we

make the model surface fully rough, the asymptotic scaling laws used to define the inner layer depth *l* often imply that the inner layer is entirely within the model roughness sublayer.

6.1 Flow over hills

As well as changing the turbulent structure of the inner layer by exaggerating the surface roughness, boundary layer wind tunnels, especially smaller ones, typically thicken the boundary layer artificially before the working section and this usually means that the inertial or logarithmic layer in the approach flow occupies a much larger fraction of the boundary layer depth than in nature (Hunt and Fernholz, 1975; Gong and Ibbetson, 1989; Finnigan et al. 1990). The effect of this on the shear in the approach flow impacts the modelled speed up and drag because, as we discussed in Section 2.1 (Belcher et al. 1993), both these features are sensitive to the upwind shear. Conversely, if the approach flow boundary layer is allowed to grow naturally, then the hill may occupy a significant fraction of the total boundary layer depth. For example in the multiple ridge simulations of Athanassiadou and Castro (2001) the model hills were $0.2z_i$ and $0.33z_i$ respectively, implying that the prototype hills stretched the strict criterion for boundary layer hills set out by Belcher and Hunt (1988) (see Section 1, above). Another ploy used by some researchers has been to generate a fully rough approach flow but then relax to geometric similarity on the model hill itself. Unfortunately, this means that interpretation has to contend with the complex effects of both hill and roughness change (e.g. Pearse et al., 1981; Takahashi et al. 2005; and see the discussion in Section 2.2 above). Indeed, abrupt combinations of roughness changes and hill effects are only just now being modelled successfully (e.g. Grant et al., 2016).

Despite all these caveats, wind tunnel studies provided a great deal of guidance as theory and understanding was being developed in the 1970s and 80s. The experiment of Britter et al. (1981) clarified the nature of turbulence changes in the rapid distortion region above the inner layer while Finnigan et al (1990) analysed turbulence dynamics over a fully rough model in streamline coordinates, which illuminated the competing effects of shear, plane strain and curvature on turbulence development over the hill. The comprehensive measurements of Gong and Ibbetson (1989) tested the predictions of

2017 competing theories for the HLR88 outer layers but not those features that depended in an
2018 essential way on the inner layer dynamics, while the wind tunnel simulations of
2019 Askervein by Teunissen and Shokr (1985a,b) and Teunissen et al. (1987), where the
2020 model surfaces were smooth or transitional, were invaluable in interpreting the field data
2021 from that campaign.

2022 The second area where the nature of the surface drag mechanism can be critical is
2023 modelling flow separation. Wind tunnel studies have been very valuable in defining the
2024 gross geometric determinants of separation on 2D and 3D hills (see Finnigan, 1988) but,
2025 when the hill steepness is close to the critical angle that promotes separation, the surface
2026 roughness has a large effect. A hill that does not separate when the surface is smooth can
2027 fully separate when it is rough. This feature is particularly striking when the hill is
2028 covered by a tall canopy as we have already noted. Finnigan (1988) discusses the
2029 mechanism of rough wall turbulent separation at some length and also compares the large
2030 number of wind tunnel studies of flow separation performed through the 1970s and 1980s
2031 to derive general guidelines for the steepness required for separation when hills are 2D
2032 versus 3D and rough versus smooth.

2033 One area that has received relatively less attention is the effect of repeated hills.
2034 There have only been a few attempts to model this situation in boundary layer wind
2035 tunnels (Gong et al., 1996; Athanassiadou and Castro, 2001) and water flumes (Poggi et
2036 al. 2007a,b). The configuration in each case has been one of repeated 2D ridges and a
2037 particular focus has been the development of the flow as it comes into equilibrium with
2038 the periodic distortion and whether linear theory still applies. Repeated ridges come
2039 closer to real complex topography than most isolated hills but even so, multiply repeated
2040 2D ridges are scarce in nature, the field study of Mason and King (1984) in South Wales
2041 or even Perdigao, where only two ridges are present, being rare examples. Intriguingly,
2042 both wind tunnel simulations show the development of secondary flows, which can be
2043 attributed to large scale streamwise vortices and which produce significant spanwise
2044 variation in the mean flow and statistics. A similar phenomenon was observed in an
2045 earlier unpublished study of flow over repeated ridges in the CSIRO Australia boundary
2046 layer wind tunnel by Dr W. Gong, Prof. P. Taylor and Dr K. Ayotte (K Ayotte. *pers.*
2047 *comm*.), suggesting that such secondary flows, possibly generated by a Craik-Leibovich

Type-2 instability, may be an important feature of atmospheric flow over real complex terrain.

The flume experiments of Poggi et al. (2007) over a train of gentle smooth-surfaced cosine hills explored the interplay between the viscous sublayer and the inner layer. Recognising our earlier caveats about fully rough simulations, that experiment revealed that many aspects of the inner layer, including the 2D shape of the mean velocity and Reynolds stress profiles, follow the JH75, theory provided the approaching mean velocity profile is appropriately specified. The experiment also showed that the hydrostatic pressure approximation, the linearization of the longitudinal mean advection term and the minor contribution from the perturbed vertical velocity to the overall advection in the mean momentum balance-simplifications all adopted in JH75-are acceptable.

6.2 Stability effects

So far we have discussed neutrally stratified flow. A different set of modelling considerations apply when the flow is diabatically stable or unstable. In such cases, as well as trying to match the Reynolds Number between real life and model, we need to match the Froude Number, $F_L = \frac{U_0}{NL} = \frac{U_0}{L} \Big/ \left(\frac{g}{\Theta_0} \frac{\Delta\bar{\theta}}{H} \right)$ For significant buoyancy effects in the atmosphere, we require $|F_L| < 1$ but to achieve this in the wind tunnel where both L and H are scaled down by 10^3–10^4, U_0 must be as small and $\Delta\bar{\theta}$ as large as possible. There are practical limitations on how large $\Delta\bar{\theta}$ can be made while the need for small U_0 conflicts with the need to have Re as large as possible and realistic simulations of stable and unstable flows over hills have only been possible in a few specialist wind tunnels around the world, e.g. Ross et al. (2004), Takahashi et al. (2005), Loureiro and Silva Freire (2005), and Pospisil et al. (2017). Of these, only the results of Ross et al., who compared neutral and stable flow over steep hills with an emphasis on how well flow separation can be modelled, are sufficiently well characterized to easily contribute to a general understanding of hill flow dynamics. The other studies mentioned, while of

relevance to their specific wind engineering applications are difficult to generalize or in some cases to interpret in terms of atmospheric stability measures..

Strong stable stratification in the atmosphere leads to phenomena like flow blocking in front of 2D ridges or, on 3D hills, the dividing streamline effect, where above some level the air flows over the hill while below it, the air flows around the hill. This phenomenon was studied in a towing tank where the water was stratified with salt solution (Hunt and Snyder, 1980). This allowed values of F_L as low as 0.1 to be achieved but at the expense of abandoning Re similarity. This is another example of flows that do not satisfy the criteria for boundary layer hills set out in Section 1.

6.3 Physical modelling of canopy covered hills

The wind tunnel study of Finnigan and Brunet (1995) has already been referenced. They placed an aeroelastic canopy model over a 2D cosine shaped ridge. The model configuration had dimensions, H=150mm, L=500, h_c=50mm, z_i=700mm. Since the hill and canopy occupied such a large fraction of the model boundary layer depth, most of the conditions of the analytic theories like JH and HLR were voided but the striking changes to the canopy and shear stress layer flow fields that were observed (see Section 3.) led to a wave of interest including *inter alia* the theoretical study of FB04. The predictions of FB04 in turn prompted a series of experimental investigations.

In the mid to late 2000s, detailed flume experiments were undertaken to measure the mean flow and turbulence structure inside canopies covering the train of gentle cosine hills already studied with smooth surfaces by Poggi et al. (2007). Since the initial focus was on the assumptions and results of FB04, the components of the mean longitudinal momentum balance were investigated first (Poggi and Katul, 2007b). That revealed that the presence of a recirculation region within the canopy is sufficiently large to distort the hydrostatic pressure perturbation assumption and to negate the mixing length hypothesis of FB04 entirely in the recirculation zone. Moreover, an alternative to the FB04 model for the deeper layers of the canopy was proposed that maintained the same interplay between the drag force and the mean pressure gradient but included a linearized mean advection term. The revised model was shown to delineate the onset of the recirculation zone better (Poggi et al., 2008) and out-performed FB04 in the deeper layers of the

canopy, suggesting that mean advection remains a leading order term there. Advection in the upper canopy was subsequently included in the extensions to FB04 by Harman and Finnigan (2010, 2013) and increased the range of applicability of the model.

The flume experiments also explored the shape of the higher-order statistics up to triple moments and the properties of the ejection-sweep cycle contributing to momentum transport (Poggi and Katul, 2007c). These experiments showed that sweeps dominate momentum transport within the roughness sublayer whereas ejections dominate momentum transport above the roughness sublayer and showed that the interface where sweeps and ejections are in approximate balance proved to be a pragmatic definition of the roughness sublayer thickness on hilly terrain. The study also showed that third-order cumulant expansion methods (i.e. correcting for asymmetry only in the joint probability density function of w' and u') as used by Nakagawa and Nezu (1977) and Raupach (1981) in smooth and rough-wall boundary layers, can also be used to link the ejection-sweep ratio to the flux transport term ($\overline{w'w'u'}$) in the more complex hill-canopy flow, thereby establishing a bridge between conditional sampling methods, quadrant analysis, and RANS closure schemes. Finally, the flume experiments also contrasted the shapes of the turbulent intensities and turbulent spectra over bare hills and hills covered by a canopy (Poggi and Katul, 2008). The key finding from those studies is that rapid distortion theories proved successful at predicting the turbulent intensities in the outer layer but not the inner or roughness sublayers, confirming the fundamental assumption in the JH75, HLR88 and FB04 analyses.

Returning to the wind tunnel, Harman and Finnigan (2013) made measurements over a model in which the well-studied 'tombstone' model canopy (Raupach et al, 1986), whose equilibrium characteristics were well characterised, was placed on a 2D ridge in the CSIRO Australia boundary layer wind tunnel. The objective of the experiment was to test extensions made to the FB04 model by Harman and Finnigan (2010), which incorporated advection in the upper canopy and a more sophisticated coupling of the lower and upper canopy solutions as they affected the overall pressure perturbation on the hill. These extension were motivated by the RANS modelling of Ross and Vosper (2005), the flume experiments of Poggi and Katul (2007b,c) and the LES modelling of Patton and Katul (2009). The experiment focussed on the mean flow and pressure fields but was also

2138 able to show that some of the impacts on scalar transport, particularly those relevant to
2139 measuring carbon exchange from eddy flux towers, as discussed in Section 3, might be
2140 smaller than predicted by FB04.
2141 As discussed at length in Section 3.2, the fundamental mechanics of momentum
2142 and scalar transport at leaf level ensure that a very stable layer develops in forest or crop
2143 canopies at night, when radiative cooling is active. Finnigan and Hughes (2008) modelled
2144 this situation in a novel way by placing the hill-canopy model of Harman and Finnigan
2145 (2013), whose surface and canopy elements could be electrically heated, on the roof of
2146 the tunnel. This reversed gravity so the heated surface and canopy elements generated a
2147 strongly stable layer within the canopy. A model stably stratified flow produced in this
2148 way is self-limiting in its depth and has the advantage that the stable layer is generated
2149 naturally by surface heating. This is in contrast to stable flows that are 'the right way up',
2150 where a stable temperature gradient has to be generated in the approach flow by a grid of
2151 heating and cooling elements (e.g. Ross et al. 2004). The Harman and Finnigan
2152 experiment covered a range of Froude numbers and for $F_L \le 0.3$, it was observed that,
2153 while flow over the hill above the canopy was fully turbulent with shear stress profiles
2154 identical to the neutral case $\left(F_L = \infty\right)$, a downslope gravity current filled the canopy layer
2155 on both upwind and downwind slopes (see Section 3.2). Surprisingly, the downslope
2156 current on the upwind face of the hill, which was in the opposite direction to the flow
2157 above the canopy, penetrated upwind a distance of $11L$ at which point the surface and
2158 canopy were no longer heated. This confirmed that as long as the canopy remains cool
2159 enough, the flows above and within canopy can be completely decoupled.
2160 Physical modelling is one of the three pillars on which our understanding of
2161 atmospheric flow has traditionally rested, the others being theory and field experiments.
2162 Today, increases in computing power have advanced large eddy simulations (Section 2.4)
2163 to the point that they can be considered a fourth pillar. Each approach has its strengths
2164 and weaknesses and they are deployed most powerfully when they are used together,
2165 each filling in gaps in the other techniques and suggesting fruitful new lines of attack.
2166 Physical modelling in particular sometimes reveals important new physics. The collapse
2167 of turbulence and establishment of a resilient stable layer in a radiatively cooling night-

time canopy was first seen in a wind tunnel experiment. It was later shown to be a consequence of basic transfer physics at leaf level and so a ubiquitous feature of canopy flow. Furthermore the theoretical result that followed showing that the strength of a resulting gravity current depended on the temperature deficit and slope length rather than slope angle (Section 5.4) explained many perplexing observations from flux towers on very gentle terrain.

As we have seen in this section, wind tunnel and flume simulations have played a major role in shaping our understanding of hill flow dynamics and should continue to do so in the future. Modern instrumentation, particularly the ready availability of laser doppler and particle image velocimetry has now removed many of the difficulties of measuring flows of very high turbulent intensity or which regularly reverse direction such as inevitably occurs in canopies and in hill separation regions. The ability to stratify the flow in a limited number of specialised tunnels or by resorting to the subterfuge of Finnigan and Hughes for the stable case suggests that the very large investment in field campaigns like Perdigao could benefit enormously from concomitant physical modelling as was the case in the 1970s and 1980s.

6.4 Gravity Driven Flows

Gravity driven slope flows do not seem to have been modelled in wind tunnels (except in the example just discussed above). Scaling considerations indicate that gravity currents generated on a rough or smooth plate of wind tunnel dimensions would be extremely thin. Most physical modelling of gravity currents has therefore been of density currents in water in an oceanographic context (see Baines, 2001 and references therein). However, the study of a katabatic water current flow through a canopy of bluff obstacles by Hatcher et al. (2000) has already been noted (see Section 4.3) as it is of direct relevance to gravity driven flows through plant canopies in the atmosphere. Similarly, the study of turbulent entrainment into atmospheric slope flows by Princevac et al. (2005) used a set of laboratory experiments on density current flows in water tanks as benchmarks against which their atmospheric measurements could be assessed. The references in Princevac et al. (2005) and in Hatcher et al. (2000) are also a good guide to laboratory work that is of direct relevance to atmospheric gravity currents.

7 Bringing it all back Home: New Challenges and new scientific directions

As we foreshadowed in the introduction, we have seen how the study of boundary layer flow over complex topography has gone through several phases. The 1970s and 1980s saw the development of analytic theory that clarified the fundamental physics. Basic questions such as, why the speed-up in the mean wind over hill crests was so much larger than the hill slope would suggest, were answered qualitatively and, to a large degree, quantitatively (Section 2.1). Numerical RANS models developed in parallel with analysis and, for a while, used the simplifications suggested by theory to produce fast computations for gentle terrain but then turned to more complex formulations to deal with steeper hills and changing surface cover (Section 2.2). These refinements and developments of RANS models continue apace driven by a host of practical applications, especially wind energy and NWP. However, for the first application especially, the weaknesses of RANS approaches in dealing with separation and the turbulent structure of the separated and near-wake flow are clear. RANS approaches work best when the model equations are effectively parabolic but the feedback on the driving pressure field that occurs with separation makes the equations unavoidably elliptic. In addition, the challenge of simultaneously parameterising the fine-scale surface processes that determine the separation point and the O[H] size eddies in the separation bubble and wake, stretch the abilities of most RANS closure schemes past breaking point.

As predicted by Wood (2000) in his prescient review, the last two decades has seen the increased use of LES approaches to capture this wide dynamic range and, perhaps as importantly, to give insights into the turbulence structure that were difficult to deduce from the sparse sampling of field experiments (Section 2.3; Section 5.). Wind tunnel simulations gave more detailed information about turbulence but over rough hills, the need to have aerodynamically fully-rough models precluded proper simulation of the shear stress dominated inner layer. Moreover, until the ready availability of Laser-Doppler- and Particle-Image-Velocimetry systems over the last decade, use of the standard wind tunnel turbulence sensor, the hot wire anemometer or even the pulsed wire

2230 sensor, precluded the proper characterisation of the 3D reversing flow in the separation
2231 region (Section 6.1).
2232 While this development of hill flow dynamics relied on a constant interplay
2233 between theory and dedicated field experiments on ‘ideal’ topography, supported in
2234 critical areas by wind tunnel simulations, the analogous study of gravity-driven flows, on
2235 hill and valley slopes, which began in earnest at the end of the 1970s, faced different
2236 challenges (Section 4). Even the simplest examples of these flows, such as katabatic
2237 winds down extensive uniform slopes under weak synoptic forcing, develop in both space
2238 and time and require a correspondingly extensive instrument deployment to characterise
2239 them properly in the field. At the same time, insights from physical modelling have not
2240 been as directly applicable to atmospheric gravity currents as they were to hill flows.
2241 Laboratory simulations generally involved dense water currents in less dense ambient
2242 fluid and were biased towards simulating large scale oceanographic or geophysical
2243 phenomena (Section 6.4). Finally, the many possible topographical configurations that
2244 generate gravity flows are difficult to represent by a single archetype equivalent to an
2245 isolated hill. Instead, field studies have ranged from ‘ideal’ simple slopes to the sides of
2246 steep valleys, where the gravity flows themselves coalesce to form hill-valley wind
2247 systems. These in turn add complexity to the downslope currents (Section 4.5). Despite
2248 these difficulties, considerable progress has been made in characterising the structure and
2249 dynamics of gravity flows and the main obstacles to theoretical progress have been
2250 identified as achieving better scaling laws and parameterisations of the fundamentally
2251 inhomogeneous turbulence of these wall-jet type flows.
2252 In the last two decades also, a good deal of effort has been devoted to
2253 understanding flow over hills covered by tall plant canopies (Section 3). As well as their
2254 important application to quantifying the terrestrial carbon cycle, analytic models that
2255 resolve the flow in the canopy and dedicated simulations in wind tunnels and flumes have
2256 resulted in a deeper understanding of hill-flow dynamics more generally such as the
2257 mechanics of flow separation on rough hills, surface roughness being in effect, simply a
2258 shallow canopy. The coupling of hill-flow and canopy dynamics has also revealed
2259 important new physical processes that were previously unsuspected such as the inevitable
2260 collapse of turbulence in a radiatively cooling canopy at night and the generation of

robust and persistent downslope flows (Section 4.4). Moreover, research teams are finding still more surprising consequences of combining canopies and hills; currently unpublished data from wind tunnel experiments and LES indicate that the flow patterns that appear on 3D hills covered with tall canopies are significantly more complex than on 2D ridges (Dr I. G. Harman, Dr E. G. Patton *pers. comm*.). There is clearly still much more to be discovered about the elementary building blocks of complex terrain flows. One point that has not been emphasised enough in the literature is the feedback between canopy processes at the individual hill scale and topographic drag at the landscape scale. The mechanisms of 'separated sheltering' in flow over low hills, which is exaggerated when a canopy is present (Belcher et al. 1993; Finnigan and Belcher, 2004) and of earlier separation caused by the canopy can easily double the topographic drag of relatively gentle topography if a rough surface is replaced by a canopy.

Despite these remaining knowledge gaps, it seems clear that we have reached a point where hill flow and gravity flow studies are poised to coalesce with valuable information to be exchanged between the two fields. The urgent driver for this is the need for information on the impacts of global heating on local climate at scales where operational decisions must be made. This means that climate and weather models must be resolved at the 1-10km scale and implies that the sub boundary-layer scale dynamics we have been discussing in this review are critical These imperatives are driving two responses. First we increasingly see resources and collaboration being donated to multinational measurement campaigns in regions of complex topography such as MAP-Riviera (Rotach et al. 2004), MATERHORN-X (Fernando and Pardyjak 2013; Fernando et al. 2015; Di Sabatino 2016), Perdigão (Fernando et al. 2019 and see Section 5) and others in the planning stage today. Second, we are seeing serious attempts to bridge the gap between eddy-resolving models on coarse meso-scale grids that can reproduced terrain-forced wind and temperature patterns around larger topographic features and the 'classic' LES models discussed in Section 2.3, which resolve the dynamics of boundary layer turbulence as it responds to topographic forcing. As this coalescence of modelling scales and the results from new field experiments that will test its success are likely to shape the research efforts of the coming decade, it is appropriate to end this review with some detailed remarks on where we now stand.

For some years, one theme of hill-flow research has been the use of LES to represent the coupling between terrain and turbulence in meso-scale regional and climate modelling systems, for example the widely used weather research and forecasting system (WRF) https://www.mmm.ucar.edu/weather-research-and-forecasting-model. At the same time, researchers using those larger-scale models have been pushing their simulations to finer and finer scales as they realized that unresolved processes associated with surface interactions directly impact their predictive skill, especially over longer time scales. The advent of grid nesting capabilities has enabled many larger-scale numerical modelling codes to now refine their meshes sufficiently to include an LES-mode in the innermost domain (e.g., Chow et al. 2006; Golaz et al., 2009). While the idea of nesting an LES within a larger-scale model might seem straightforward, doing so accurately remains an ongoing challenge (e.g., Wyngaard, 2004; Talbot et al., 2012; Muñoz-Esparza et al., 2014; Shin and Hong, 2015; Honnert, 2016; Rai et al., 2016; Muñoz-Esparza et al., 2017; Bao et al., 2018; Muñoz-Esparza and Kosovic, 2018; Hald et al., 2019; Arthur et al., 2020). Indeed, Cuxart (2015) argues for a more stringent definition rather than simply describing this style of calculation as LES. The fundamental interplay between larger-scale dynamics and mountain boundary-layer turbulence drives these efforts. To take just two recent examples: Kirshbaum (2017) used a nested-LES framework to identify regimes and scaling associated with the influence of hill-induced thermal forcing on boundary-layer turbulence and how the hill-induced pressure distribution results in upstream blocking of larger scale dynamical processes, while Babić and de Wekker (2019) found that complex terrain reduces the aspect ratios of boundary-layer rolls and cells compared to what is expected over horizontally-homogeneous terrain.

Wyngaard (2004) pointed out that one of the key differences between micro-scale models used to study turbulence and meso- to larger-scale models used to study weather and climate is the ratio of the energy-containing scales of turbulence to the filter-scale of the model. In ‘classic’ LES the filter-scale falls deep in the inertial subrange, whose statistical properties are simple and well understood and can be parametrised with confidence. Conversely, to simulate large domains, larger-scale models filter the flow at scales notably larger than the largest scales of boundary-layer turbulence, which range from tens of meters to a few kilometres, so the physics that a model of the unresolved

processes needs to represent must change with the scale at which the equations are filtered, a concept now called ‘scale-aware parameterization’.

These challenges were clearly expressed in the penetrating analyses of boundary layer structure in mountainous terrain by Rotach and Zardi (2007) and Weigel et al. (2007). Based on experience from many large scale measurement campaigns they were able to make two crucial observations. First, the exchange of scalars between these deeply corrugated regions and the free troposphere was predominantly by the ventilation of hill-valley systems, whose flow patterns were dominated by local thermally-driven ridge-valley flows. These flows themselves were modulated by the interaction of synoptic winds and the topography. Under certain conditions this ‘topographic venting’ could be several times larger than the turbulent exchange (Henne et al. 2004; Weigel et al. 2007). Second, was the observation that despite the highly complex and heterogeneous structure of the hill-valley flows, characteristic and transferable patterns in the turbulence structures and larger scale flow patterns could be found.

It might be instructive to compare this state of affairs with that which faced researchers into canopy turbulence thirty years ago. There too it was necessary to integrate the complex interacting patterns of mean flow and turbulence around canopy elements, which, if we include urban canopies, varied in size from leaves to buildings. There were even many studies of flow around individual leaves or twigs or branches in the hope that these could be combined into an average ‘canopy flow’. Although flow patterns around individual canopy elements were heterogeneous and distinct, three conceptual advances eventually allowed real progress to be made. The first was the use of formal spatial averaging to deduce conservation equations for the whole canopy (Raupach and Shaw, 1982; Finnigan and Shaw, 2008). The second was arriving at a detailed understanding of the differences between the spatially-averaged properties of turbulence in the canopy airspace and that in the free air above (e.g. Finnigan, 2000). The third was the realisation that at the whole-canopy scale,’ emergent properties’, which could not be deduced by analysis of the element flows alone, determined the interaction of the canopy with the overlying boundary layer (Raupach et al. 1996).

In mountainous regions individual hill and hill-valley flow systems play the part of canopy elements. The definition of form drag around hills is exactly analogous to the

form drag around canopy elements that is produced in canopy-flow momentum equations by spatial averaging. The distinctly different natures of within-canopy and boundary-layer turbulence manifests itself in different scaling laws, different ratios of turbulence moments and different spectral dynamics. The analogy to this in flow in and around topography may be a new approach to flow scaling that takes the irreducible anisotropy of boundary layer turbulence in complex topography at face value (e.g. Stiperski, 2017; Stiperski et al. 2019). This approach may be what is needed to write sub-filter scale parameterisations for eddy-resolving models that resolve Wyngaard's dilemma by a physically-based statistical treatment of the unresolved motions in complex topography. Presumably, this would use the statistics of the topography to inform the statistics of the space-time structure of the airflow. An analogy to the third element in the modern description of canopy turbulence-the emergent nature of large scale energy-containing eddies that result from the inflexion point in the mean velocity profile-is harder to predict. It may be resolved by the application of the modern understanding of the thermodynamic constraints on the energy and entropy balances of topographical flow (e.g. Kleidon, 2016) or by approaches currently hidden somewhere in the large span of work we have surveyed here.

References

Allen T, Brown AR (2002) Large-Eddy Simulation of Turbulent Separated Flow over Rough Hills. Boundary-Layer Meteorol 102: 177–98

Amanatidis GT, Papadopoulos KH, Bartzis JG, Helmis CG (1992) Evidence of katabatic flows deduced from a 84 m meteorological tower in Athens, Greece. Boundary-Layer Meteorol 58:117–132

Arduini G, Staquet C, Chemel C (2016) Interactions Between the Nighttime Valley-Wind System and a Developing Cold-Air Pool. Boundary-Layer Meteorol 161:49–72

Arritt RW, Pielke RA (1986) Interactions of nocturnal slope flows with ambient winds. Boundary-Layer Meteorol 37:183–195

Arthur RS, Lundquist KA, Wiersema DJ, Bao J, Chow FK (2020) Evaluating Implementations of the Immersed Boundary Method in the Weather Research and Forecasting Model. Mon Weather Rev 148 (5): 2087–2109

2389 Athanassiadou M, Castro IP (2001) Neutral flow over a series of rough hills: a laboratory experiment.
2390 Boundary-Layer Meteorol 101:1–30

2391
2392 Aubinet M, Feigenwinter C, Heinesch B, Bernhofer C, Canepa F, Lindroth A, Montagnani L, Rebmann C,
2393 Sedlak P, Van Gorsel E (2010) Direct advection measurements do not help to solve the night-time CO2
2394 closure problem: Evidence from three different forests. Agric For Meteorol 150: 655–664

2395
2396 Axelsen SL, van Dop H (2009a) Large-eddy simulation of katabatic winds. Part 1: Comparison with
2397 observations. Acta Geophys 57:803–836

2398
2399 Axelsen SL, van Dop H (2009b) Large-eddy simulation of katabatic winds. Part 2: Sensitivity study and
2400 comparison with analytical models. Acta Geophys 57:837–856

2401 Ayotte KW (1997) Optimization of upstream profiles in modelling flow over complex terrain. Boundary-
2402 Layer Meteorol 83: 285–309

2403 Ayotte KW (2008) Computational modelling for wind energy assessment, J Wind Eng Ind Aerodyn 96:
2404 1571–1590

2405 Ayotte KW, Hughes DE (2004.) Observations of boundary-layer wind-tunnel flow over isolated ridges of
2406 varying steepness and roughness. Boundary-Layer Meteorol 112: 525–556

2407
2408 Ayotte KW, Taylor PA (1995) A mixed spectral-finite difference 3D model of neutral planetary boundary-
2409 layer flow over topography. J Atmos Sci 52: 3523–3537

2410 Ayotte KW, Xu D, Taylor PA (1994) The impact of turbulence schemes on predictions of the mixed
2411 spectral finite-difference model of flow over topography. Boundary-Layer Meteorol 68:1–33.

2412
2413 Babić N, De Wekker SFJ (2019) Characteristics of Roll and Cellular Convection in a Deep and Wide
2414 Semiarid Valley: A Large-Eddy Simulation Study. Atmos Res 223:74–87.
2415

2416 Bader DC, Mckee TB (1983) Dynamical Model Simulation of the Morning Boundary Layer Development
2417 in Deep Mountain Valleys. J Appl Meteorol Climatol 22:341–351

2418 Baines PG (2001) Mixing in flows down gentle slopes into stratified environments. J Fluid Mech 443: 237–
2419 270

2420 Baldocchi, DD Meyers TP (1988) A Spectral and Lag-correlation Analysis of Turbulence in a Deciduous
2421 Forest Canopy. Boundary-Layer Meteorol 45:31–58.

2422 Bao J, Chow FK, Lundquist KA (2018) Large-Eddy Simulation over Complex Terrain Using an Improved
2423 Immersed Boundary Method in the Weather Research and Forecasting Model. Mon Weather Rev 146
2424 (9):2781–2797

2425
2426 Basu S, Lacser A (2017) A Cautionary Note on the Use of Monin–Obukhov Similarity Theory in Very High-
2427 Resolution Large-Eddy Simulations. Boundary-Layer Meteorol 163:351–355

2428 Beare, RJ, MacVean MK, Holtslag AAM, Cuxart J, Esau I, Golaz J-C, Jimenez MA, Khairoutdinov, M,
2429 Kosović B, Lewellen D, Lund TS, Lundquist J K, McCabe A, Moene AF, Noh Y, Raasch S, Sullivan PP
2430 (2006) An Intercomparison of Large-Eddy Simulations of the Stable Boundary Layer. Boundary-Layer
2431 Meteorol 118: 247–272

2432 Bechmann A, Sørensen NN, Berg J, Mann, J, Réthoré PE (2011.) The Bolund Experiment, Part II: Blind
2433 Comparison of Microscale Flow Models. Boundary-Layer Meteorol 141: 245–271

2434
2435 Belcher SE (1990) Turbulent Boundary Layer Flow over Undulating Surfaces. Ph.D. Dissertation,
2436 Cambridge University, U.K.
2437
2438 Belcher SE, Hunt JCR (1998) Turbulent Flow over Hills and Waves. Annu Rev Fluid Mech. 30:507–538.

2439 Belcher SE, Wood N (1996) Form and wave drag due to stably stratified turbulent flow over low ridges. Q
2440 J R Meteorol Soc 122:863–902

2441
2442 Belcher, SE, Finnigan JJ, Harman IN (2008) Flows through forest canopies in complex terrain. Ecol Appl.
2443 18:1436–1453.

2444
2445 Belcher SE, Harman IN, Finnigan JJ (2012) The wind in the willows: Flows in forest canopies in complex
2446 terrain. Annu Rev Fluid Mech 44:479–504.

2447 Belcher SE, Newley T, Hunt JCR (1993) The drag on an undulating surface induced by the flow of a
2448 turbulent boundary layer. J Fluid Mech 249:557–596.

2449 Beljaars ACM, Walmsley JL, Taylor PA (1987) Mixed Spectral Finite-Difference Model for Neutrally
2450 Stratified Boundary-Layer Flow over Roughness Changes and Topography. Boundary-Layer Meteorol 38:
2451 273–303.

2452 Berg J, Mann J, Bechmann A, Courtney MS, Jørgensen HE (2011) The Bolund Experiment, Part I: Flow
2453 over a Steep, Three-Dimensional Hill. Boundary-Layer Meteorol 141: 219–243

2454 Bleeg J, Digraskar D, Woodcock J, Corbett J-F (2014) Modelling stable thermal stratification and its
2455 impact on wind flow over topography, 18: 369–383

2456 Blumen W (1990) Atmospheric Processes over Complex Terrain. American Meteorological Society.
2457 Meteorological Monograph. Vol. 23, No.45.

2458 Bou-Zeid E (2014) Challenging the Large Eddy Simulation Technique with Advanced a Posteriori Tests, J
2459 Fluid Mech 764:1–4

2460 Bowen AJ, Mortensen, NG (2004) WAsP prediction errors due to site orography. Riso-R-995(EN), ISBN
2461 87-550- 2320-7, Roskilde, Denmark.

2462 Bradley EF (1980) An Experimental Study of the Profiles of Wind Speed, Shearing Stress and Turbulence
2463 at the Crest of a Large Hill. Q J R Meteorol Soc 106:101–124.

2464 Bradley EF (1983) The influence of thermal stability and angle of incidence on the acceleration of wind up
2465 a slope. J Wind Eng Ind Aerodyn 15: 231–242.

Britter RE, Hunt JCR, Richards KJ (1981) Air flow over a two-dimensional hill: Studies of velocity speed-up, roughness effects and turbulence Q J R Meteorol Soc 107: 91–110.

Brown AR, Wood N (2001) Turbulent Form Drag on Anisotropic Three-Dimensional Orography. Boundary-Layer Meteorol 101: 229–241.

Brown AR Athanassiadou M, Wood N (2003) Topographically induced waves within the stable boundary layer. Q J R Meteorol Soc 129: 3357–3370

Brown AR, Hobson JM, Wood N (2001) Large-Eddy Simulation of Neutral Turbulent Flow over Rough Sinusoidal Ridges. Boundary-Layer Meteorol 98: 411–41.

Burkholder BA, Fedorovich E, Shapiro A (2011) Evaluating Subgrid-Scale Models for Large-Eddy Simulation of Turbulent Katabatic Flow. In: Salvetti, MV Geurts B, Meyers J, Sagaut P (eds) Quality and Reliability of Large-Eddy Simulations II, Dordrecht, The Netherlands: Springer. pp149–60.

Burns P, Chemel C (2014) Evolution of Cold-Air-Pooling Processes in Complex Terrain. Boundary-Layer Meteorol 150:423–447.

Burns P, Chemel C (2015) Interactions Between Downslope Flows and a Developing Cold-Air Pool. Boundary-Layer Meteorol 154:57–80.

Businger JA, Wyngaard JC, Izumi Y, Bradley EF (1971) Flux-Profile Relationships in the Atmospheric Surface Layer. J Atmos Sci 28:181–189.

Carruthers DJ, Choularton TW (1982) Airflow over hills of moderate slope. Q J R Meteorol Soc 108: 603–624.

Carruthers DJ, Hunt JCR (1990) (1982) Fluid Mechanics of Airflow over Hills: Turbulence, Fluxes and Waves in The Boundary Layer. In: Blumen W (ed) Atmospheric Processes over Complex Terrain. Amer. Meteor. Soc. Meteorological Monograph. Vol. 23, No. 45. pp 83–107.

Catalano F, Moeng CH (2010) Large-Eddy Simulation of the Daytime Boundary Layer in an Idealized Valley Using the Weather Research and Forecasting Numerical Model. Boundary-Layer Meteorol 137: 49–75.

Chávez Arroyo R, Sanz Rodrigo J, Gankarski P (2014) Modelling of atmospheric boundary-layer flow in complex terrain with different forest parameterizations. J. Phys.: Conf. Ser. 524 012119

Chen B, Chamecki M, Katul GG (2019) Effects of topography on in-canopy transport of gases emitted within dense forests, Q J R Meteorol Soc 145: 2101–2114,

Choukulkar A, Calhoun R, Billings B, Doyle J (2012) Investigation of a Complex Nocturnal Flow in Owens Valley, California Using Coherent Doppler Lidar. Boundary-Layer Meteorol 144:359–378.

Chow FK, Weigel AP, Street RL, Rotach MW, Xue M (2006) High-Resolution Large-Eddy Simulations of Flow in a Steep Alpine Valley. Part I: Methodology, Verification, and Sensitivity Experiments. J Appl Meteorol Climatol 45 (1): 63–86.

2504 Chow FK, Street RL (2009) Evaluation of Turbulence Closure Models for Large-Eddy Simulation over
2505 Complex Terrain: Flow over Askervein Hill. J Appl Meteorol Climatol 48 (5):1050–65.
2506
2507 Clark TL (1977) A Small-Scale Dynamic Model Using a Terrain-Following Coordinate Transformation. J
2508 Comput Phys 24 (2): 186–215.

2509
2510 Clements WE, Nappo CJ (1983) 'Observations of Katabatic Flow on a Simple Slope' J Appl Meteorol
2511 Climatol 22: 331–335.

2512 Coppin PA, Bradley EF, Finnigan JJ (1994) Measurements of flow over an elongated ridge and its thermal
2513 stability dependence: the mean field. Boundary-Layer Meteorol 69: 173–199.

2514 Cuxart J (2015) When Can a High-Resolution Simulation over Complex Terrain Be Called LES? Frontiers
2515 in Earth Sci 3:1–6.

2516 Dar AS, Berg J, Troldborg N, Patton EG (2019.) On the Self-Similarity of Wind Turbine Wakes in a
2517 Complex Terrain Using Large Eddy Simulation. Wind Energy 4 (4): 633–44.

2518 Deardorff JW (1970a) A Numerical Study of Three-Dimensional Turbulent Channel Flow at Large
2519 Reynold's Numbers. J Fluid Mech 41: 453–80.

2520 Deardorff JW (1970b) A Three-Dimensional Numerical Investigation of the Idealized Planetary Boundary
2521 Layer. Geophysical Astrophysical Fluid Dynamics 1(3): 377–410.

2522 Deardorff JW (1972a) Numerical Investigation of Neutral and Unstable Planetary Boundary Layers. J
2523 Atmos Sci 29: 91–115

2524 Deardorff JW (1972b) Three-Dimensional Numerical Modeling of the Planetary Boundary Layer. In:
2525 Haugen DA (ed) Workshop on Micrometeorology, American Meteorological Society. Boston, MA:
2526 pp271–311

2527 Deaves DM (1975) Wind over Hills: A Numerical Approach. J Wind Eng Ind Aerodyn 1: 371–91.

2528
2529 De Bruyn Kops S, Riley J (2019) The effects of stable stratification on the decay of initially isotropic
2530 homogeneous turbulence. J Fluid Mech 860:787–821.
2531
2532 Denby B (1999) Second-Order Modelling of Turbulence in Katabatic Flows. Boundary-Layer Meteorol
2533 92:65–98

2534
2535 Defant F (1949) Zur Theorie der Hangwinde, nebst Remerkungen zur Theorie der Berg- und Talwinde [A
2536 Theory of Slope Winds, Along With Remarks on the Theory of Mountain Winds and Valley Winds]. Archiv
2537 fuer Meteorologie Geophysik und Biolimatologie Ser. A, 1:421–450

2538

2539 Desmond CJ, Watson SJ, Hancock PE (2017) Modelling the wind energy resources in complex terrain and
2540 atmospheres. Numerical simulation and wind tunnel investigation of non-neutral forest canopy flows. J
2541 Wind Eng Ind Aerodyn 166: 48–60.

Diebold M, Higgins C, Fang, J, Bechmann A, Parlange MB (2013) Flow over Hills: A Large-Eddy Simulation of the Bolund Case. Boundary-Layer Meteorol 148: 177–94.

Di Sabatino S (2016) Boundary-Layer Atmospheric Processes in Mountainous Terrain: Results from MATERHORN-X. Boundary-Layer Meteorol 159:465–467

Doran JC (1991) The effects of ambient winds on valley drainage flows. Boundary-Layer Meteorol 55:177–189

Doran JC, Horst TW, Whiteman CD (1990) The development and structure of nocturnal slope winds in a simple valley. Boundary-Layer Meteorol 52:41–68

Dörnbrack, A, Schumann U (1993) Numerical Simulation of Turbulent Convective Flow over Wavy Terrain. Boundary-Layer Meteorol 65: 323–55.

Dupont S, Brunet Y, Finnigan JJ (2008) Large-Eddy Simulation of Turbulent Flow over a Forested Hill: Validation and Coherent Structure Identification. Q J R Meteorol Soc 134: 1911–1929.

Dyer AJ (1967) The turbulent transport of heat and water vapour in an unstable atmosphere. Q J R Meteorol Soc 93: 501–508

Feigenwinter C, Bernhofer C, Vogt R (2004,)The influence of advection on the short term CO2 budget in and above a forest canopy, Boundary-Layer Meteorol 113: 201–224.

Fernando HJS, Pardyjak ER (2013) Field Studies Delve Into the Intricacies of Mountain Weather. Eos Trans AGU 94:313–315

Fernando HJS, Pardyjak ER, Di Sabatino S (2015) The MATERHORN: Unraveling the Intricacies of Mountain Weather. Bull Am Meteorol Soc 96:1945–1967

Fernando HJ (2019) The Perdigão: peering into microscale details of mountain winds. Bull Am Meteorol Soc 100:799–819

Finnigan JJ (2000) Turbulence in Plant Canopies. Annu Rev Fluid Mech 32:519–571

Finnigan JJ, Raupach MR (1987). Transfer processes in plant canopies in relation to stomatal characteristics. In: Zeiger E, Farquhar G, Cowan IR (eds) Stomatal Function. Stanford University Press, Stanford, California. pp 385–429

Finnigan JJ (1988). Air flow over complex terrain. In: Steffen WL, Denmead OT (eds) Flow and Transport in the Natural Environment: Advances and Applications, Springer-Verlag: Heidelberg. pp183–229

Finnigan JJ, Raupach MR, Bradley EF, Aldis GK (1990) A wind tunnel study of turbulent flow over a two-dimensional ridge. Boundary-Layer Meteorol 50:277–317.

Finnigan JJ, Shaw RH, Patton EG (2009) Turbulence Structure above Vegetation Canopies J Fluid Mech 637: 387–424.

Finnigan JJ (2006) Turbulent flow in canopies on complex topography and the effects of stable stratification. In: Gayev Y, Hunt JCR (eds) Flow and Transport Processes with Complex Obstructions. Proceedings of the 2003 NATO Advanced Studies Workshop, Kiev, Ukraine. Springer, Berlin. pp 199–219

Finnigan JJ, Brunet Y (1995) Turbulent airflow in forests on flat and hilly terrain. In: Coutts MP, Grace J. (eds) Wind and Trees, Cambridge Univ. Press. Cambridge, UK pp 3–40

Finnigan JJ (2008) Introduction to flux measurements in difficult conditions. Ecol Appl 18:1340–1350

Finnigan JJ, Belcher. SE (2004) Flow over a Hill Covered with a Plant Canopy. Q J R Meteorol Soc 130:1–29

Finnigan JJ, Shaw RH, Patton EG (2009) Turbulence Structure above vegetation canopies. J Fluid Mech 637: 387–424.

Finnigan JJ, Harman IN. Ross AN, Belcher SE (2015) First-order turbulence closure for modelling complex canopy flows. Q J R Meteorol Soc 141:2907–2916.

Finnigan JJ, Hughes D (2008) A wind tunnel study of stably stratified flow on a ridge covered with a tall plant canopy. 18th AMS Symposium on Boundary layers and Turbulence http://ams.confex.com/ams/pdfpapers/140135.pdf

Finnigan JJ, Shaw RH (2008) Double-averaging methodology and its application to turbulent flow in and above vegetation canopies. Acta Geophys 5: 534–561

Fitzjarrald DR (1984) Katabatic Wind in Opposing Flow. J Atmos Sci 41:1143–1158

Foken T (2008) Micrometeorology. Springer-Verlag Berlin Heidelberg.

Forrer J, Rotach MW (1997) On the turbulence structure in the stable boundary layer over the Greenland ice sheet. Boundary-Layer Meteorol 85:111–136

Foster CS, Crosman ET, Horel JD (2017) Simulations of a Cold-Air Pool in Utah's Salt Lake Valley: Sensitivity to Land Use and Snow Cover. Boundary-Layer Meteorol 164:63–87.

Fox DG, Lilly DK (1972) Numerical Simulation of Turbulent Flows. Rev. Geophys 10 (1): 51–72

Gallée H, Schayes G (1992) Dynamical aspects of katabatic wind evolution in the Antarctic coastal zone. Boundary-Layer Meteorol 59:141–161

Gal-Chen T, Somerville RCJ (1975) On the Use of a Coordinate Transformation for the Solution of the Navier-Stokes Equations. J. Comput Phys 17: 209–28.

Geiss A, Mahrt L (2015) Decomposition of Spatial Structure of Nocturnal Flow over Gentle Terrain. Boundary-Layer Meteorol 156:337–347

Giometto MG, Grandi R, Fang J (2017) Katabatic Flow: A Closed-Form Solution with Spatially-Varying Eddy Diffusivities. Boundary-Layer Meteorol 162:307–317

Giometto MG, Katul GG, Fang J, Parlange MB (2017b) Direct numerical simulation of turbulent slope flows up to Grashof number Gr= 2.1 x 1011, J Fluid Mech 829:589–620

Goger B, Rotach MW, Gohm A (2018) The Impact of Three-Dimensional Effects on the Simulation of Turbulence Kinetic Energy in a Major Alpine Valley. Boundary-Layer Meteorol 168:1–27

Golaz J-C, Doyle, JD Wang S (2009) One-Way Nested Large-Eddy Simulation over the Askervein Hill. J Adv Model Earth Syst 1 (3) https://doi.org/10.3894/JAMES.2009.1.6.

Gong W, Ibbetson A (1989). A wind tunnel study of turbulent flow over model hills. Boundary-Layer Meteorol 49: 113–148

Gong W, Taylor PA, Dornbrack A (1996) Turbulent Boundary-Layer Flow over Fixed Aerodynamically Rough Two-Dimensional Sinusoidal Waves. J Fluid Mech 312: 1–37.

Goulden ML, Miller SD, da Rocha HR (2006) Nocturnal cold air drainage and pooling in a tropical forest. J Geophys Res 111 (D8)D08S04.

Grachev AA, Leo LS, Sabatino SD (2016) Structure of Turbulence in Katabatic Flows Below and Above the Wind-Speed Maximum. Boundary-Layer Meteorol 159:469–494.

Grant ER, Ross AN, Gardiner BA (2016) Modelling canopy flows over complex terrain. Boundary-Layer Meteorol 161: 417–437.

Grant ER, Ross AN, Gardiner BA, Mobbs SD (2015) Field observations of canopy flows over complex terrain. Boundary-Layer Meteorol 156: 231–251.

Grisogono B, Oerlemans J (2001) Katabatic Flow: Analytic Solution for Gradually Varying Eddy Diffusivities. J Atmos Sci 58:3349–3354

Grisogono B, Axelsen SL (2012) A Note on the Pure Katabatic Wind Maximum over Gentle Slopes. Boundary-Layer Meteorol 145:527–538

Grubisic V, Doyle JD, Kuettner J, Mobbs SD, Smith RB, Whiteman CD, Dirks R, Czyzyk S, Cohn SA, Vosper S, Weissmann M, Haimov S, Stephan F, de Wekker jJ, Pan LI, Chow FK (2008) The terrain-induced rotor experiment: a Field Campaign Overview Including Observational Highlights. Bull Am Meteorol Soc 89(10):1513–1534.

2663 Gryning S-E, Mahrt L, Larsen S (1985) Oscillating nocturnal slope flow in a coastal valley. Tellus A
2664 37A:196–203

2665
2666 Hahn CJ (1981) A study of the diurnal behavior of boundary-layer winds at the Boulder Atmospheric
2667 Observatory. Boundary-Layer Meteorol 21:231–245

2668 Hald C, Zeeman M, Laux P, Mauder M, Kunstmann H (2019) Large-Eddy Simulations of Real-World
2669 Episodes in Complex Terrain Based on Era-Reanalysis and Validated by Ground-Based Remote Sensing
2670 Data. Mon Weather Rev 147(12): 4325–43.

2671
2672 Haiden T, Whiteman CD, Hoch SW, Lehner M (2010) A Mass Flux Model of Nocturnal Cold-Air
2673 Intrusions into a Closed Basin. J Appl Meteorol Climatol 50:933–943

2674
2675 Harman IN, Finnigan JJ (2007) A simple unified theory for flow in the canopy and roughness sublayer.
2676 Boundary-Layer Meteorol 123:339–363
2677
2678 Harman IN, Finnigan JJ (2008) Scalar concentration profiles in the canopy and roughness sublayer.
2679 Boundary-Layer Meteorol 129:323–351
2680
2681 Harman IN, Finnigan JJ (2010) Flow Over Hills Covered by a Plant Canopy: Extension to Generalised
2682 Two-Dimensional Topography. Boundary-Layer Meteorol 135:51–65
2683
2684 Harman IN, Finnigan JJ (2013) Flow Over a Narrow Ridge Covered with a Plant Canopy: A Comparison
2685 Between Wind-Tunnel Observations and Linear Theory. Boundary-Layer Meteorol 147:1–20
2686
2687 Hatcher L, Hogg AJ, Woods AW. (2000) The effects of drag on turbulent gravity currents. J Fluid Mech
2688 416:297–314
2689
2690 Heinemann G (2004) Local Similarity Properties of the Continuously Turbulent Stable Boundary Layer over
2691 Greenland. Boundary-Layer Meteorol 112:283–305.

2692
2693 Henne S, Furger M, Nyeki S, Steinbacher M, Neininger B, DeWekker SFJ, Dommen J, Spichtinger N,
2694 Stohl A, Prevot ASH. (2004) Quantification of topographic venting of boundary-layer air to the free
2695 troposphere. Atmos Chem Phys 4: 497–509
2696
2697 Hennemuth B (1986) Thermal asymmetry and cross-valley circulation in a small alpine valley. Boundary-
2698 Layer Meteorol 36:371–394.

2699
2700 Heinemann G (1999) The Kabeg'97 field experiment: an aircraft-based study of katabatic wind dynamics
2701 over the Greenland ice sheet, Boundary-Layer Meteorol 93: 75–116

2702 Henn DS, Sykes RI (1999) Large-Eddy Simulation of Flow over Wavy Surfaces. J Fluid Mech 383:75–112

2703
2704 Honnert R (2016) Representation of the Grey Zone of Turbulence in the Atmospheric Boundary Layer.
2705 Adv Sci Res 13: 63–67
2706
2707 Horst TW, Doran JC (1986) Nocturnal drainage flow on simple slopes. Boundary-Layer Meteorol 34:263–
2708 286.

Horst TW, Doran JC (1988) The Turbulence Structure of Nocturnal Slope Flow. J Atmos Sci 45:605–616.

Hunt JCR (1980) Wind over Hills. Survey paper for AMS workshop on the planetary boundary layer. Amer. Meteor. Soc., Boulder, pp101–157

Hunt JCR, Leibovich S, Richards KJ (1988a) Turbulent shear flows over low hills. Q J R Meteorol Soc 114:1435–1470.

Hunt JCR, Richards KJ, Brighton PWM (1988b) Stably stratified shear flow over low hills. Q J R Meteorol Soc 114: 859–886.

Hunt JCR, Snyder WH (1980) Experiments on stably and neutrally stratified flow over a model three - dimensional hill. J Fluid Mech 96, 671–704

Hunt JCR, Weng WS, Carruthers DJ (1988c) Modelling Deposition Fluxes on Hills. In: van Dop H (ed) Air Pollution Modelling and its Applications, Plenum Publishing Corp.

Hunt JCR Fernholz H (1975) Wind-Tunnel Simulation of the Atmospheric Boundary Layer: A Report on Euromech 50, J Fluid Mech 70:543–559

Hunt JCR, Carruthers DJ (1990) Rapid distortion theory and the 'problems' of turbulence. J Fluid Mech 212:497–532

Huntingford C, Blyth EM, Wood N, Hewer FE, Grant ALM (1998) The Effect of Orography on Evaporation. Boundary-Layer Meteorol 86:487–504

Iizuka S, Hiroaki K (2004) Performance of Various Sub-Grid Scale Models in Large-Eddy Simulations of Turbulent Flow over Complex Terrain. Atmospheric Environment 38: 7083–91

Izuka S, Hiroaki K (2006.) Large-Eddy Simulations of Turbulent Flow over Complex Terrain Using Modified Static Eddy Viscosity Models. Atmospheric Environment 40: 925–35

Jackson PS, Hunt JCR (1975) Turbulent Wind Flow over a Low Hill. Q J R Meteorol Soc 101: 929–955.

Jensen DD, Nadeau DF, Hoch SW, Pardyjak ER (2017) The evolution and sensitivity of katabatic flow dynamics to external influences through the evening transition. Q J R Meteorol Soc 143:423–438

Jenkins GJ, Mason PJ, Moores WH, Dykes RI (1981) Measurements of the flow structure around Ailsa Craig, a steep, three-dimensional, isolated hill. Q. J. Roy. Meteorol. Soc. 107: 749–984

Kaimal JC, Finnigan JJ (1994) Atmospheric Boundary Layer Flows: Their Structure and Measurement. Oxford University Press.

Kaimal JC, Wyngaard JC (1990) The Kansas and Minnesota Experiments. Boundary-Layer Meteorol 50: 31–47

Katul GG, Finnigan JJ, Poggi D, Leuning R, Belcher SE (2006) The influence of hilly terrain on canopy-atmosphere carbon dioxide exchange, Boundary Layer Meteorol 118: 189–216

Katul GG, Mahrt L, Poggi D, Sanz C (2004) One- and two-equation models for canopy turbulence. Boundary-Layer Meteorol 113: 81–109.

King J (1989) Low-level wind profiles at an Antarctic coastal station. Antarctic Science, 1(2): 169–178.

Kirshbaum DJ (2017) On Upstream Blocking over Heated Mountain Ridges. Q J R Meteorol Soc 143 (702): 53–68.

Kleidon A (2016) Thermodynamic foundations of the earth system. Cambridge University Press.

Kondo J, Sato T (1988) A simple model of drainage flow on a slope. Boundary-Layer Meteorol 43:103–123.

Kottmeier C (1986) Shallow gravity flows over the Ekström ice shelf. Boundary-Layer Meteorol 35:1–20.

Kuwagata T, Kimura F (1997) Daytime Boundary Layer Evolution in a Deep Valley. Part II: Numerical Simulation of the Cross-Valley Circulation. J Appl Meteorol 36: 883–895

Lareau NP, Horel JD (2015) Dynamically Induced Displacements of a Persistent Cold-Air Pool. Boundary-Layer Meteorol 154:291–316.

Lee HN, Kau WS (1984) Simulation of three-dimensional wind flow over complex terrain in the atmospheric boundary layer. Boundary-Layer Meteorol 29:381–396

Lee X, Barr, AG (1998), Climatology of gravity waves in a forest. Q J R Meteorol Soc 124:1403–1419

Lee X, Hu X (2002) Forest-air fluxes of carbon, water and energy over non-flat terrain. Boundary Layer Meteorol 103: 277–301

Lehner M, Whiteman CD, Hoch SW (2015) A Case Study of the Nocturnal Boundary Layer Evolution on a Slope at the Foot of a Desert Mountain. J Appl Meteorol Climatol 54:732–751.

Lewis HW, Mobbs SD, Vosper SB, Brown AR (2008a) The Effects of Surface Heating on Hill-Induced Flow Separation. Boundary-Layer Meteorol 129:269–287

Lewis HW, Mobbs SD, Lehning M (2008b.) Observations of cross-ridge flows across steep terrain. Q J R Meteorol Soc 134:801–816

Litt M, Sicart J-E, Helgason WD, Wagnon P (2015) Turbulence Characteristics in the Atmospheric Surface Layer for Different Wind Regimes over the Tropical Zongo Glacier (Bolivia, S). Boundary-Layer Meteorol 154:471–495

Łobocki L (2017) Turbulent Mechanical Energy Budget in Stably Stratified Baroclinic Flows over Sloping Terrain. Boundary-Layer Meteorol 164:353–365

Loureiro JBR, Silva Freire AP (2005) Experimental investigation of turbulent boundary layers over steep two-dimensional elevations. Journal of the Brazilian Society of Mechanical Sciences and Engineering 27(4) DOI: 10.1590/S1678-58782005000400001

Mahrt L. (1982) Momentum balance of Gravity Flows. J. Atmos. Sci 39: 2701–2711.

Mahrt L, Larsen S (1982) Small scale drainage front. Tellus 34:579–587

Mahrt L, Vickers D, Nakamura R (2001) Shallow Drainage Flows. Boundary-Layer Meteorol 101:243–260

Mahrt L, Larsen S (1990) Relation of slope winds to the ambient flow over gentle terrain. Boundary-Layer Meteorol 53:93–102.

Mahrt L (1999) Stratified Atmospheric Boundary Layers. Boundary-Layer Meteorol 90:375–396

Mahrt L (2010) Variability and Maintenance of Turbulence in the Very Stable Boundary Layer. Boundary-Layer Meteorol 135:1–18.

Mahrt L, Thomas CK, Grachev AA, Persson POG (2018) Near-Surface Vertical Flux Divergence in the Stable Boundary Layer. Boundary-Layer Meteorol 169:373–393

Manins PC (1992) Vertical fluxes in katabatic flows. Boundary-Layer Meteorol 60:169–178.

Manins PC, Sawford BL (1979a) Katabatic winds: A field case study. Q J R Meteorol Soc 105:1011–1025.

Manins PC, Sawford BL (1979b) A Model of Katabatic Winds. J Atmos Sci 36:619–630.

Mann J, Angelou N, Arnqvist J, Callies D, Cantero E, Chávez Arroyo R, Courtney M (2017) Complex Terrain Experiments in the New European Wind Atlas. Philos Trans R Soc *A* 375: 20160101. http://dx.doi.org/10.1098/rsta.2016.0101

Martínez D, Jiménez MA, Cuxart J, Mahrt L (2010) Heterogeneous Nocturnal Cooling in a Large Basin Under Very Stable Conditions. Boundary-Layer Meteorol 137:97–113.

Mason PJ (1985) On the Parametrization of Orographic Drag. In: ECMWF Seminar on Physical Parametrization for Numerical Models of the Atmosphere, ECMWF, Shinfield Park, Reading, U.K., pp. 139–165.

Mason PJ (1986) Flow over the Summit of an Isolated Hill, Boundary-Layer Meteorol 37: 385–405.

Mason PJ, Sykes RI (1979) Flow over an isolated hill of moderate slope. Q J R Meteorol Soc 105: 383–395.

Mason PJ, King JC (1984) Atmospheric Flow over a Succession of Nearly Two Dimensional Ridges and Valleys. Q J R Meteorol Soc 110: 821–845.

Mason PJ, King JC (1985) Measurements and Predictions of Flow and Turbulence over an Isolated Hill of Moderate Slope, Q J R Meteorol Soc 111: 617–640.

Mayr GJ, Armi L, Gohm A, Zangl G, Durran D R, Flamant C, Gabersek S, Mobbs SD, Ross AN, Weissmann M (2007) Gap flows: Results from the Mesoscale Alpine Programme. Q J R Meteorol Soc 133: 881–896

Mickle RE Cook NJ Hoff AM Jensen NO, Salmon JR, Taylor PA, Tetzlaff G, Teunissen HW (1988) The Askervein Hill Project: Vertical Profiles of Wind and Turbulence. Boundary-Layer Meteorol 43: 143–169.

Mobbs SD, Vosper SB, Sheridan PF, Cardoso R, Burton RR, Arnold SJ (2005) Observations of downslope winds and rotors in the Falkland Islands. Q J R Meteorol Soc 131:329–351

Monti P, Fernando HJS, Princevac M (2002) Observations of Flow and Turbulence in the Nocturnal Boundary Layer over a Slope. J Atmos Sci 59:2513–2534.

Mortensen NG, Tindal A, Landberg L (2008) Field validation of the RIX performance indicator for flow in complex terrain. Paper presented at 2008 European Wind Energy Conference and Exhibition, Brussels, Belgium.

Muñoz-Esparza D, Kosovic.B (2018) Generation of Inflow Turbulence in Large-Eddy Simulations of Nonneutral Atmospheric Boundary Layers with the Cell Perturbation Method. Mon Weather Rev 146 (6): 1889–1909

Muñoz-Esparza D, Kosović B, Mirocha J, van Beeck J (2014) Bridging the Transition from Mesoscale to Microscale Turbulence in Numerical Weather Prediction Models. Boundary-Layer Meteorol 153: 409–40.

Muñoz-Esparza D, Lundquist JK, Sauer JA, Kosović B, Linn RR (2017.) Coupled Mesoscale- LES Modeling of a Diurnal Cycle during the CWEX-13 Field Campaign: From Weather to Boundary-layer Eddies. J Adv Model Earth Syst 9:1572–94.

Nadeau DF, Pardyjak ER, Higgins CW (2012) Flow during the evening transition over steep Alpine slopes. Q J R Meteorol Soc 139:607–624

Nadeau DF, Pardyjak ER, Higgins CW, Parlange MB (2013) Similarity Scaling Over a Steep Alpine Slope. Boundary-Layer Meteorology 147:401–419.

Nakagawa H, Nezu I (1977) Prediction of the contributions to the Reynolds stress from bursting events in open-channel flows. J Fluid Mech 80:99–128.

Nanni SC, Tampieri F (1985) A Linear Investigation on Separation in Laminar and Turbulent Boundary Layers over Low Hills and Valleys, Nuovo Cimento 8C: 579–601.

Neininger B, Rucker M, Weber H, Weiss A, De Wecker S, Zappa M (2004) The turbulence structure and exchange processes in an Alpine valley: The Riviera project. Bull Am Meteorol Soc 85(9):1367–1385

Newley TMJ (1985) Turbulent Airflow over Hills. Ph.D. Dissertation, Cambridge University, U.K.

Nieuwstadt FTM (1984a) The Turbulent Structure of the Stable, Nocturnal Boundary Layer. J Atmos Sci 41:2202–2216.

Nieuwstadt FTM (1984b) Some aspects of the turbulent stable boundary layer. Boundary-Layer Meteorol 30:31–55.

Noppel H, Fiedler F (2002) Mesoscale Heat Transport Over Complex Terrain By Slope Winds-A Conceptual Model And Numerical Simulations. Boundary-Layer Meteorol 104:73–97.

Obukhov AM (1971) Turbulence in an atmosphere with a non-uniform temperature. Boundary-Layer Meteorol 2:7–29.

Oldroyd HJ, Katul GG, Pardyjak ER, Parlange MB (2014) Momentum balance of katabatic flow on steep slopes covered with short vegetation. Geophys Res Lett 41:4761–4768.

Oldroyd HJ, Pardyjak ER, Higgins CW, Parlange MB (2016) Buoyant Turbulent Kinetic Energy Production in Steep-Slope Katabatic Flow. Boundary-Layer Meteorol 161:405–416.

Padro J (1987) Boundary-Layer Pollutant Concentrations over Complex Terrain Boundary-Layer Meteorol 38:17–28.

Padro J, Walmsley JL (1990) A Mixed Spectral-Finite Difference Model for Pollutant Concentrations over a Hill. Boundary-Layer Meteorol 51:343–363.

Palma J M L M, Silva Lopes A, Costa Gomes VM, Veiga Rodrigues C, Menke R, Vasiljevic N, Mann J (2019) Unravelling the wind flow over highly complex regions through computational modeling and two-dimensional lidar scanning. Journal of Physics: Conference Series. DOI: 10.1088/1742-6596/1222/1/012006

Papadopoulos KH, Helmis CG (1999) Evening and Morning Transition of Katabatic Flows. Boundary-Layer Meteorol 92:195–227.

Parish TR, Cassano JJ (2003) The Role of Katabatic Winds on the Antarctic Surface Wind Regime. Mon Weather Rev 131:317–333

Parmhed O, Oerlemans J, Grisogono B (2004) Describing surface fluxes in katabatic flow on Breidamerkurjökull, Iceland. Q J R Meteorol Soc 130:1137–1151

Patton EG, Katul GG (2009) Turbulent Pressure and Velocity Perturbations Induced by Gentle Hills Covered with Sparse and Dense Canopies. Boundary-Layer Meteorol 133: 189–217.

Patton EG, Sullivan PP, Ayotte KW (2006) Turbulent Flow over Isolated Ridges: Influence of Vegetation. In: 17th American Meteorological Society Symposium on Boundary Layers and Turbulence. San Diego, CA. http://ams.confex.com/ams/pdfpapers/110925.pdf.

Patton EG, Sullivan PP, Shaw RH Finnigan JJ, Weil JC (2016) Impact of atmospheric stability on coupled boundary-layer-canopy turbulence. J Atmos Sci 73:1621–1647,

Pearse JR, Lidley D, Stevenson DC (1981) Wind flow over ridges in simulated atmospheric boundary layers. Boundary-Layer Meteorol 21:77–92.

Phillips NA (1957) A Coordinate System Having Some Special Advantages for Numerical Forecasting. J Meteorol 14 (2): 184–85.

Poggi D, Katul GG (2007a) Turbulent flows inside forested hilly terrain: the recirculation region Q J R Meteorol Soc 133:1027–1039.

Poggi D, Katul GG (2007b) An experimental investigation of the mean momentum budget inside dense canopies on narrow gentle hilly terrain, Agric For Meteorol 144:1–13.

Poggi D, Katul GG (2007c) The ejection-sweep cycle over gentle hills covered with bare and forested surfaces, Boundary Layer Meteorol 122:493–515

Poggi D, Katul GG, Albertson JD, Ridolfi L (2007) An experimental investigation of turbulent flows over a hilly surface. Phys Fluids 19, DOI: 10.1063/1.2565528

Poggi D, Katul GG (2008) Turbulent intensities and velocity spectra for bare and forested gentle hills: flume experiments, Boundary Layer Meteorol 129: 25–46

Poggi D, Katul GG, Finnigan JJ, Belcher SE (2008) Analytical models for the mean flow inside dense canopies on gentle hilly terrain, Q J R Meteorol Soc 134:1095–1112

Pospíšil S, Kuznetsov S, Kozmarb H, Michalcovác V (2017) Wind-tunnel Simulation Of Thermally Unstable Atmospheric Flow In Complex Terrain. Procedia Engineering 190 : 575–580

Prandtl L (1942) Führer durch die Strömungslehre. Vieweg und Sohn, Braunschweig

Princevac M, Fernando HJS, Whiteman CD (2005) Turbulent entrainment into natural gravity-driven flows. J Fluid Mech 533:259–268

Princevac M, Hunt JCR, Fernando HJS (2008) Quasi-Steady Katabatic Winds on Slopes in Wide Valleys: Hydraulic Theory and Observations. J Atmos Sci **65:**627–643

Queney P (1948)The Problem of Air Flow over Mountains: A Summary of Theoretical Studies. Bull Am Meteorol Soc 29:16–26.

Rai RK, Berg LK, Kosović B, Mirocha JD, Pekour MS, Shaw WJ (2017) Comparison of Measured and Numerically Simulated Turbulence Statistics in a Convective Boundary Layer Over Complex Terrain. Boundary-Layer Meteorol 163: 69–89.

Rao KS, Snodgrass HF (1981) A nonstationary nocturnal drainage flow model. Boundary-Layer Meteorol 20:309–320

Raupach MR (1981) Conditional Statistics of Reynolds Stress in Rough-Wall and Smooth-Wall Turbulent Boundary Layers. J Fluid Mech 108:363–382

Raupach MR Shaw RH (1982) Averaging procedures for flow within vegetation canopies, Boundary-Layer Meteorol 22:79–90.

Raupach MR, Coppin PA, Legg BJ (1986) Experiments on scalar dispersion within a model plant canopy part I: The turbulence structure. Boundary-Layer Meteorol 35:21–52.

Raupach MR, Antonia RA, Rajagopalan S (1991) Rough-Wall Turbulent Boundary Layers. Appl Mech Rev 44(1):1–25

Raupach MR, Weng WS, Carruthers DJ, Hunt JCR (1992) Temperature and Humidity Fields and Fluxes over Low Hills Q J R Meteorol Soc 118:191–225.

Raupach MR, Finnigan JJ, Brunet Y (1996) Coherent eddies in vegetation canopies-the mixing layer analogy. Boundary-Layer Meteorol 78:351–382.

Raupach MR, Finnigan JJ (1997) The Influence of Topography on Meteorological Variables and Surface-Atmosphere Interactions. J Hydrol 190:182–213.

Ross AN (2012) Boundary-layer flow within and above a forest canopy of variable density. Q J R Meteorol Soc 138:1259–1272.

Ross AN (2011) Scalar Transport over Forested Hills. Boundary-Layer Meteorol 141:179–199

Ross AN, Arnold S, Vosper SB, Mobbs SD, Dixon N, Robins AG (2004) A comparison of wind-tunnel experiments and numerical simulations of neutral and stratified flow over a hill. Boundary-Layer Meteorol 113:427–459.

Ross AN, Baker TP (2013) Flow over partially forested ridges. Boundary-Layer Meteorol 146:375-392.

Ross AN (2008) Large eddy simulations of flow over forested ridges. Boundary-Layer Meteorol 128:59–76.

Ross AN, Harman IN (2015) The impact of source distribution on scalar transport over forested hills. Boundary-Layer Meteorol. 156:211–230.

2992 Ross AN, Vosper SB (2005) Neutral turbulent flow over forested hills. Q J R Meteorol Soc 131:1841–
2993 1862.

2994 Rotach MW, Calanca PL, Vogt R, Steyn D, Graziani G, Andretta M, Christen A, Cieslik S, Conolly R,
2995 Galmarini S, Van Gorsel E, Gurtz J, Kadygrov E, Kadygrov V, Miller E, Neininger B, Rucker M, Weber
2996 H, Weiss A, De Wecker S, Zappa, M (2004) The turbulence structure and exchange processes in an Alpine
2997 valley: The Riviera project. Bull Am. Meteorol Soc 85(9):1367–1385

2998
2999 Rotach MW, Zardi D (2007) On the boundary-layer structure over highly complex terrain: Key findings from
3000 MAP. Q J R Meteorol Soc133:937–948

3001
3002 Rotach MW, Andretta M, Calanca P (2008) Boundary layer characteristics and turbulent exchange
3003 mechanisms in highly complex terrain. Acta Geophys 56:194–219

3004

3005 Salmon JR, Teunissen HW, Mickle RE, Taylor PA (1988) The Kettles Hill Project: Field Observations,
3006 Wind Tunnel Simulations and Numerical Model Predictions for Flow over a Low Hill, Boundary-Layer
3007 Meteorol. 43:309–343.
3008
3009 Schmidli J, Rotunno, R (2010) Mechanisms of Along-Valley Winds and Heat Exchange over Mountainous
3010 Terrain. J. Atmos. Sci. 67(9): 3033–3047

3011 Schumann U (1990) Large-Eddy Simulation of the Upslope Boundary Layer. Q J R Meteorol Soc 116:
3012 637–70

3013
3014 Scorer RS (1949) Theory of Waves in the Lee of Mountains Q J R Meteorol Soc 76:41–56.
3015
3016 Serafin S, De Wekker SFJ, Knievel JC (2016) A Mesoscale Model-Based Climatography of Nocturnal
3017 Boundary-Layer Characteristics over the Complex Terrain of North-Western Utah. Boundary-Layer
3018 Meteorol 159:495–519.

3019
3020 Sfyri E, Rotach MW, Stiperski I (2018) Scalar-Flux Similarity in the Layer Near the Surface Over
3021 Mountainous Terrain. Boundary-Layer Meteorol 169:11–46

3022
3023 Shapiro A, Burkholder B, Fedorovich E (2012) Analytical and Numerical Investigation of Two-Dimensional
3024 Katabatic Flow Resulting from Local Surface Cooling. Boundary-Layer Meteorol 145:249–272

3025
3026 Shapiro A, Fedorovich E (2014) A Boundary-Layer Scaling for Turbulent Katabatic Flow. Boundary-Layer
3027 Meteorol 153:1–17

3028 Shaw RH, Schumann U (1992) Large-Eddy Simulation of Turbulent Flow above and within a Forest.
3029 Boundary-Layer Meteorol 61: 47–64.

3030
3031 Sheridan WP, Vosper SB, Mobbs SD. (2004) Rotors and downslope winds in
3032 the Falklands. Bull Am Meteorol Soc 85(8):1059–1060

Sheridan PF, Horlacher V, Rooney GG, Hignett P, Mobbs SD, Vosper SB (2007) Influence of lee waves on the near-surface flow downwind of the Pennines. Q J R Meteorol Soc 133:1353–1369

Shin HH, Hong SY (2015) Representation of the Subgrid-Scale Turbulent Transport in Convective Boundary Layers at Gray-Zone Resolutions. Mon Weather Rev 143: 250–71.

Silva Lopes A, Palma JMLM, Castro FA (2007) Simulation of the Askervein Flow. Part 2: Large-Eddy Simulations. Boundary-Layer Meteorol 125:85–108.

Skyllingstad E D (2003) Large-Eddy Simulation of Katabatic Flows. Boundary-Layer Meteorol 106: 217–43.

Smeets CJPP, Duynkerke PG, Vugts HF (1998) Turbulence Characteristics of the Stable Boundary Layer Over a Mid-Latitude Glacier. Part I: A Combination of Katabatic and Large-Scale Forcing. Boundary-Layer Meteorol 87:117–145.

Smeets CJPP, Duynkerke PG, Vugts HF (2000) Turbulence Characteristics Of The Stable Boundary Layer Over A Mid-Latitude Glacier. Part II: Pure Katabatic Forcing Conditions. Boundary-Layer Meteorol 97:73–107.

Smith CM, Skyllingstad ED (2005) Numerical Simulation of katabatic Flow with Changing Slope Angle. Mon Weather Rev 133:3065-3080

Söderberg S, Parmhed O (2006) Numerical Modelling of Katabatic Flow Over a Melting Outflow Glacier. Boundary-Layer Meteorol 120:509–534

Sogachev A (2009) A note on two-equation closure modeling of canopy flow. Boundary-Layer Meteorol 130:423–435.

Sogachev A, Panferov O (2006) Modification of two-equation models to account for plant drag. Boundary-Layer Meteorol 121:229–266.

Soler MR, Infante C, Buenestado P, Mahrt L (2002) Observations Of Nocturnal Drainage Flow In A Shallow Gully. Boundary-Layer Meteorol 105:253–273

Soler MR, Udina M, Ferreres E (2014) Observational and Numerical Simulation Study of a Sequence of Eight Atmospheric Density Currents in Northern Spain. Boundary-Layer Meteorol 153:195–216

Stiperski I, Rotach MW (2016) On the Measurement of Turbulence Over Complex Mountainous Terrain. Boundary-Layer Meteorol 159:97–121

Stiperski I, Calaf M (2017) Dependence of near-surface similarity scaling on the anisotropy of atmospheric turbulence. Q J R Meteorol Soc 144:641–657

Stiperski I, Calaf M, Rotach MW (2019) Scaling, Anisotropy, and Complexity in Near-Surface Atmospheric Turbulence. J Geophys Res 16; 124(3): 1428–1448

Sykes R (1980) An asymptotic theory of incompressible turbulent boundary layer flow over a small hump. J Fluid Mech 101: 647–670.

Takahashi, T, Kato S, Murakami S, Ooka R, Fassy Yassin M, Kono, R (2005) Wind tunnel tests of effects of atmospheric stability on turbulent flow over a three-dimensional hill. J Wind Eng Ind Aerodyn 9:155–169

Talbot C, Bou-Zeid E, Smith J (2012) Nested Mesoscale Large-Eddy Simulations with WRF: Performance in Real Test Cases. J Hydrometeorol 13 (5):1421–41.

Tampieri F (1987) Separation Features of Boundary-Layer Flow over Valleys. Boundary-Layer Meteorol 40:295–307.

Tamura T, Okuno A, Sugio Y (2007) LES Analysis of Turbulent Boundary Layer over 3D Steep Hill Covered with Vegetation. J Wind Eng Ind Aerodyn 95:1463–75.

Taylor PA (1977a) Some numerical studies of surface boundary layer flow above gentle topography. Boundary-Layer Meteorol 11:439–465.

Taylor PA (1977b) Numerical Studies of Neutrally Stratified Planetary Boundary-Layer Flow above Gentle Topography: Two-Dimensional Cases. Boundary-Layer Meteorol 12: 37–60.

Taylor PA, Gent PR (1974) A Model of Atmospheric Boundary-Layer Flow above an Isolated Two-Dimensional “Hill”; An Example of Flow above “Gentle Topography”. Boundary-Layer Meteorol 7:349–362.

Taylor PA, Gent PR, Keen J M (1976) Some Numerical Solutions for Turbulent Boundary Layer Flow above Fixed, Rough, Wavy Surfaces, ***Geophysical Journal Internationa***l 44 (1):177–201.

Taylor, PA, Walmsley J, Salmon JR (1983) A Simple Model of Neutrally Stratified Boundary-Layer Flow over Real Terrain Incorporating Wavenumber-Dependent Scaling, Boundary-Layer Meteorol 26:169–189.

Taylor PA, Teunissen HW (1985) The Askervein Hill Project; Report on the September/October 1983 Main Field Experiment, Internal Report MSRB-84-6, Atmospheric Environment Service, Downsview, Ontario, Canada.

Taylor PA, Teunissen HW (1987) Askervein Hill Project: Overview and Background Data. Boundary-Layer Meteorol 39:15–39

Taylor PA, Lee R J (1984) Simple Guidelines for Estimating Wind Speed Variations Due to Small Scale Topographic Features, Climatological Bulletin 18 (2), 3–32.

Taylor PA, Mason PJ, Bradley EF (1987) Boundary-layer flow over low hills. Boundary-Layer Meteorol 39:107–132

Taylor PA, Sykes R I, Mason PJ (1989) On the Parametrization of Drag over Small-Scale Topography in Neutrally-Stratified Boundary-Layer Flow, Boundary-Layer Meteorol 48: 409–422.

Teunissen HW, Shokr ME (1985a) The Askervein Hill Project: Wind-Tunnel Simulation (Smooth Model) at Length Scale 1: 1200, Research Report MSRB-85–1, Atmospheric Environment Service, Downsview, Ontario, Canada.

Teunissen HW, Shokr M E (1985b) Wind-Tunnel/Full-Scale Comparisons of Boundary-Layer Flow over Askervein Hill, Scotland, Proc. Asia Pacific Symposium on Wind Engineering, held at Univ. of Roorkee, Roorkee, India, December 5–7, 1985.

Teunissen HW, Shokr ME, Bowen AJ (1987) The Askervein Hill Project: Wind-tunnel simulations at three length scales. Boundary-Layer Meteorol 40:1–29.

Trachte K, Nauss T, Bendix J (2010) The Impact of Different Terrain Configurations on the Formation and Dynamics of Katabatic Flows: Idealised Case Studies. Boundary-Layer Meteorol 134:307–325

Troen I, Petersen E L (1989) The European Wind Atlas. Risø National Lab., Roskilde, Denmark.

Umphrey C, DeLeon R, Senocak I (2017) Direct Numerical Simulation of Turbulent Katabatic Slope Flows with an Immersed-Boundary Method. Boundary-Layer Meteorol 164:367–382

Undheim O, Andersson HI, Berge E (2006) Non-Linear, Microscale Modelling of the Flow over Askervein Hill. Boundary-Layer Meteorol 120: 477–95.

Van Der Avoird E, Duynkerke PG (1999) Turbulence in a Katabatic Flow. Boundary-Layer Meteorol 92:37–63

van Gorsel E, Christen A, Feigenwinter C, Parlow E, Vogt R (2003) Daytime turbulence statistics above a steep forested slope. Boundary-Layer Meteorol 109**:**311–329.

van Gorsel E, Harman IN, Finnigan JJ, Leuning R (2011) Decoupling of airflow above and in plant canopies and gravity waves affect micrometeorological estimates of net scalar exchange, Agric For Meteorol 151:927–933

Vasiljević N, Palma J M L M, Angelou N, Carlos Matos J. , Menke, R, Lea G, Mann J, Courtney M, Frölen Ribeiro L, Gomes VMMGC (2017) Perdigão 2015: Methodology for atmospheric multi-Doppler lidar experiments, Atmos. Meas. Tech. 10:3463–3483

Vosper SB, Mobbs SD (1997) Measurement of the pressure field on a mountain. Q J R Meteorol Soc 123:129–144.

Vosper SB, Mobbs SD, Gardiner BA. (2002) Measurements of the near-surface flow over a hill. Q J R Meteorol Soc 128: 2257–2280

Wagner A (1938) Theorie und Beobachtung der periodischen Gebirgswinde [English Translation from Atmospheric studies in complex terrain. Technical progress report, FY 1979-FY 1983]. Gerlands Beitraege zur Geophysik 52:408–449

Walko RL, Cotton WR, Pielke RA (1992) Large-Eddy Simulations of the Effects of Hilly Terrain on the Convective Boundary Layer. Boundary-Layer Meteorol 58:133–50.

Walmsley JL, Salmon JR, Taylor PA (1982) On the Application of a Model of Boundary-Layer Flow Over Low Hills to Real Terrain, Boundary-Layer Meteorol 23:17–46.

Walmsley JL, Taylor PA (1996) Boundary-layer Flow Over Topography: Impacts of the Askervein Study, Boundary-Layer Meteorol 78:291–320.

Walmsley JL, Taylor PA, Keith T (1986) A Simple Model of Neutrally Stratified Boundary-Layer Flow over Complex Terrain with Surface Roughness Modulations (MS3DJH/3R). Boundary-Layer Meteorol 36:157–86.

Wan F, Porté-Agel F (2011) Large-Eddy Simulation of Stably-Stratified Flow over a Steep Hill. Boundary-Layer Meteorol 138:367–84.

Watanabe T (1994) Bulk parameterization for a vegetated surface and its application to a simulation of nocturnal drainage flow, Boundary-Layer Meteorol 70:13–35

Weigel AP, Chow FK, Rotach MW (2007) The effect of mountainous topography on moisture exchange between the “surface” and the free atmosphere. Boundary-Layer Meteorol 125:227–244

Weng W (1997) Stably Stratified Boundary-Layer Flow over Low Hills: A Comparison of Model Results and Field Data, Boundary-Layer Meteorol 85:223–241.

Weng W, Chan L, Taylor PA, Xu D (1997) Modelling Stably Stratified Boundary Layer Flow over Low Hills’, Q J R Meteorol Soc 123:1841–1866.

Weng W, Taylor PA (2011) A Non-Linear Mixed Spectral Finite-Difference 3-D model for planetary boundary-layer flow over complex terrain, Adv Sci Res 6:75-78

Whiteman CD (1990) Observations of thermally developed wind systems in mountainous terrain. In: Blumen W (ed.) Atmospheric Processes over Complex Terrain, Meteorological Monographs Vol. 23 No. 45, American Meteorological Society. pp 5–42

Whiteman CD, Hoch SW, Lehner M, Haiden T (2010) Nocturnal Cold-Air Intrusions into a Closed Basin: Observational Evidence and Conceptual Model. J Appl Meteorol Climatol 49:1894–1905

Whiteman CD, Zhong S (2008) Downslope flows in a low-angle slope and their interactions with valley inversions. part I: Observations, J Appl Meteorol Climatol 47:2023–2038.

Wilson JD, Finnigan JJ, Raupach MR (1998) A first-order closure for disturbed plant-canopy flows and its application to winds in a canopy on a ridge, Q J R Meteorol Soc 124:705–732.

Wood N (1995) The onset of flow separation in neutral, turbulent flow over hills. Boundary-Layer Meteorol 76:137–164

Wood N, Mason PJ (1991), The influence of static stability on the effective roughness lengths for momentum and heat transfer. Q J R Meteorol Soc 117:1025–1056.

Wood N, Mason PJ (1993) The pressure force induced by neutral, turbulent flow over hills. Q J R Meteorol Soc 119:1233-1267.

Wood N (2000) Wind Flow over Complex Terrain: A Historical Perspective and the Prospect for Large-Eddy Modelling. Boundary-Layer Meteorol 96:11–32.

Wyngaard J C (2004) Toward Numerical Modeling in the ``Terra Incognita". J Atmos Sci 61:1816–18226.

Xu D, Taylor PA (1992) A Non-Linear Extension of the Mixed Spectral Finite Difference Model for Neutrally Stratified Turbulent Flow over Topography, Boundary-Layer Meteorol 59:177–186.

Xu D, Ayotte KW, Taylor PA (1994) Development of a Non-Linear Mixed Spectral Finite Difference Model for Turbulent Boundary Layer Flow over Topography, Boundary-Layer Meteorol 70:341–367.

Ye ZJ, Garratt JR, Segal M, Pielke RA (1990) On the impact of atmospheric thermal stability on the characteristics of nocturnal downslope flows. Boundary-Layer Meteorol 51:77–97

Yi C, Monson RK, Zhai Z, Anderson DE, Lamb B, Allwine G, Turnipseed AA, Burns S P (2005) Modeling and measuring the nocturnal drainage flow in a high-elevation, subalpine forest with complex terrain, J Geophys Res 110, D22303, doi:10.1029/2005JD006282.

Yu Y, Cai X, King JC, Renfrew IA (2005) Numerical simulations of katabatic jumps in coats land, Antarctica. Boundary-Layer Meteorology 114:413–437

Yu Y, Cai X-M (2006) Structure and Dynamics of Katabatic Flow Jumps: Idealised Simulations. Boundary-Layer Meteorol 118:527–555

Zardi D, Whiteman CD (2013) Diurnal Mountain Wind Systems. In: Chow FK, De Wekker SFJ, Snyder BJ (eds) Mountain Weather Research and Forecasting: Recent Progress and Current Challenges. Springer Netherlands, Dordrecht, pp 35–119

Zeman O, Jensen NO (1987) Modification of Turbulence Characteristics in Flow over Hills, Q J R Meteorol Soc 113:55–80

Zeri M, Rebmann C, Feigenwinter C, Sedlake P (2010) Analysis of periods with strong and coherent CO2 advection over a forested hill. Agric For Meteorol 150:674–683

Zilitinkevich SS, Elperin T, Kleeorin N (2009) Energy- and Flux-Budget Turbulence Closure Model for Stably Stratified Flows. Part II: The Role of Internal Gravity Waves. Boundary-Layer Meteorol 133:139–164